DØ Note 5709
Version 0.5
August 18, 2008

# Search for neutral Higgs bosons in $\phi b \to b\bar{b}b$ using RunIIb data

Daniela Bauer, Gavin Davies, Jonathan Hays, Per Jonsson, Tim Scanlon
Imperial College London
Fabrice Couderc, Boris Tuchming
Dapnia/Spp, Saclay
Anna Goussiou, Prolay Mal
University of Washington

**Abstract**

The RunIIb data sample recorded with trigger list version 15 at DØ has been analyzed to search for Neutral Higgs bosons produced in association with $b$-quarks at high $\tan\beta$ within the MSSM framework. The search has been performed in the three $b$-quarks channel using multi-jet triggered events corresponding to an integrated luminosity of $\sim 1.6$ fb$^{-1}$. No statistically significant excess of events with respect to the predicted background is observed. Limits are set on the cross section times branching ratio in the mass range 90 to 260 GeV/$c^2$. The result from this search is combined with that from the RunIIa search [1] and combined limits and exclusions in the MSSM parameter space are set.

## Contents

**1 Introduction** **1**
1.1 Overview of Updates and Changes with respect to p17 . . . . . 1

**2 Data sample** **1**
2.1 Data quality . . . . . 1
2.2 Trigger . . . . . 2
2.3 Jets . . . . . 2

**3 Monte Carlo samples** **5**
3.1 *hb* signal simulation . . . 6
3.2 Background simulation . . . 6
3.3 Corrections to full simulation . . . 6

**4 Analysis overview** **7**
4.1 Event selection . . . 7
4.2 Sample composition . . . 10
4.3 Likelihood discriminant . . . 19
4.4 Background model . . . 19
4.5 Data/Background prediction comparison . . . 20
4.6 Likelihood Output Comparison . . . 24
4.7 Agreement in the low-likelihood region . . . 24
4.8 Agreement in the high-likelihood region . . . 24

**5 Systematic Uncertainties** **31**
5.1 Signal Uncertainties . . . 31
5.2 Background Uncertainties . . . 31
5.3 Systematics . . . 32

**6 Limit Setting** **35**
6.1 Exclusion limit within different MSSM scenarios . . . 37

**A Trigger** **41**
A.1 L1 Jets . . . 41
A.2 Level 2 . . . 49
A.3 L3 Jets . . . 50
A.4 Closure Tests . . . 52
A.5 IP Tagger at Level 3 . . . 57

**B Data Background Comparison** **58**
B.1 Low Mass Likelihood . . . 58
B.2 High Mass Likelihood . . . 67

**C Data Monte Carlo Comparison** **73**
C.1 Low Likelihood Sample . . . 73
C.2 High Likelihood Sample . . . 91

**D Likelihoods** **109**
D.1 Low Mass Likelihood . . . 109
D.2 High Mass Likelihood . . . 112

**E Taggability** **115**

**F Luminosity Reweighting** **119**

**G Deficit Crosschecks** **121**
G.1 High Likelihood Region . . . . . 121
G.2 Deficit Mass Region . . . . . 126

# 1 Introduction

This note presents an update to the analysis in DØNote 5341 [1] using RunIIb data. The analysis procedure remains fundamentally the same. An overview of the updates and changes with respect to the p17 analysis can be found in section 1.1 below.

## 1.1 Overview of Updates and Changes with respect to p17

- A total of 1.6 $\text{fb}^{-1}$ of data collected with trigger list v15 have been analyzed.
- New p20 Monte Carlo (MC) signal and background samples were used.
- All trigger parameterizations have been re-derived. See appendix A.
- The taggability corrections have been re-derived. The results are shown in appendix E.
- $b$-tagging: The official $b$-ID ICHEP [2] tag rate functions (TRFs) were used to model the data tagging rate on MC.
- MC was reweighted to match instantaneous luminosity profiles between data and Monte Carlo.
- The background composition was updated (see sec. 4.2).
- The program `collie` [3] was used to calculate the limits at 95% C.L.

# 2 Data sample

The data sample used in this analysis is based on events from the 3JET skim [4] comprising runs 221993 - 240743, recorded between June 2006 and March 2008 with trigger list version 15. The data were reconstructed with the appropriate p20 versions of d0reco. The 3JET skim demands one uncorrected JCCB jet reconstructed with $p_T > 20\,\text{GeV}/c$ and two others with $p_T > 15\,\text{GeV}/c$. From the 3JET skim, CAFTrees were produced with p21 versions of the DØ software. The recommended versions of jet energy scale (JES) and $b$-tagging were applied. The CAFTrees were then processed through the higgs_hb package in p21.11.00.

## 2.1 Data quality

A bad luminosity block list (from dq_defs and lm_access run for the $h^0 b\bar{b}$ trigger) and detector (Muon, Calorimeter, SMT, CFT) good run list (from caf_dq) were used. This selection rejected 14 % of the events. Flags rejecting events which are subject to known calorimeter issues significantly affecting the data quality were applied event by event. An additional 6 % of the events were rejected by these. About 120 million events remained in the sample.

## 2.2 Trigger

The trigger used to collect the data was JT2_3JT15L_IP_VX. This trigger had four separate Level-2 branches in trigger list v15. Only the L2 $H_T$ and missing $H_T$ based branches were used to collect the events in the present analysis. Table 1 shows the L1, L2 and L3 requirements of the trigger.

| Level | v15 |
|---|---|
| L1 | CSWJT(3,8,$\|\eta\| < 3.2$)CSWJT(2,15,$\|\eta\| < 2.4$)CSWJT(1,30,$\|\eta\| < 2.4$) |
| L2 | JT(1,30,$\|\eta\| < 2.6$) JT(2,15,$\|\eta\| < 2.6$) JT(3,8,$\|\eta\| <$ X) HT(75,6) MJT(10,10) OR JT(1,30,$\|\eta\| < 2.6$) JT(2,15,$\|\eta\| < 2.6$) JT(3,8,$\|\eta\| <$ X) HT(100,6) |
| L3 | JT(3,15,$\|\eta\| < 3.6$) JT(2,25,$\|\eta\| < 3.6$) $\|z_{PV}\| < 35$ cm $\text{Prob}_b(0.4)$ |
| Name | JT2_3JT15L_IP_VX |

Table 1: The trigger conditions for the $h^0 b\bar{b}$ trigger in the v15 trigger list. The CSWJT(x,y,$|\eta| <$ z) term corresponds to x L1 jets above y GeV and within $|\eta| <$ z. The JT(x,y,$|\eta| <$ z) term corresponds to x jets reconstructed at L2 or L3 with $p_T > y$ GeV/$c$ and $|\eta| <$ z. The HT(x,y) term is used only at L2 and requires that the sum of the transverse momenta of L2 jets with $p_T > y$ GeV/$c$ is above x GeV. The MJT(x,y) term corresponds to a missing transverse energy $>$ x GeV calculated from jets with $E_T >$ y GeV. The $\text{Prob}_b(0.4)$ term is used only at L3 and corresponds to a cut of 0.4 on the probability for the event to not contain a $b$-quark.

Starting with trigger list v16.00, a STT IP condition was added to the $h^0 b\bar{b}$ trigger at Level 2, these data will be added to the analysis at a later time.
The total integrated luminosity after exclusion of bad luminosity blocks was 1.614 fb$^{-1}$ (1.222 fb$^{-1}$ and 0.392 fb$^{-1}$ of which was recorded before and after the 2007 shutdown respectively).

## 2.3 Jets

Jets were reconstructed with the Run II Improved Legacy Cone Algorithm and required to pass selection cuts to eliminate fake jets and EM objects. The recommended p20 jet energy scale corrections from jetcorr p21-br-07 were applied to all jets. Additionally, jets containing a medium muon (nseg = 3, $|\eta| < 2.$) within $\Delta R(\mu$, jet axis)$< 0.5$ were considered to originate from a semileptonic $b$-quark and were corrected for the momentum carried away by the muon and the neutrino. The JES correction applied to data is shown in Fig. 1.
Fig. 2 shows the properties of the jets in the data sample. There are neither significant spikes nor bumps in the $p_T$ and $\eta$ spectra which would be signs of remaining detector problems. The $\eta - \phi$ distributions of the jets after requiring various numbers of $b$-tagged jets in the event are also shown in Fig. 3. No irregularities are observed.

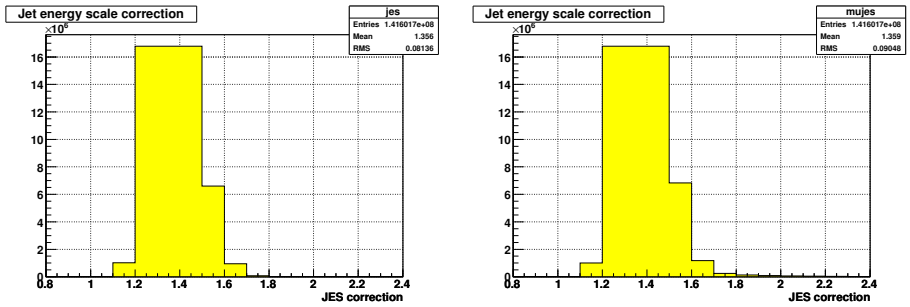


(a) (b)

Figure 1: (a) The basic jet energy scale correction in data and (b) after additional correction of semileptonic $b$-jets.

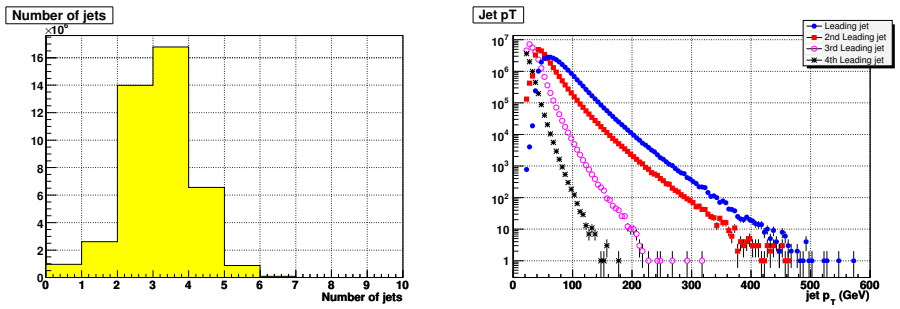


(a) Number of jets

(b) JES corrected $p_T$ of the four leading jets

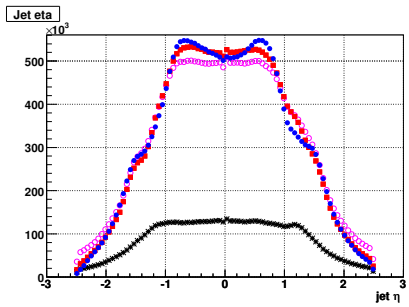


(c) Pseudo rapidity of the 4 leading jets

Figure 2: Basic jet distributions. For each plot, jets must pass quality cuts and taggability requirements, each event must pass the $h^0 b\bar{b}$ trigger and have a primary vertex within $\pm$ 35 cm.

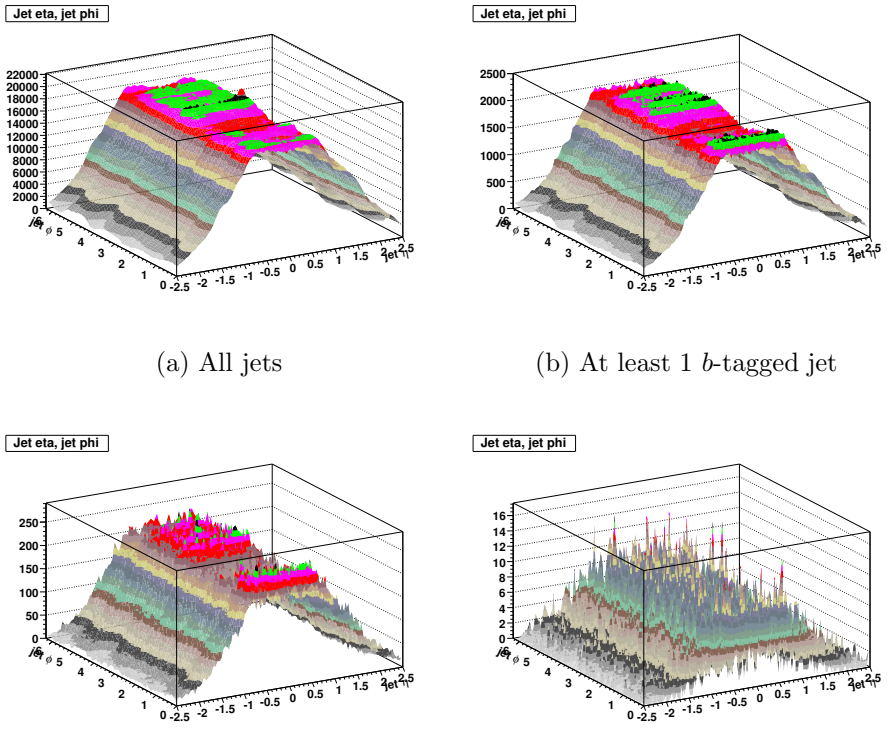


(a) All jets

(b) At least 1 $b$-tagged jet

(c) At least 2 $b$-tagged jets

(d) At least 3 $b$-tagged jets

Figure 3: The $\eta - \phi$ distributions of jets in events with 0 and at least 1, 2 or 3 tight NN $b$-tags.

# 3 Monte Carlo samples

The Monte Carlo samples used in this analysis are listed in table 2.

| $M_h$( GeV/$c^2$) | Number of events | request ids |
|---|---|---|
| 90 | 150000 | 88672 |
| 100 | 300000 | 88673, 88689 |
| 110 | 300000 | 88652, 88654 |
| 120 | 300000 | 88674, 88690 |
| 130 | 300000 | 88675, 88691 |
| 140 | 300000 | 88676, 88692 |
| 150 | 300000 | 88677, 88693 |
| 160 | 300000 | 88678, 88694 |
| 170 | 300000 | 88679, 88695 |
| 180 | 150000 | 88653 |
| 190 | 300000 | 88680, 88696 |
| 200 | 300000 | 88681, 88697 |
| 210 | 150000 | 88682 |
| 220 | 300000 | 88683, 88699 |
| 230 | 300000 | 88684, 88700 |
| 240 | 300000 | 88685, 88701 |
| 250 | 300000 | 88686, 88702 |
| 260 | 300000 | 88687, 88703 |

| Backgrounds | Number of events | request ids |
|---|---|---|
| $b\bar{b}j$ exclusive | 1000000 | 88493, 88494, 88495, 88496, 88497 |
| $b\bar{b}jj$ inclusive | 1000000 | 88472, 88473, 88474, 88475, 88476 |
| $b\bar{b}b\bar{b}$ inclusive | 2000000 | 86852, 86853, 86854, 86855, 86856 |
| $c\bar{c}j$ exclusive | 200000 | 88498 |
| $c\bar{c}jj$ inclusive | 200000 | 88492 |
| $b\bar{b}c\bar{c}$ inclusive | 1248000 | 87414, 87415, 87416, 87417, 87418, 87419 |

Table 2: The number of events simulated for each signal and background process. Currently we are only using signal events up to $m_H = 220$ GeV.

Signal and background events were generated using the p20.09.02/03 simulation chain, including zero bias event overlay, followed by the production of CAF Trees [5]. The CAFTrees were then processed through the higgs_hb package in p21.11.00 with

the recommended version of p20 JES being applied. At the generator level, Pythia [6] or ALPGEN [7] were run with the parton distribution function (PDF) set CTEQ6L1.

## 3.1 *hb* signal simulation

As the main difference between the MSSM Higgs bosons and the SM Higgs boson is the enhanced production cross-section, the $hb$ signal was simulated with the Monte Carlo program Pythia using its process $gb \to hb$ [6]. However, this simulates only the leading order production corrected by initial and final state radiation (ISR and FSR). As the process $gb \to hb$ has been calculated at the next-to-leading order [8, 9], this simulation needs to be corrected. MCFM [10] was used to compute the required corrections. The details of this procedure and the corrections can be found in section 2.2.1 of [1]. The experimental acceptance of the simulated events was also corrected by weighting each simulated signal event according to the kinematic parameters $(p_T, \eta)$ of the leading $b$-jet which is not from the decay of the Higgs. The same procedure as for the p17 analysis was used again.

## 3.2 Background simulation

The main backgrounds for high multiplicity final states with 3 b-tagged jets arise from QCD multi-jet production processes ($j$ stands for light parton):

1. $p\bar{p} \to jjj(j)$
2. $p\bar{p} \to bjj(j)$
3. $p\bar{p} \to b\bar{b}j(j)$
4. $p\bar{p} \to b\bar{b}b(b)$

The first process is difficult to simulate given the number of diagrams contributing to the final state. The processes with $b$-quark production were simulated with ALPGEN [7], based on LO matrix elements. A summary of the cross-sections obtained with ALPGEN, as well as the kinematic cuts, is given in table 3. The larger cross section for the $b\bar{b}c\bar{c}$ sample compared to the p17 analysis is due to the 5 GeV/$c$ lower $p_T(b)$ cut in p20.

## 3.3 Corrections to full simulation

To account for the discrepancies between Monte Carlo and data the corrections listed below were applied. These are fundamentally the same corrections which were applied during the p17 analysis, but the actual functions were updated for the p20 analysis.

- The $b$-tagging [11] rate (ICHEP08) and taggability of jets which were derived from data (see [12] for a description of the method) were applied as weight factors to the simulated events. Details of the taggability can be found in appendix E.

| Process | Cross-section (pb) | Generator cuts ($p_T$ in GeV/$c$) |
|---|---|---|
| $c\bar{c}jj$ inclusive | 5499 | $p_T(j) > 15$, $p_T(c) > 20$ , $\|\eta\| < 3$, $\Delta R < 0.4$ |
| $c\bar{c}j$ exclusive | 8187 | $p_T(j) > 15$, $p_T(c) > 20$ , $\|\eta\| < 3$, $\Delta R < 0.4$ |
| $b\bar{b}jj$ inclusive | 4710 | $p_T(j) > 15$, $p_T(b) > 20$ , $\|\eta\| < 3$, $\Delta R < 0.4$ |
| $b\bar{b}j$ exclusive | 7855 | $p_T(j) > 15$, $p_T(b) > 20$ , $\|\eta\| < 3$, $\Delta R < 0.4$ |
| $b\bar{b}b\bar{b}$ inclusive | 213 | 2 b's with $p_T(b) > 20$ , 3b's with $p_T(b) > 15$ |
| $b\bar{b}c\bar{c}$ inclusive | 630 | 2 b's with $p_T(b) > 20$ , 3b/c's with $p_T(b/c) > 15$ |

Table 3: Cross-section for the generated background events. "X exclusive" means exactly "X" in the final state. "X inclusive" means "X" plus an arbitrary number of extra light jets in the final state.

- JSSR (Jet Smeared Shift and Removed) was used to correct for jet-id efficiency, jet energy scale and resolution [13].
- Skimming cuts were simulated using the jetcorr package.
- Full trigger efficiencies have been measured and were simulated using the higgs_hb package, see appendix A for full details.
- The luminosity profiles of the MC samples were reweighted to agree with the profile from data. Details can be found in appendix F.

# 4 Analysis overview

This section describes the event selection, likelihood discriminant and background modeling in the analysis.

## 4.1 Event selection

The event selection cuts were largely equivalent to the cuts used in the p17 analysis.

- The event was required to have fired the $h^0 b\bar{b}$ trigger.
- Events had to pass a primary vertex cut of $|z_{\text{vtx}}| < 35$ cm.
- Between 3 and 5 good, taggable jets with JES corrected $p_T > 20\,\text{GeV}/c$ within $|\eta| < 2.5$ were required.
- At least 2 of these jets with $p_T > 25\,\text{GeV}/c$ were required to pass a tight NN $b$-tag criteria.
- At least one additional tight NN $b$-tagged jet was required.

| | Number of events | Fraction relative to previous level |
|---|---|---|
| Events in 3JET skim (v15) | 121,457,747 | - |
| Pass hbb trigger | 51,973,882 | 0.428 |
| Pass z vertex cut | 51,690,017 | 0.995 |
| 3/4/5 good taggable jets | 26,606,009/6,558,214/876,572 | 0.515/0.127/0.017 |
| 2 NN tight $b$-tag jets ($p_T > 25\,\mathrm{GeV}/c$) | 211,177/72,127/12,473 | 0.008/0.011/0.014 |
| 3 NN tight $b$-tag jets | 4,668/3,387/848 | 0.022/0.047/0.068 |

Table 4: The number of events and relative fraction of events in data passing each cut. As we later split the data into 3-, 4- and 5 jet sub-samples, these numbers are reported separately in the last 3 rows.

The data were split into separate 3, 4 and 5 jet channels for the analysis. A jet is only counted if it is taggable and its $p_T$ is $> 20$ GeV/$c$ and its $|\eta| < 2.5$. Table 4 shows the number of events in data at different levels of the event selection. For all events in the selected sample the two leading jet pairs (i.e. jet 1 and 2, and jet 1 and 3) were considered as possible Higgs candidates. The $\Delta R$ for each such jet pairing must be $> 1.0$, to remove jet pairs from gluon splitting.
The acceptance for MC signal events generated at masses of 100, 150 and 190 GeV is reported in tables 5, 6 and 7. The numbers of events in these tables correspond to the SM cross section normalized to the actual luminosity and assuming 100% branching fraction to $b\bar{b}$.

| | Number of events | Fraction relative to previous level | Fraction relative to total |
|---|---|---|---|
| Initial number | 16.5528 | | |
| pass z vertex cut | 13.8148 | 0.835 | 0.8346 |
| 3-5 good taggable jets | 2.0023 | 0.145 | 0.1210 |
| pass skimming cuts | 1.4157 | 0.707 | 0.0855 |
| pass trigger | 0.4115 | 0.291 | 0.0249 |
| pass 2 NN tight $b$-tag ($p_T > 25$) | 0.1738 | 0.422 | 0.0105 |
| pass 3 NN tight $b$-tag | 0.0444 | 0.255 | 0.0027 |
| in separate channels: | | | |
| 3-jets | 0.0274 | 0.619 | 0.0017 |
| 4-jets | 0.0144 | 0.325 | 0.0009 |
| 5-jets | 0.0025 | 0.057 | 0.0002 |

Table 5: For $m_A = 100$ GeV the number of events, and relative and total fraction of signal events passing each cut.

| | Number of events | Fraction relative to previous level | Fraction relative to total |
|---|---|---|---|
| Initial number | 2.8418 | | |
| pass z vertex cut | 2.3659 | 0.833 | 0.8325 |
| 3-5 good taggable jets | 0.6097 | 0.258 | 0.2146 |
| pass skimming cuts | 0.4909 | 0.805 | 0.1727 |
| pass trigger | 0.2531 | 0.516 | 0.0891 |
| pass 2 NN tight $b$-tag ($p_T > 25$) | 0.1032 | 0.408 | 0.0363 |
| pass 3 NN tight $b$-tag | 0.0244 | 0.237 | 0.0086 |
| in separate channels: | | | |
| 3-jets | 0.0162 | 0.663 | 0.0057 |
| 4-jets | 0.0069 | 0.284 | 0.0024 |
| 5-jets | 0.0013 | 0.053 | 0.0005 |

Table 6: For $m_A = 150$ GeV the number of events, and relative and total fraction of signal events passing each cut.

| | Number of events | Fraction relative to previous level | Fraction relative to total |
|---|---|---|---|
| Initial number | 0.8749 | | |
| pass z vertex cut | 0.7287 | 0.833 | 0.8330 |
| 3-5 good taggable jets | 0.2673 | 0.367 | 0.3056 |
| pass skimming cuts | 0.2279 | 0.852 | 0.2605 |
| pass trigger | 0.1482 | 0.650 | 0.1694 |
| pass 2 NN tight $b$-tag ($p_T > 25$) | 0.0581 | 0.392 | 0.0664 |
| pass 3 NN tight $b$-tag | 0.0131 | 0.225 | 0.0150 |
| in separate channels: | | | |
| 3-jets | 0.0086 | 0.655 | 0.0098 |
| 4-jets | 0.0038 | 0.292 | 0.0044 |
| 5-jets | 0.0007 | 0.053 | 0.0008 |

Table 7: For $m_A = 190$ GeV the number of events, and relative and total fraction of signal events passing each cut.

#### 4.1.1 Signal efficiency loss

There has been a notable loss in signal efficiency between the p17 and p20 analysis. This loss is up to 47% at 100 GeV and 18% at 190 GeV. The vast majority of this loss in signal efficiency can be attributed to the much tighter trigger requirements in the L1 trigger. Tables 8 - 10 show the predicted p17 and p20 trigger efficiencies on

the 100, 150 and 190 GeV p20 MC signal samples respectively. There is a notable loss in signal efficiency between the p17 and p20 trigger which ranges from 35% at 100 GeV to 15% at 190 GeV.

| Version | Level 1 | Level 2 | Level 3 | Total |
|---|---|---|---|---|
| p17 | 0.869 | 0.833 | 0.504 | 0.435 |
| p20 | 0.538 | 0.777 | 0.407 | 0.283 |

Table 8: The predicted p17 and p20 trigger efficiencies on the $m_A = 100$ GeV signal sample.

| Version | Level 1 | Level 2 | Level 3 | Total |
|---|---|---|---|---|
| p17 | 0.947 | 0.919 | 0.723 | 0.672 |
| p20 | 0.759 | 0.892 | 0.644 | 0.532 |

Table 9: The predicted p17 and p20 trigger efficiencies on the $m_A = 150$ GeV signal sample.

| Version | Level 1 | Level 2 | Level 3 | Total |
|---|---|---|---|---|
| p17 | 0.971 | 0.951 | 0.82 | 0.786 |
| p20 | 0.846 | 0.94 | 0.762 | 0.67 |

Table 10: The predicted p17 and p20 trigger efficiencies on the $m_A = 190$ GeV signal sample.

## 4.2 Sample composition

The technique to derive the sample composition is described in detail in the p17 analysis note [1]. To first order the sample composition is derived on the 3 jet sample considering the following backgrounds: $jjj$, $cjj$, $cjj$, $ccc$, $bjj$, $bbj$, $bcc$, $bbc$, $bbb$. The fraction of each component is measured in bins of $H_T = \sum_{jets} p_T$ by comparing the MC samples to data, taking into account the $b$-tagging efficiency and the cross-section of each process. To limit the number of unknown variables a number of assumptions based on p17 studies have been made:

- $x_{bjj} = x_{cjj}$ and $x_{bbj} = x_{ccj}$ for events with $H_T > 50$ GeV.
- $x_{bcc} = x_{bbc} = x_{bbb}$. From Alpgen.
- $x_{ccc}$ is negligible.

With updates to the MC generators, triggers and the introduction of Layer 0 we expect the sample composition in RunIIb to differ from RunIIa. The results for RunIIb are shown in Figs. 4, 5, 6 and 7 for the three jet channel and in Figs. 8, 9, 10 and 11 for the four jet channel.

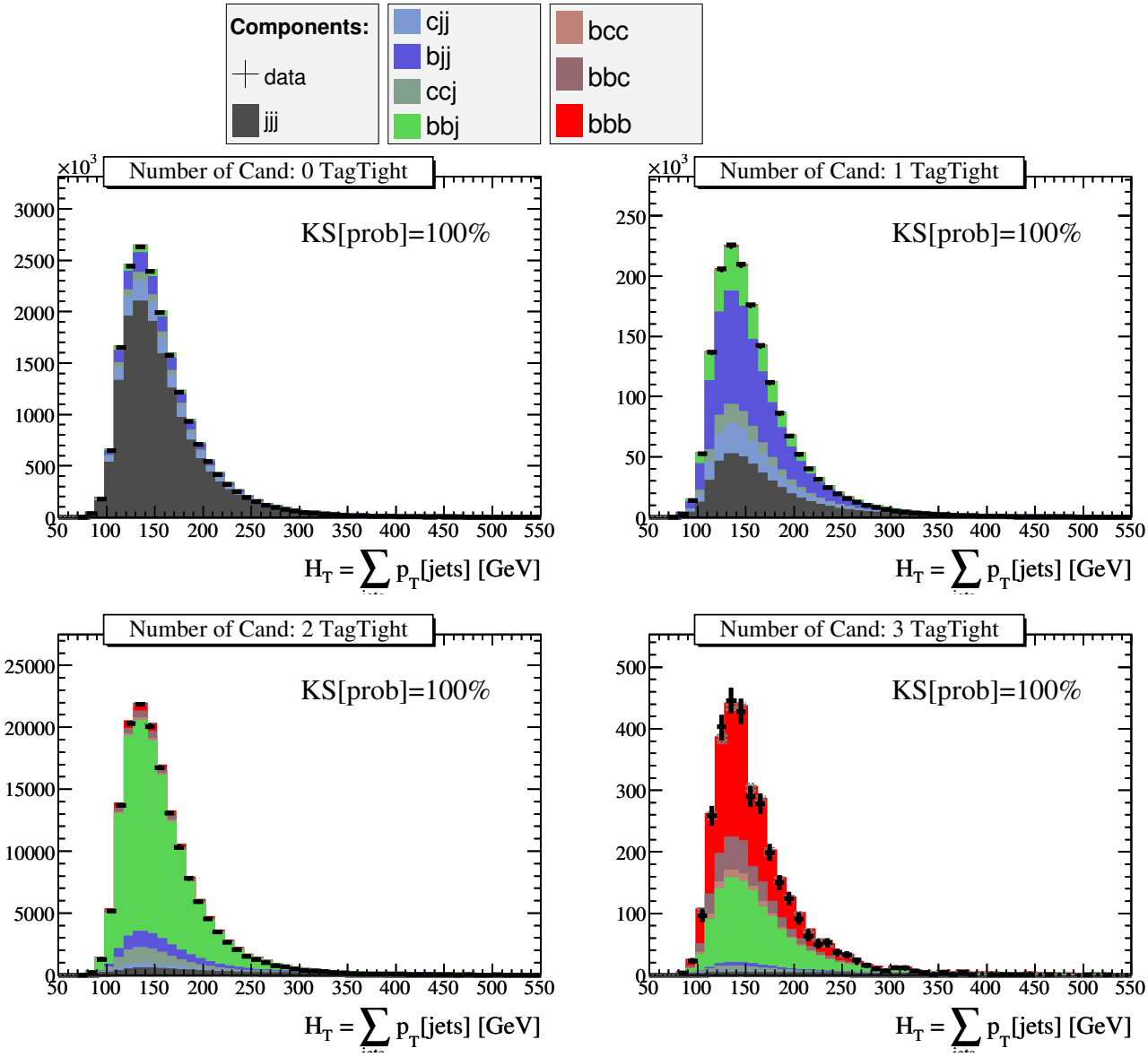


Figure 4: Composition of zero to three $b$-tagged three jet data samples. Numerical values for the each of the $b$-tagged samples are shown in table 11.

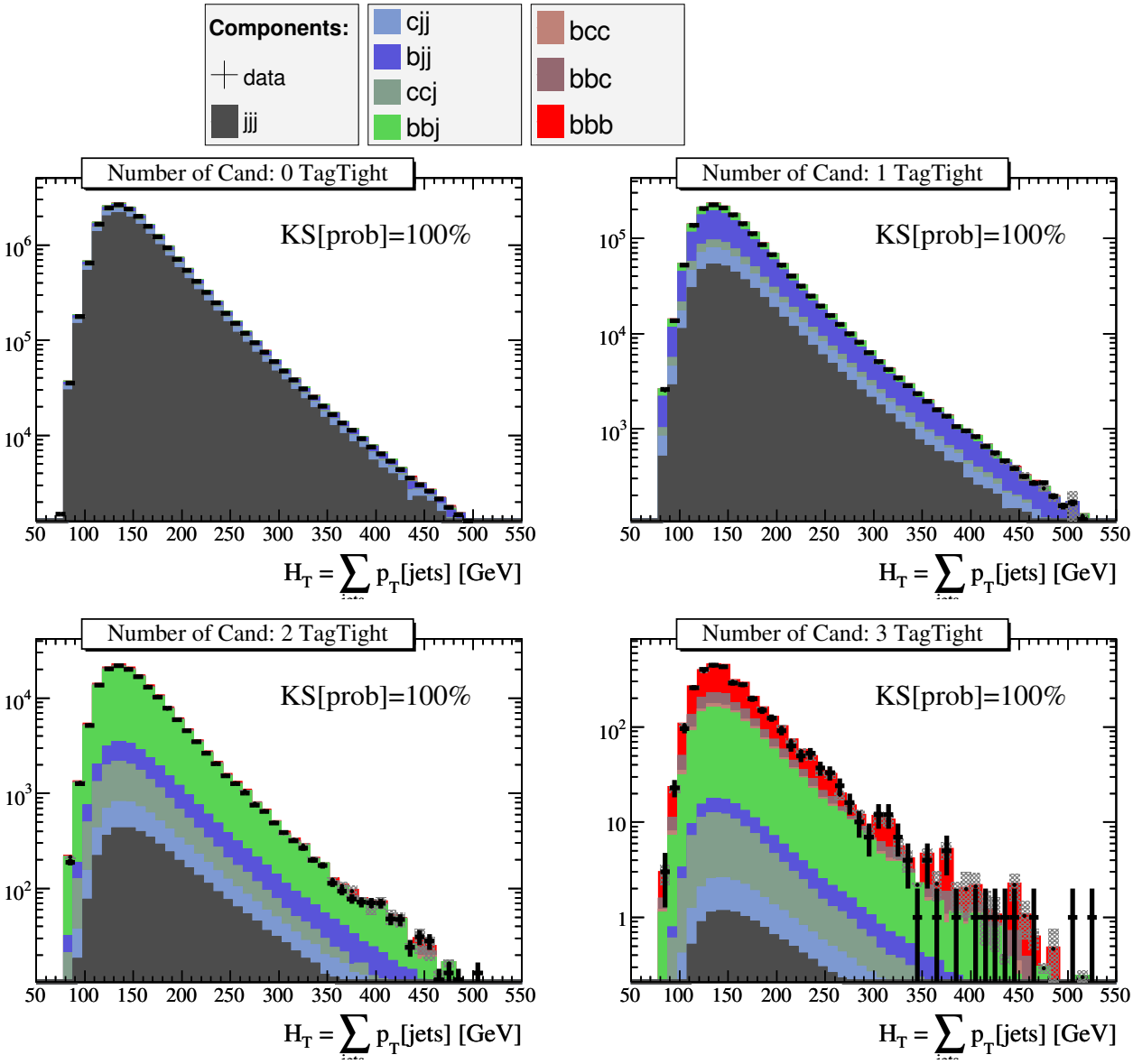


Figure 5: Composition of zero to three $b$-tagged three jet data samples on a logarithmic scale. Numerical values for the each of the $b$-tagged samples are shown in table 11.

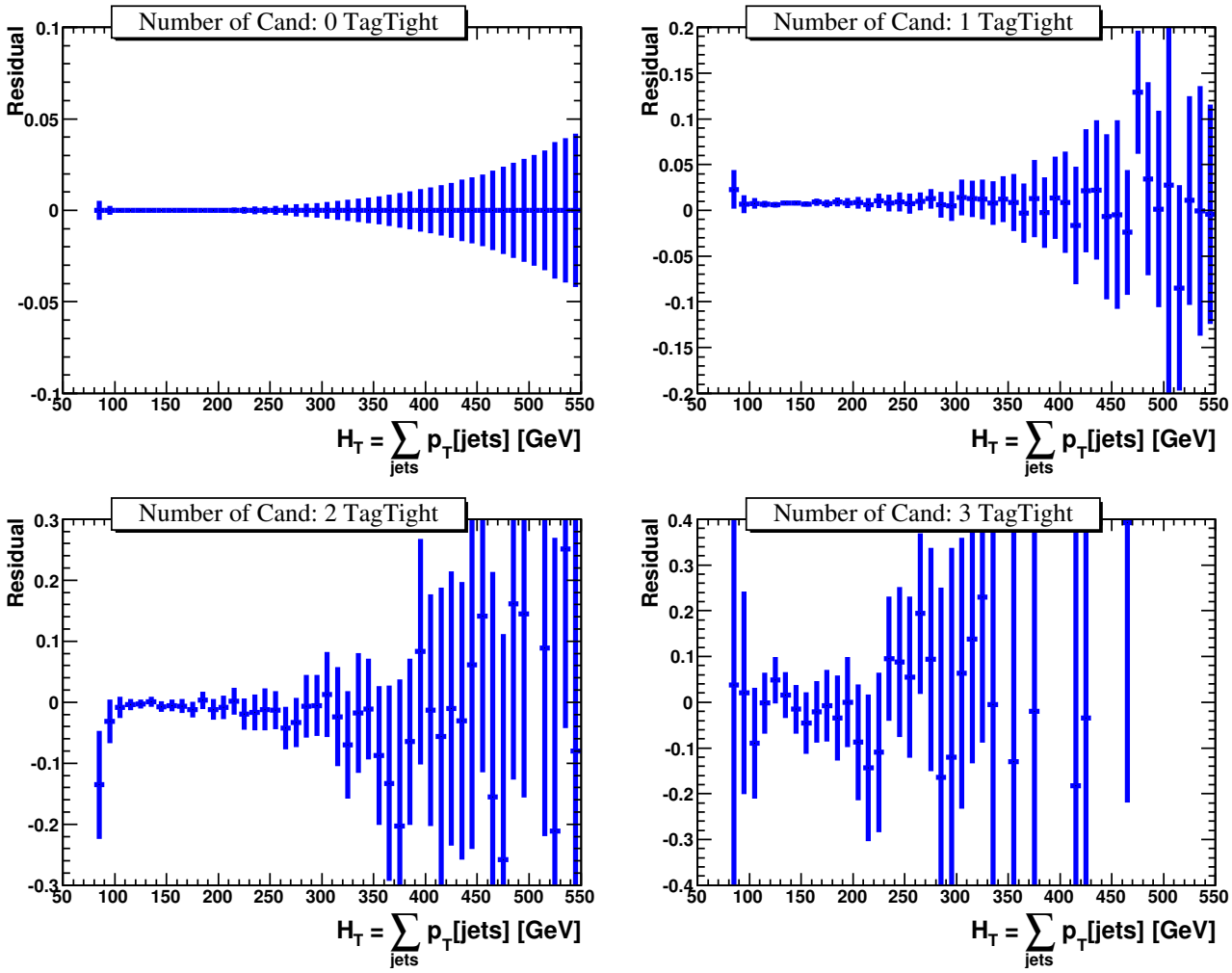


Figure 6: Residuals between data and fitted MC background for the zero to three $b$-tagged three jet data samples.

| Process | Composition % | | | |
|---|---|---|---|---|
| | 0 Tag | 1 Tag | 2 Tag | 3 Tag |
| $jjj + cjj + bjj$ | 94.1 | 76.7 | 11.1 | 2.3 |
| $ccj$ | 3.0 | 6.9 | 5.8 | 2.4 |
| $bbj$ | 2.7 | 15.3 | 76.9 | 34.6 |
| $bbc + bcc$ | 0.2 | 0.8 | 3.2 | 14.0 |
| $bbb$ | 0.1 | 0.3 | 3.0 | 46.7 |

Table 11: Contributions of different background processes to the 0, 1, 2 and 3 tagged samples in the 3-jet channel.

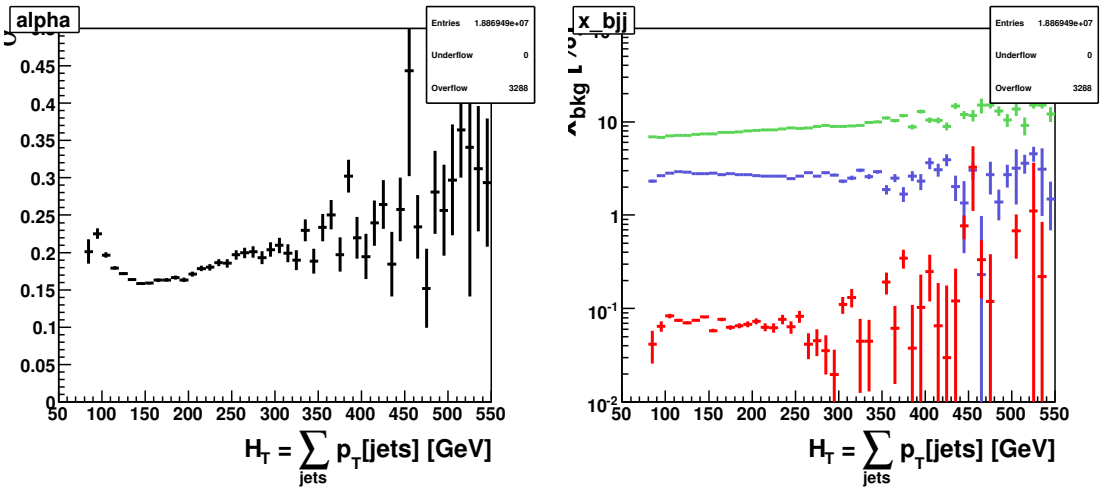


Figure 7: Left plot: To first order the parameter $\alpha$ represents a correction to the mis-tag rate, i.e. the mis-tag rate in this particular sample is $\sim 20\%$ higher than in the $b$-id sample. Right plot: The contributions of the different backgrounds $x_{bjj}$ (top), $x_{bbj}$ (middle), $x_{bbb}$ (bottom) vs $H_T$ in the three jet channel.

| Process | Composition % | | | |
|---|---|---|---|---|
| | 0 Tag | 1 Tag | 2 Tag | 3 Tag |
| $jjj + cjj + bjj$ | 90.5 | 68.6 | 10.0 | 1.9 |
| $ccj$ | 4.8 | 9.5 | 6.3 | 2.4 |
| $bbj$ | 4.4 | 20.7 | 77.3 | 33.3 |
| $bbc + bcc$ | 0.2 | 0.9 | 3.5 | 17.6 |
| $bbb$ | 0.1 | 0.3 | 2.9 | 44.8 |

Table 12: Contributions of different background processes to the 0, 1, 2 and 3 tagged samples in the 4-jet channel.

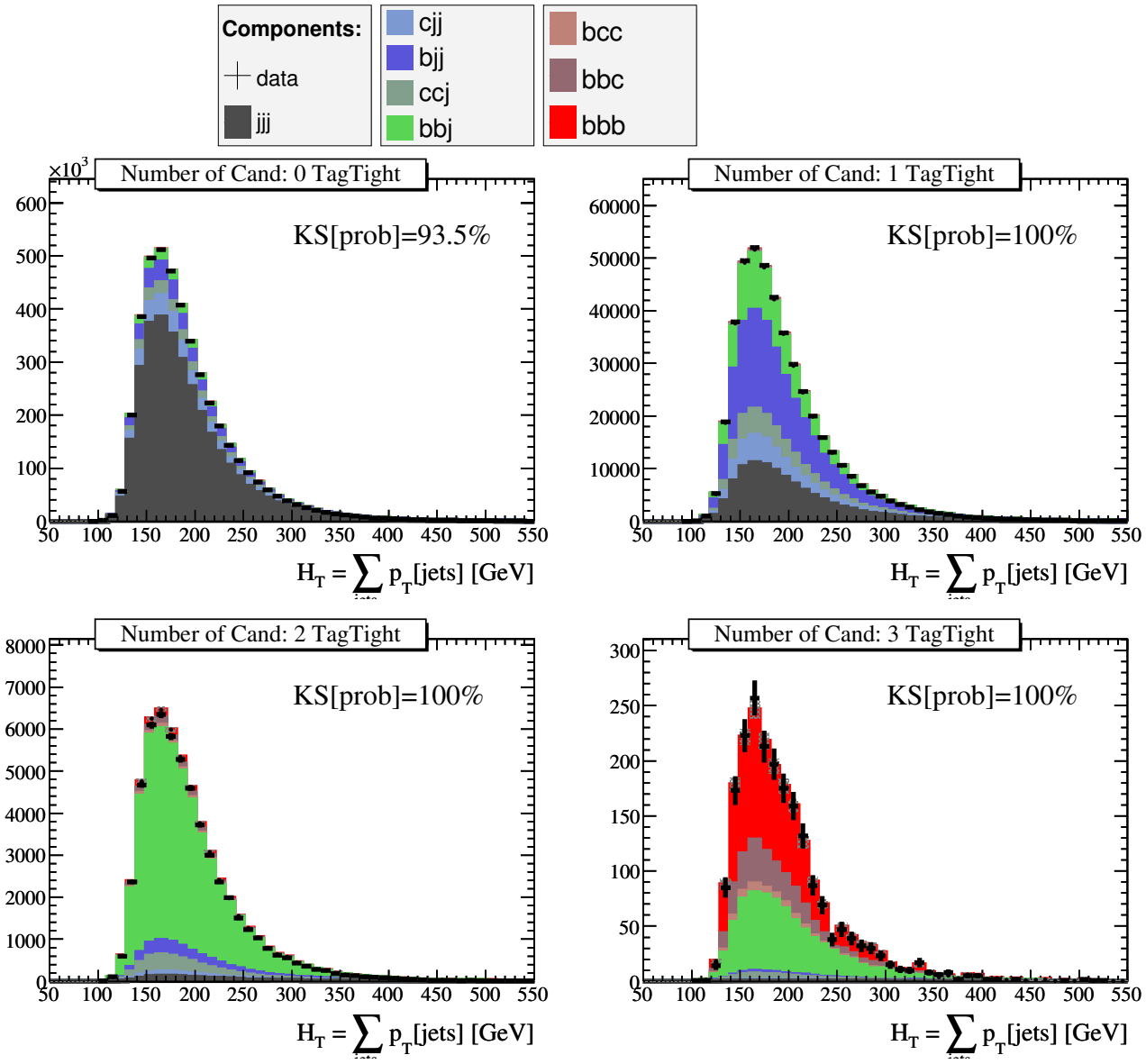


Figure 8: Composition of zero to three $b$-tagged four jet data samples. Numerical values for the each of the $b$-tagged samples are shown in table 12.

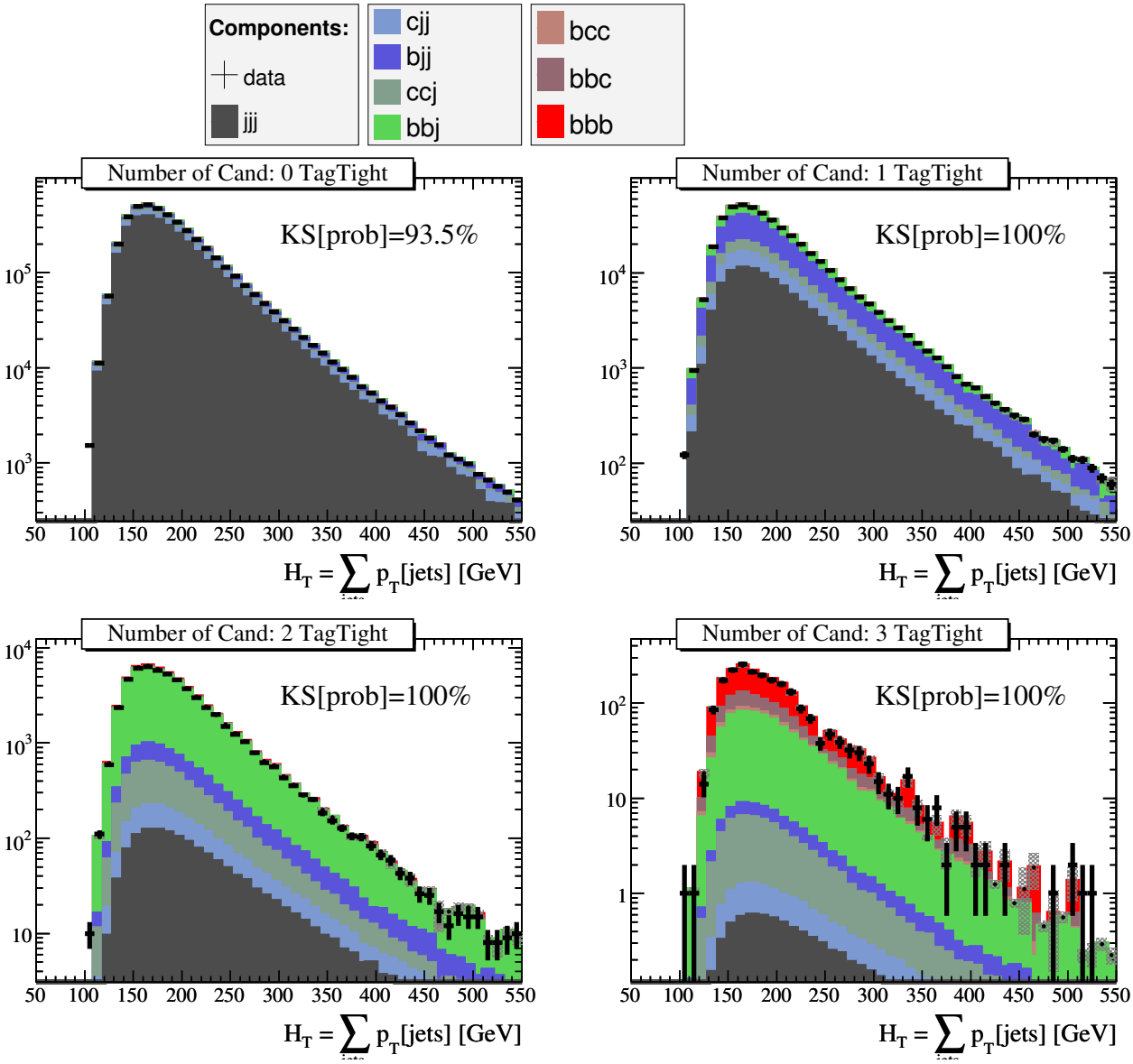


Figure 9: Composition of zero to three $b$-tagged four jet data samples on a logarithmic scale. Numerical values for the each of the $b$-tagged samples are shown in table 12.

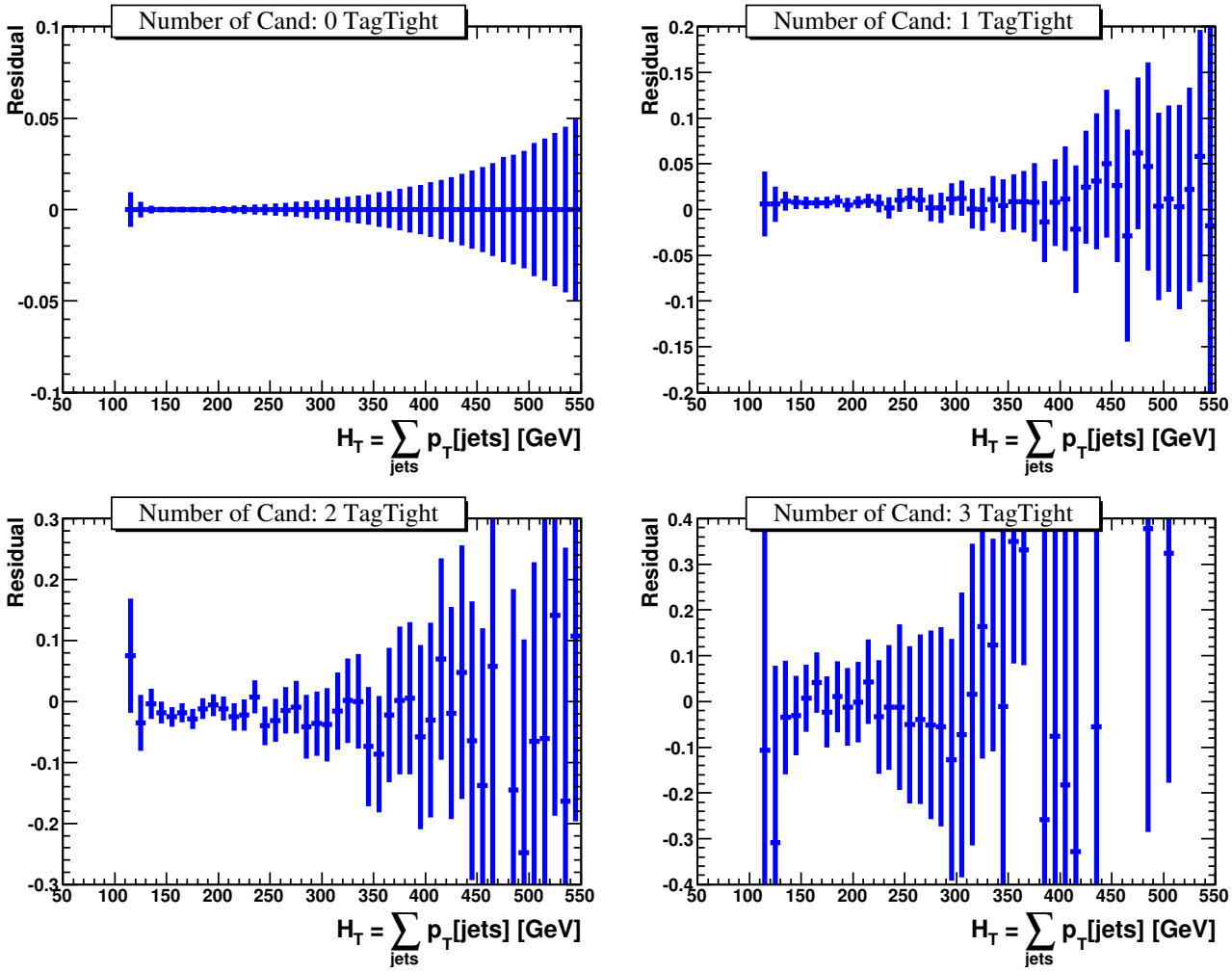


Figure 10: Residuals between data and fitted MC background for the zero to three $b$-tagged four jet data samples.

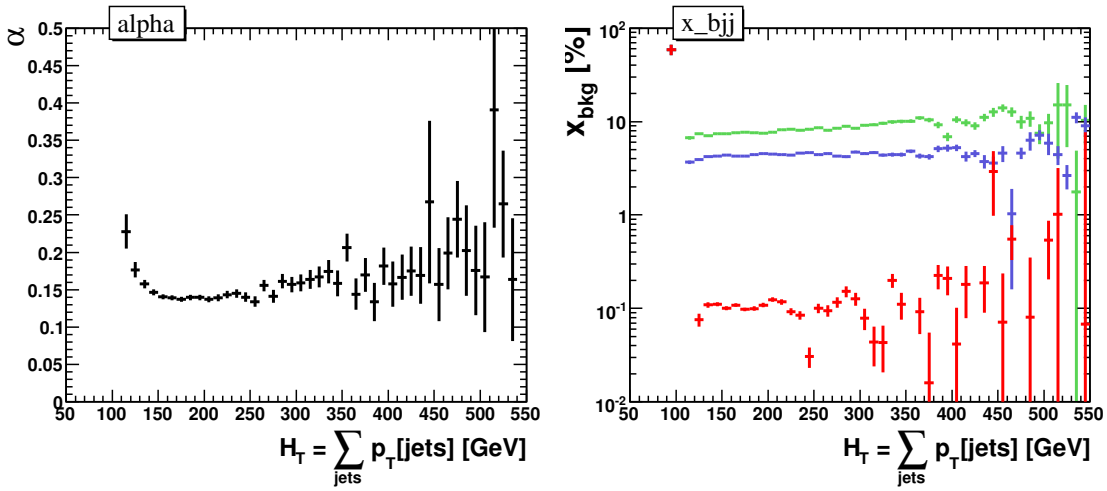


Figure 11: Left plot: To first order the parameter $\alpha$ represents a correction to the mis-tag rate, i.e. the mis-tag rate in this particular sample is $\sim 15\%$ higher than in the $b$-id sample. Right plot: The contributions of the different backgrounds $x_{bjj}$ (top), $x_{bbj}$ (middle), $x_{bbb}$ (bottom) vs $H_T$ in the four jet channel.

## 4.3 Likelihood discriminant

The calculation of the likelihood discriminant is unchanged with respect to the p17 analysis. For each invariant mass pair with $M_{bb} > 50$ GeV a likelihood between 0 and 1, where 1 indicates signal using the variables in table 13 was determined. The likelihood discriminant $\mathcal{D}$, was calculated according to:

$$\mathcal{D}(x_1, ...., x_6) = \frac{\prod_{i=1}^{6} p_i^{sig}(x_i)}{\prod_{i=1}^{6} p_i^{sig}(x_i) + \prod_{i=1}^{6} p_i^{bkg}(x_i)}, \quad (1)$$

where $p_i^{sig}$ ($p_i^{bkg}$) refers to the signal (background) probability density function (pdf) for variable $x_i$, and $(x_1, ..., x_6)$ is the set of measured kinematic variables for the jet pair. The pdfs were obtained from triple $b$-tagged signal and background simulation. Two likelihoods were built combining simulated samples in the $90-130\,\mathrm{GeV}/c^2$ ("Low-mass") and $130-220\,\mathrm{GeV}/c^2$ ("High-mass") mass ranges, providing discrimination at low and high masses, respectively. Studies from p17 showed that this division of the mass range gave the best discrimination. A cut was then placed on the likelihood discriminant to increase the sensitivity of the analysis. We used the cuts which were optimized for the p17 analysis.

| | |
|---|---|
| $\Delta\ \phi_{b1,b2}$ | Angle in $\phi$ between the two jets in the jet pair. |
| $\Delta\ \eta_{b1,b2}$ | Difference in $\eta$ between the two jets in the jet pair. |
| $Y_h$ | Jet pair rapidity. |
| $\frac{p^{\mathrm{b1}}-p^{\mathrm{b2}}}{p^{\mathrm{b1}}+p^{\mathrm{b2}}}$ | Momentum balance. |
| acos($\mathrm{b_1}$.h) | Angle between leading jet in jet pair and the jet pair itself. |
| Sphericity | Sphericity of the event, calculated using jets with $p_T > 15$ and $\lvert\eta\rvert < 2.5$. |

Table 13: Kinematic variables used in the likelihood.

## 4.4 Background model

Several multijet processes contribute to the background and the uncertainty on the cross sections is large. The *bbb* component may also contain a contribution that is indistinguishable from a signal and cannot be normalized from the data. To model the background we used the same method as in the p17 analysis, which relies on a combination of data and simulation. The distribution of the expected triple $b$-tagged (3Tag) sample in the two-dimensional $\mathcal{D}$ and invariant mass ($M_{bb}$) plane, $S^{exp}_{\mathrm{3Tag}}(\mathcal{D}, M_{bb})$, is obtained from the double $b$-tagged (2Tag) data shape multiplied by the ratio of the simulated (MC) shapes of the triple and double tagged events:

$$S^{exp}_{\mathrm{3Tag}}(\mathcal{D}, M_{bb}) = \frac{S^{MC}_{\mathrm{3Tag}}(\mathcal{D}, M_{bb})}{S^{MC}_{\mathrm{2Tag}}(\mathcal{D}, M_{bb})} S^{data}_{\mathrm{2Tag}}(\mathcal{D}, M_{bb}). \quad (2)$$

Many uncertainties affecting the simulation cancel in the ratio $\frac{S^{MC}_{3\text{Tag}}(\mathcal{D},M_{bb})}{S^{MC}_{2\text{Tag}}(\mathcal{D},M_{bb})}$. The 2D $(M_{bb},\mathcal{D})$ histograms for data, background model and signal MC after 3 $b$-tags are used as inputs to the `collie` limit setting program [3]. The limit setting and the results are discussed in section 6.

## 4.5 Data/Background prediction comparison

Plots 12 -14 show a comparison between data and the predicted background for the 3 jets, 3 $b$-tag channel. The corresponding plots for the 4 and 5 jet channels and for a Higgs mass of 120 GeV can be found in appendix B. Data/MC comparison plots for both the 2 and 3 $b$-tag channels for 120 and 180 GeV Higgs mass points can be found in appendix C. Figure 15 shows the flavour composition of the jet pairs as a function of the dijet mass.

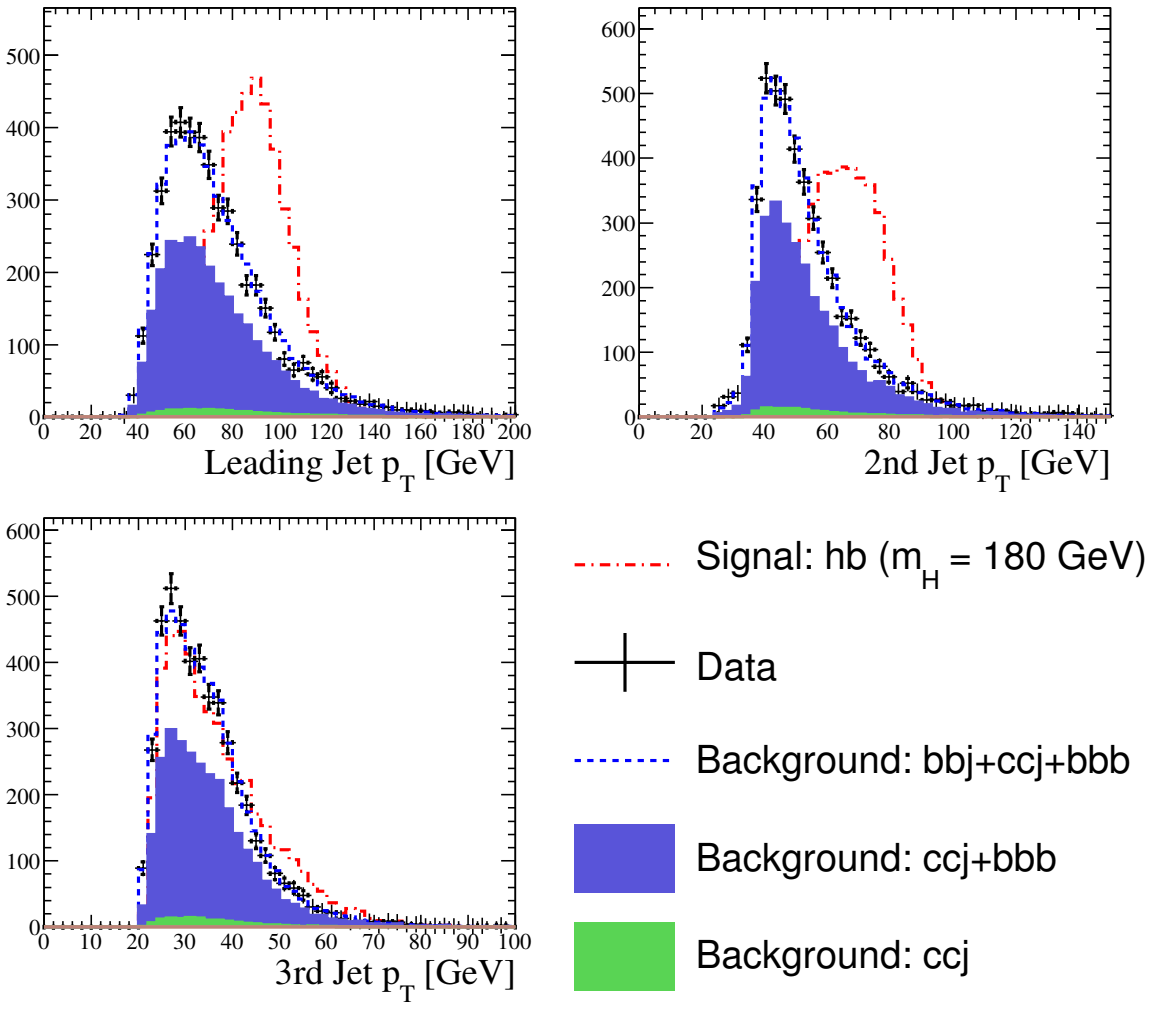


Figure 12: Data predicted background comparison for 3 jets, 3 $b$-tag sample with a 180 GeV Higgs sample used as signal. Shown is the predicted background vs data of the jet $p_T$ for the three jets with the highest $p_T$ in the event.

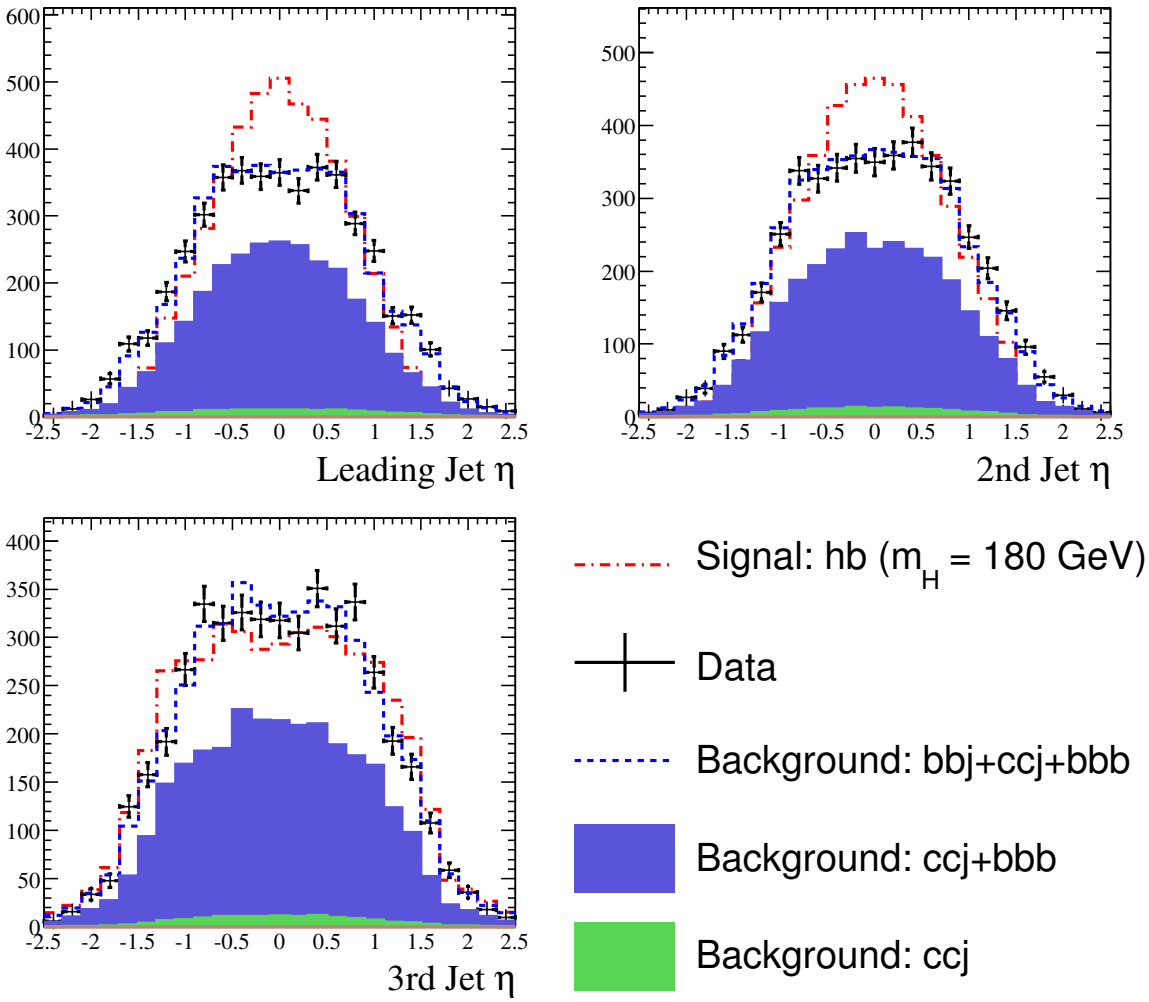


Figure 13: Data predicted background comparison for 3 jets, 3 $b$-tag sample with a 180 GeV Higgs sample used as signal. Shown is the predicted background vs data of the jet $\eta$ for the three jets with the highest $p_T$ in the event.

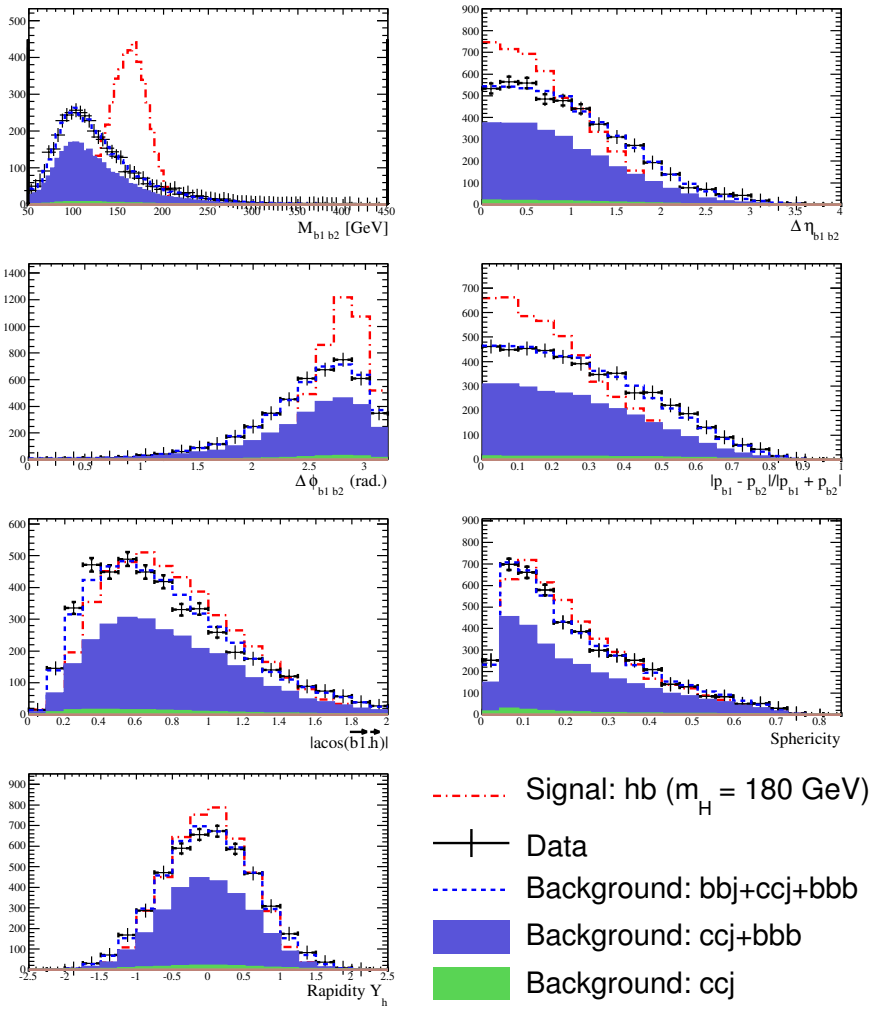


Figure 14: Data predicted background comparison for 3 jets, 3 $b$-tag sample with a 180 GeV Higgs sample used as signal. The figure shows $M_{bb}$ and the six kinematic variables used as input to the likelihood.

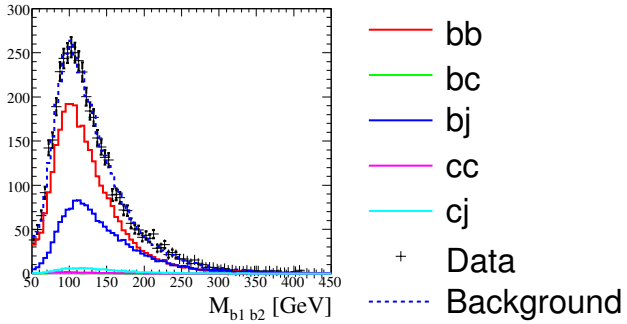


Figure 15: The flavour composition of the jet pairs for the 3 jets, 3 $b$-tag sample as a function of $M_{bb}$.

## 4.6 Likelihood Output Comparison

A Comparison between the 3Tag MC, predicted background and data is shown in Fig. 16 for the low-mass likelihood case and in Fig. 17 for the high-mass likelihood case.

## 4.7 Agreement in the low-likelihood region

The agreement in the low-likelihood region is shown for both the low and high-mass likelihoods in Fig. 18 for the 3Tag/2Tag ratios and in Fig. 19 for the invariant mass distributions.

## 4.8 Agreement in the high-likelihood region

The agreement in the low-likelihood region is shown for both the low and high-mass likelihoods in Fig. 20 for the 3Tag/2Tag ratios and in Fig. 21 for the invariant mass distributions.

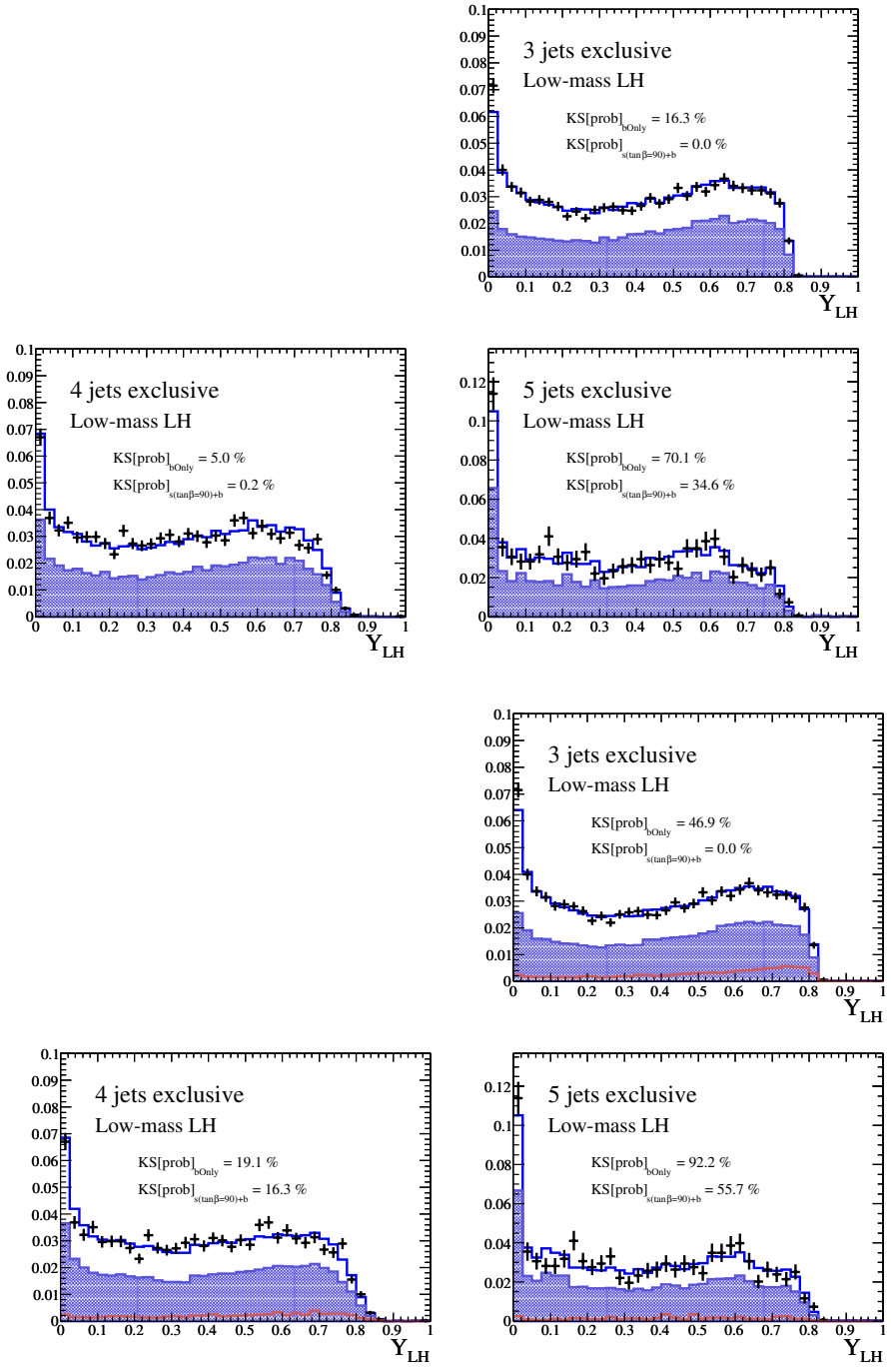


Figure 16: Three top plots: Comparison between 3Tag data and 3Tag MC likelihood distributions (low-mass case). Three bottom plots: Comparison between 3Tag data and 3Tag model (defined by Eq. 2) likelihood distributions (low-mass case). These comparisons are evaluated using a Kolmogorov-Smirnov test with and without the presence of a Higgs signal of 110 GeV/$c^2$ and $tan\beta = 90$. Black points refer to data, the blue histograms to the 3Tag models, the plain blue histograms to the *bbb* background component and the red histograms to a Higgs signal of 110 GeV/$c^2$ and $tan\beta = 90$.

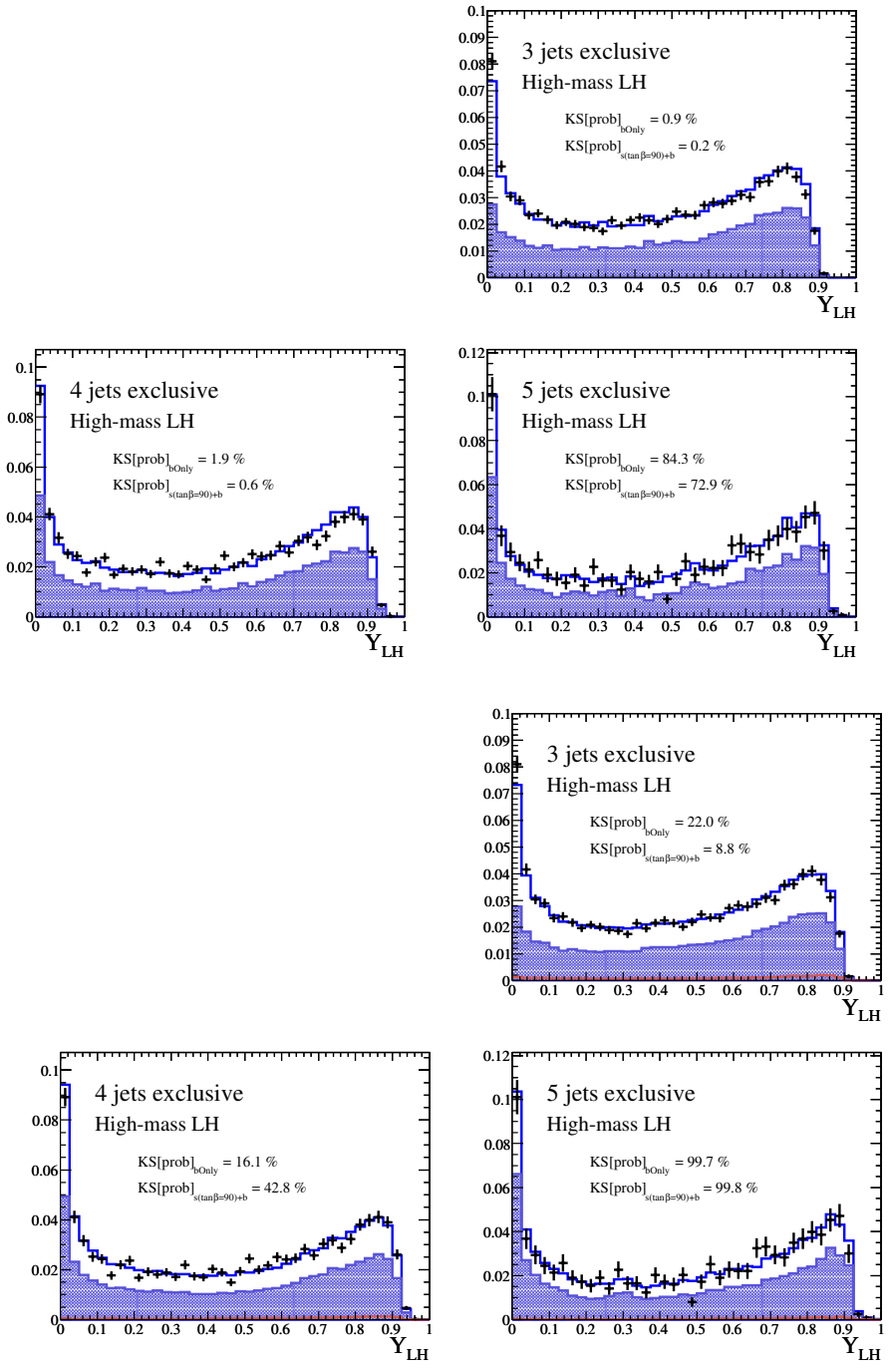


Figure 17: Three top plots: Comparison between 3Tag data and 3Tag MC likelihood distributions (high mass case). Three bottom plots: Comparison between 3Tag data and 3Tag model (defined by Eq. 2) likelihood distributions (high-mass case). These comparisons are evaluated using a Kolmogorov-Smirnov test with and without the presence of a Higgs signal of 180 GeV/$c^2$ and $tan\beta = 90$. Black points refer to data, the blue histograms to 3Tag models, the plain blue histograms to the *bbb* background component and the red histograms to a Higgs signal of 180 GeV/$c^2$ and $tan\beta = 90$.

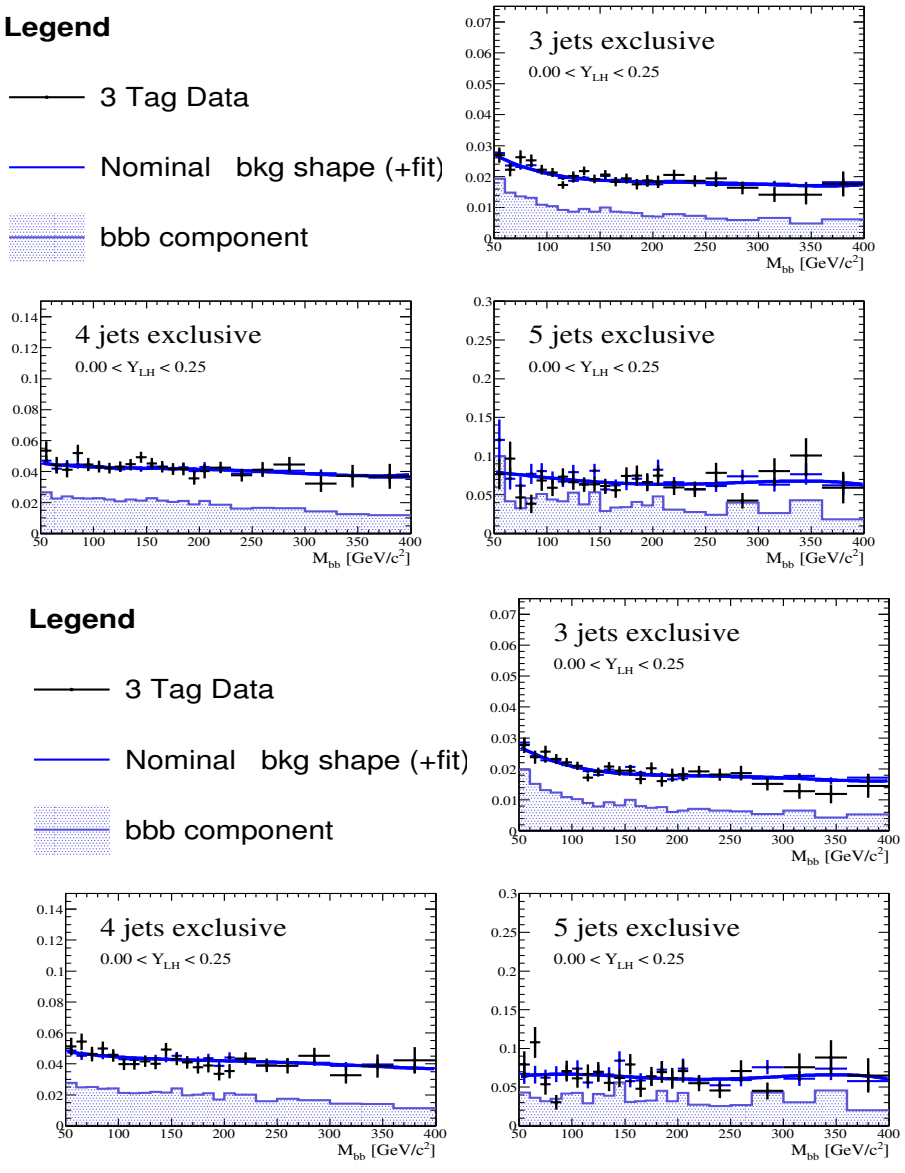


Figure 18: 3Tag/2Tag ratios for the low-likelihood control region using the low-mass likelihood (top plot) and the high-mass likelihood (bottom plot).

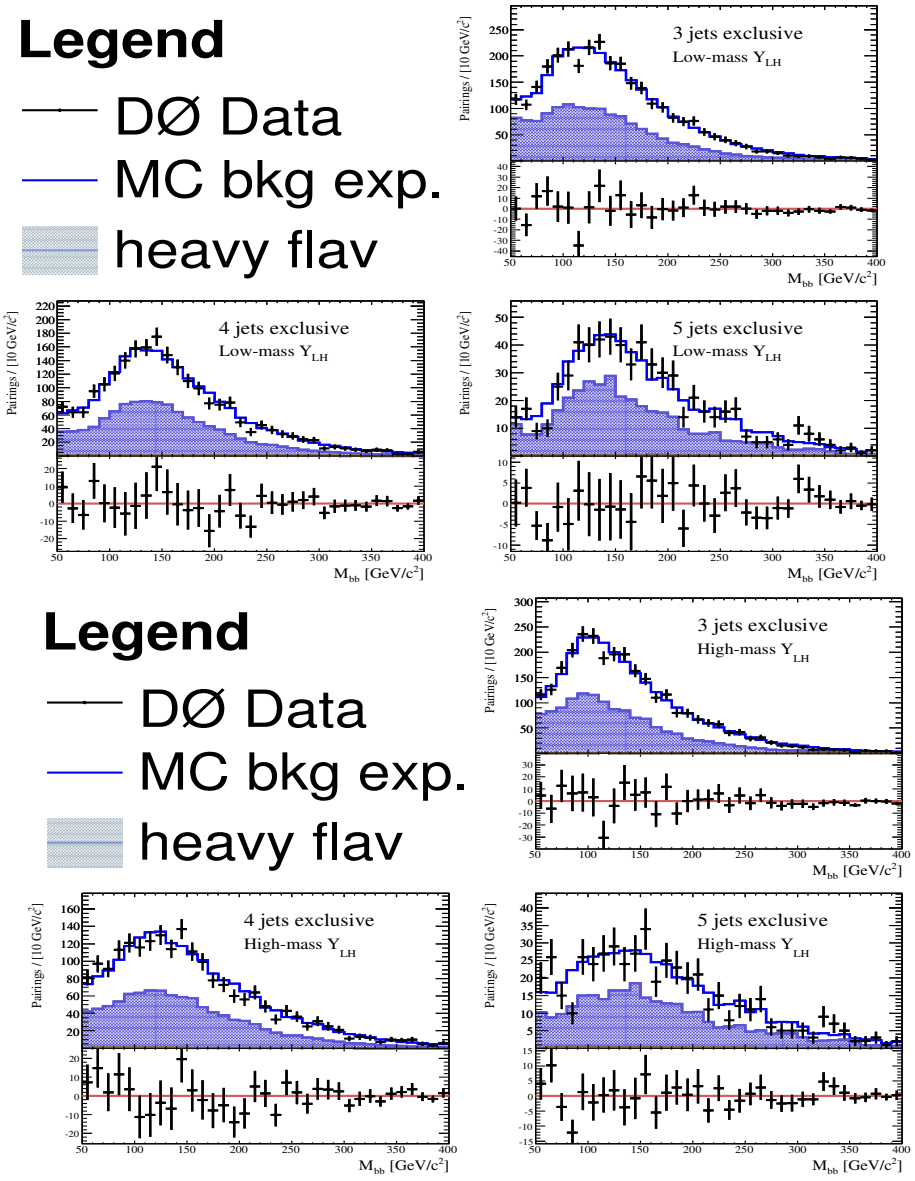


Figure 19: Invariant mass distribution for the low-likelihood control region using the low-mass likelihood (top plot) and the high-mass likelihood (bottom plot).

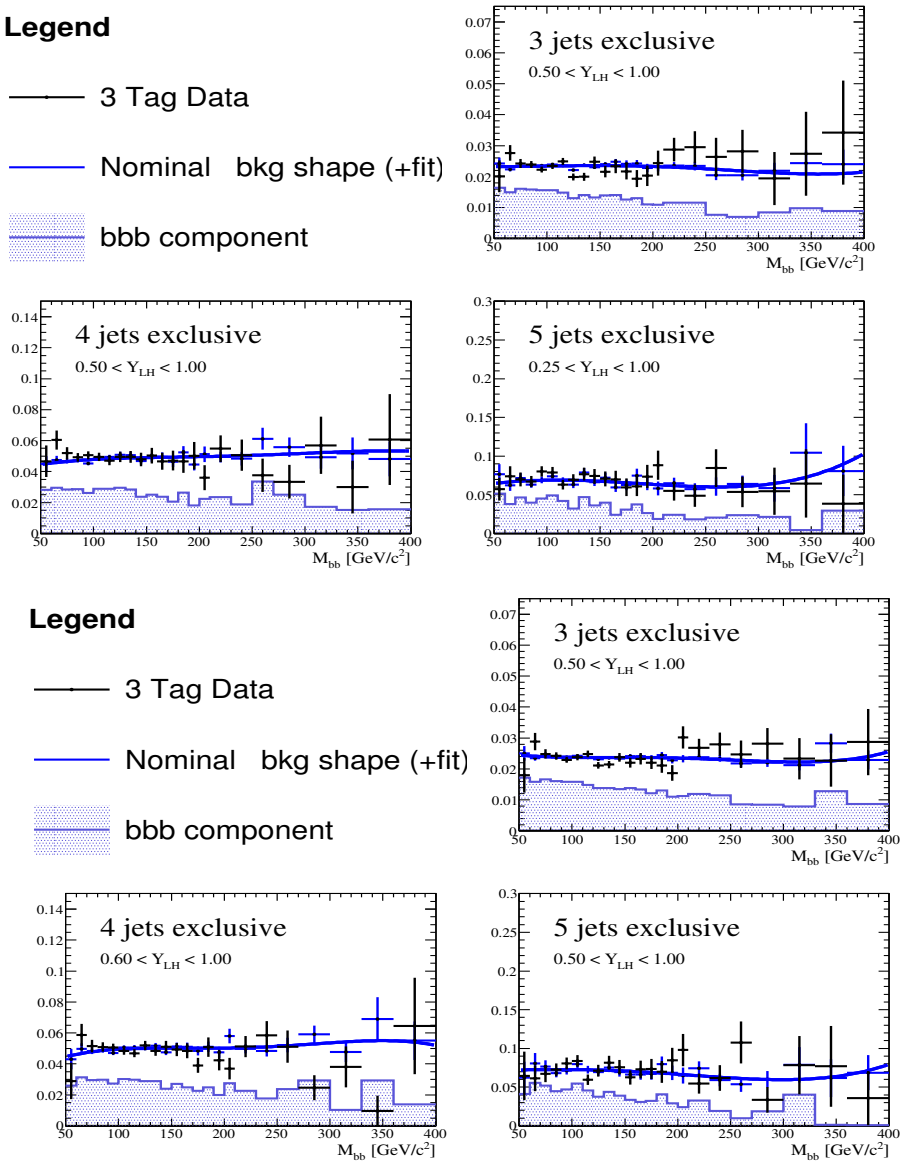


Figure 20: 3Tag/2Tag ratios for the high-likelihood region using the low-mass likelihood (top) and the high-mass likelihood (bottom).

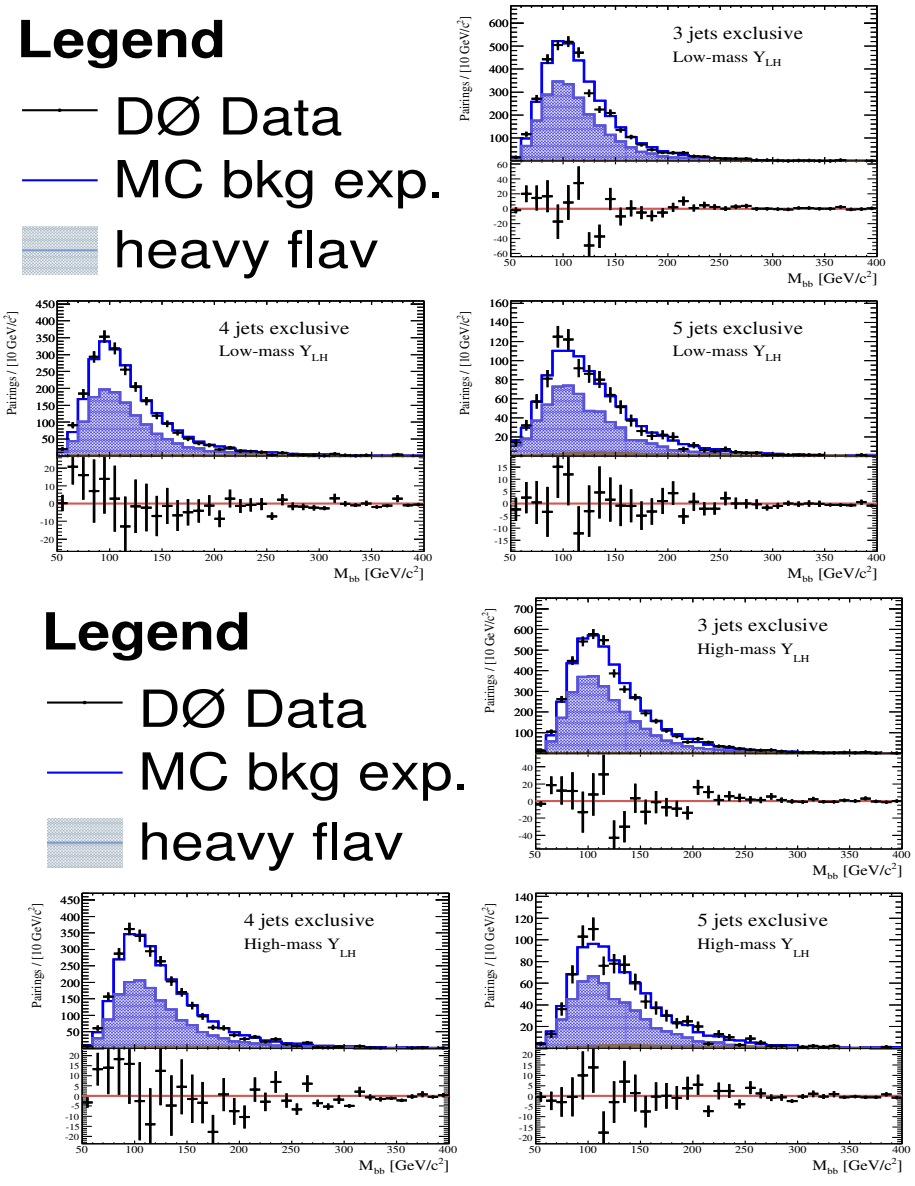


Figure 21: Invariant mass for the high-likelihood region using the low-mass likelihood (top) and the high-mass likelihood (bottom).

# 5 Systematic Uncertainties

The sources of systematic uncertainty are split into two categories: those applying to the estimated signal acceptance and yield, and those affecting the shape of the background model.

## 5.1 Signal Uncertainties

The signal normalisation is assigned a flat systematic uncertainty of 17%. The only variation from the p17 analysis is that the luminosity component has been removed and applied as a separate source of systematic uncertainty. This is to aid in the combination of these results with other analyses (such as $\Phi \rightarrow \tau\tau$) and has no effect on the final result. A detailed breakdown the contributions can be found in the p17 analysis note [14]. The dominant contributions are from theoretical uncertainties (including PDF uncertainties) at the level 12-13%, depending on the mass point; b-ID 8-9% and the luminosity contributes a 6.1% uncertainty.

## 5.2 Background Uncertainties

In the p17 analysis 6 sources of uncertainty on the shape of the background were considered.

- Composition : arising from the quality of the fit in the determination of the background composition.
- b-efficiency : arising from varying the b-tagging TRFs within their errors.
- L3-IP : derived from the modelling of the L3 Impact parameter trigger.
- *b*-res : derived by applying an additional 7% smearing to the *b*- and *c*-jet response in the MC.
- *bbb* : derived by taking half the variation between the pure Monte-Carlo description of the background and that obtained by using the 3/2 ratio as a scale-factor to the 2-tagged data sample.
- *bbj* : derived by comparing the variation in the shape of the contribution from *bbj* like events between two samples derived from the 3/2 ratio from MC applied to the 2-tagged data sample and a sample selected using a negative tag.

While the method for deriving each of these systematics has not changed substantially from the published p17 analysis new values have been derived for the p20 analysis. In the following sections the deviations from the p17 analysis will be briefly described:

### 5.2.1 b-tagging efficiency

In the p17 analysis the efficiency to tag b-jets was varied within the appropriate $1\sigma$ errors in a skewed fashion in order to produce a large and conservative systematic effect. However, in the p20 analysis it has been decided to use a standard non-skewed shifting by $\pm 1\sigma$ since it is believed that the previous method is overly conservative and non-standard when contrasted with other analyses at DØ.

### 5.2.2 Monte-Carlo modelling

The systematic from the p17 analysis described in [1] as either: "*bbb* vs *bbj* kinematics" or "MC-kinematics" has been dropped in the preliminary p20 analysis. It is poorly motivated and is believed to have a large overlap with the composition systematic. Furthermore, it essentially negates most of the benefit expected to arise due to the use of the 3/2-ratio. We have introduced a new systematic to take into account variations in the 3tag-2tag ratio as follows: an alternative background shape, $S_{alt}^{LLHD}(M_{bb})$, is constructed:

$$S_{alt}^{LLHD}(M_{bb}) = \frac{S_{\rm 3Tag}^{DATA-lowLH}(M_{bb})/S_{\rm 2Tag}^{DATA-lowLH}(M_{bb})}{S_{\rm 3Tag}^{MC-lowLH}(M_{bb})/S_{\rm 2Tag}^{MC-lowLH}(M_{bb})} \times S_{bkg}(M_{bb}), \qquad (3)$$

where $S_{\rm 3Tag}^{DATA-lowLH}(M_{bb})$ and $S_{\rm 2Tag}^{DATA-lowLH}(M_{bb})$ are the di-jet invariant mass distributions for data selected with a likelihood discriminant cut of $\mathcal{D} < 0.25$ for the 3-tagged and 2-tagged samples respectively, and $S_{\rm 3Tag}^{MC-lowLH}(M_{bb})$ and $S_{\rm 2Tag}^{MC-lowLH}(M_{bb})$ are the equivalent distributions for the Monte-Carlo background sample. $S_{bkg}(M_{bb})$ is the nominal background distribution.

### 5.2.3 b-tagging fake rate

A systematic uncertainty was assessed in the p17 analysis related to the modelling of the deformation of the shape of the $M_{jj}$ distribution for the *bbj* sample arising from the b-tagging fake rate. At present, in the p20 analysis, this systematic is undergoing further study but has been included when setting limits. The effect is at the few percent level below 200 GeV/$c^2$. In p17 this error was evaluated by comparing data with two *b*-tags and one negative tag to the *bbj* MC. Figure 22 shows the same comparison between the negative tag sample and the *bbj* expectation for p20.

## 5.3 Systematics

The relative contributions of the systematics can be seen for the 3-,4- and 5-jet channels in Figures 23, 24 and 25 respectively.
These uncertainties have been significantly reduced with respect to the previous p17 analysis. In particular, the uncertainty from the composition - which has been reassessed using p20 Monte-Carlo - is approximately 30% smaller. Both the contributions from the b-tagging efficiency and the Level 3 impact parameter trigger

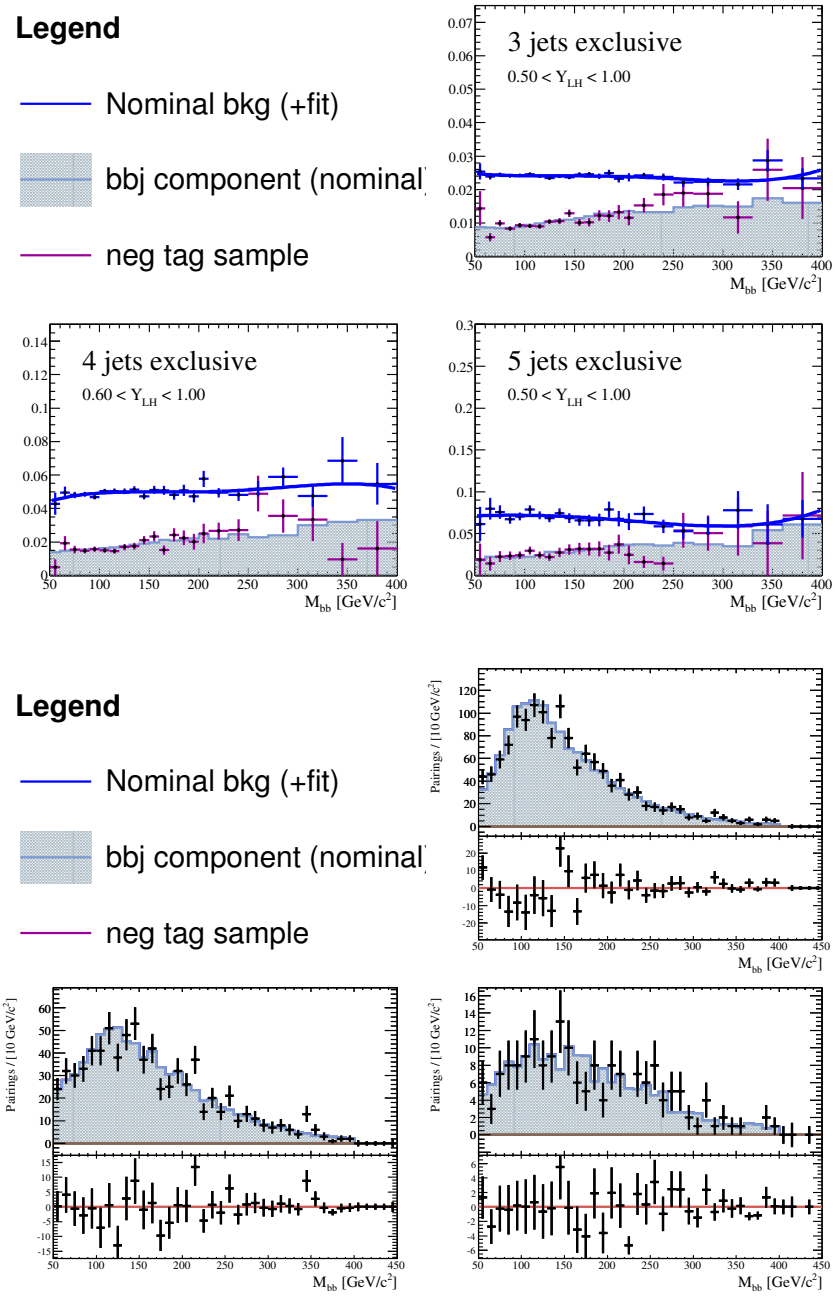


Figure 22: Top set of plots shows the 3Tag/2Tag ratio for the nominal background shape (blue), the *bbj* shape expectation (plain histogram) and the negative tag data sample (points with error bars). Note the relative difference between the *bbj* only and the full background shapes and the agreement between negative tag data and *bbj* expectation. The bottom set of plots displays the invariant mass for the *bbj* expectation (plain histogram) and the negative tag data sample (points), the histograms are normalized one to another. The lower panels show the difference between the negative tag data and the *bbj* expectation. Reminder, the negative tag is assumed to be dominated by *bbj* background (see text).

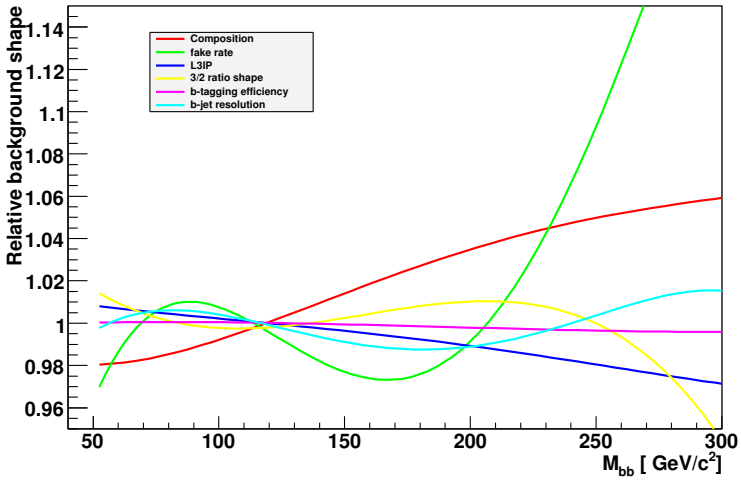


Figure 23: Ratios of the different systematic shapes to the nominal background model for the 3-jet channel.

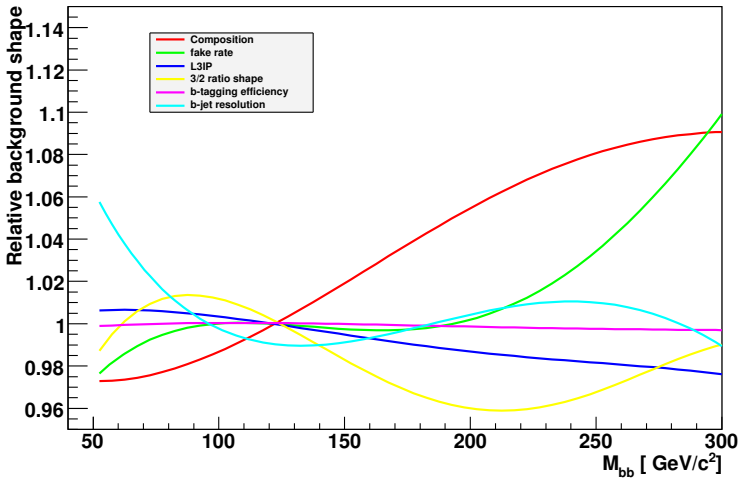


Figure 24: Ratios of the different systematic shapes to the nominal background model for the 4-jet channel.

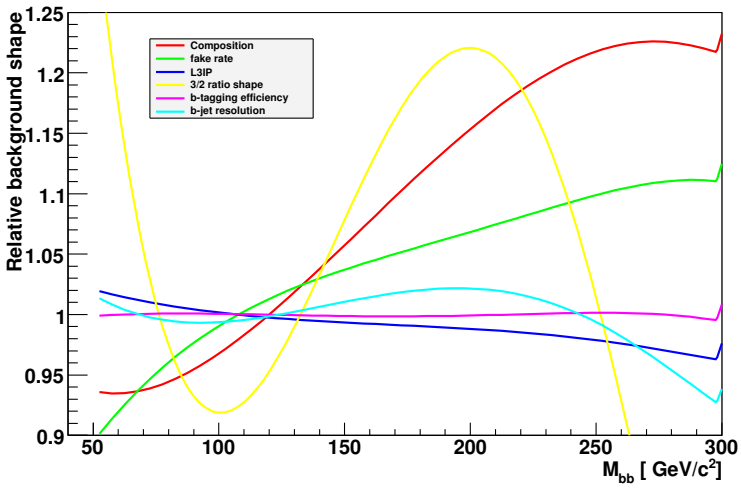


Figure 25: Ratios of the different systematic shapes to the nominal background model for the 5-jet channel.

modelling have also improved though even in the p17 analysis they only had a modest effect on the final limit.

# 6 Limit Setting

Limits are set at the 95% confidence level in the $\tan\beta - M_A$ plane using the `collie` package[3]. At present only the overall background normalisation is subject to profiling and in this case it is simply allowed to float. This procedure has been shown to be effectively equivalent to that used for the p17 analysis using hbbLimit and deals with the unknown background normalisation. All the other systematics are dealt with using Gaussian prior probability densities as in the "CLsyst" method provided by the collie package.

In the simple enhancement scenario the Higgs is assumed to be narrow and the cross section $\times$ branching ratio is taken to be $2 \times 0.9 \times \tan\beta^2 \times (\sigma \times \mathrm{Br})_{SM}$. In making the combination across the 3-, 4- and 5-jet channels in the p20 analysis all the systematic uncertainties are assumed to be correlated and similarly when combining across the same channels in p17. When combining the 3 p17 channels with the 3 p20 channels only the b-jet resolution systematic is assumed correlated between p20 and p17.

Figures 26 and 27 show the observed and expected (with $\pm$ 1 and 2 $\sigma$ uncertainties as the yellow and green bands respectively) 95% confidence level exclusion limits for the p20 and combined p17 and p20 analyses respectively. These results are summarized numerically in Tables 14 and 15.

In a previous pass of the the p20 analysis in the mass region between 120 GeV and 160 GeV there appeared to be evidence for a downward fluctuation in the data above the $2\sigma$ level. Several crosschecks were made to ensure that there were no mistakes in

| $m_A$/GeV/$c^2$ | Tan$\beta$ Obs. | Tan$\beta$ Exp. | $\sigma\times$Br. Obs./pb | $\sigma\times$Br. Exp./pb |
|---|---|---|---|---|
| 90 | 83 | $71^{+14}_{-12}$ | 200.7 | $149.1^{+63.2}_{-46.3}$ |
| 100 | 80 | $73^{+15}_{-13}$ | 121.7 | $103.8^{+47.0}_{-32.6}$ |
| 110 | 68 | $70^{+14}_{-12}$ | 58.9 | $64.2^{+28.1}_{-20.6}$ |
| 120 | 60 | $66^{+13}_{-11}$ | 32.7 | $38.9^{+17.1}_{-11.5}$ |
| 130 | 50 | $71^{+13}_{-13}$ | 15.8 | $31.4^{+12.7}_{-10.6}$ |
| 140 | 61 | $78^{+16}_{-13}$ | 16.9 | $27.4^{+12.4}_{-8.6}$ |
| 150 | 64 | $83^{+17}_{-14}$ | 13.6 | $22.6^{+10.3}_{-7.1}$ |
| 160 | 57 | $75^{+15}_{-13}$ | 7.9 | $13.5^{+6.0}_{-4.1}$ |
| 170 | 63 | $81^{+16}_{-15}$ | 7.1 | $11.6^{+5.0}_{-3.9}$ |
| 180 | 67 | $87^{+18}_{-15}$ | 5.9 | $9.9^{+4.6}_{-3.1}$ |
| 190 | 77 | $93^{+19}_{-16}$ | 6.0 | $8.8^{+3.9}_{-2.8}$ |
| 200 | 90 | $100^{+22}_{-16}$ | 6.2 | $7.7^{+3.7}_{-2.2}$ |
| 210 | 107 | $109^{+23}_{-19}$ | 6.7 | $7.1^{+3.3}_{-2.2}$ |
| 220 | 125 | $117^{+27}_{-19}$ | 7.2 | $6.3^{+3.2}_{-1.9}$ |

Table 14: Observed and expected 95% C.L. limits in Tan$\beta$ and cross section times branching ratio for the 1.6fb$^{-1}$ analysis in the negligible width scenario.

| $m_A$/GeV/$c^2$ | Tan$\beta$ Obs. | Tan$\beta$ Exp. | $\sigma\times$Br. Obs./pb | $\sigma\times$Br. Exp./pb |
|---|---|---|---|---|
| 90 | 67 | $55^{+12}_{-9}$ | 132.4 | $86.9^{+41.6}_{-25.0}$ |
| 100 | 58 | $56^{+11}_{-9}$ | 65.6 | $60.1^{+25.7}_{-17.5}$ |
| 110 | 52 | $54^{+12}_{-8}$ | 35.1 | $37.6^{+17.9}_{-10.4}$ |
| 120 | 49 | $52^{+11}_{-8}$ | 21.9 | $24.6^{+11.3}_{-7.3}$ |
| 130 | 44 | $56^{+11}_{-9}$ | 12.1 | $19.6^{+8.8}_{-5.7}$ |
| 140 | 57 | $63^{+13}_{-11}$ | 14.5 | $17.9^{+8.1}_{-5.6}$ |
| 150 | 69 | $70^{+15}_{-12}$ | 15.4 | $16.1^{+7.4}_{-4.9}$ |
| 160 | 73 | $71^{+14}_{-12}$ | 12.9 | $11.9^{+5.2}_{-3.8}$ |
| 170 | 86 | $77^{+16}_{-13}$ | 13.1 | $10.4^{+4.9}_{-3.2}$ |
| 180 | 96 | $84^{+17}_{-14}$ | 12.3 | $9.5^{+4.2}_{-2.8}$ |
| 190 | 103 | $91^{+18}_{-17}$ | 10.7 | $8.3^{+3.5}_{-2.8}$ |
| 200 | 113 | $96^{+20}_{-16}$ | 9.9 | $7.1^{+3.3}_{-2.2}$ |
| 210 | 124 | $104^{+22}_{-18}$ | 9.1 | $6.4^{+2.9}_{-2.0}$ |
| 220 | 137 | $111^{+23}_{-21}$ | 8.7 | $5.7^{+2.6}_{-1.9}$ |

Table 15: Observed and expected 95% C.L. limits in Tan$\beta$ and cross section times branching ratio for the 2.6fb$^{-1}$ analysis in the negligible width scenario.

the analysis procedure which could be responsible for this effect (see appendix G). With the addition of the fake-rate and new MC-modelling systematics and a small correction to the limit setting procedure this effect has been reduced.

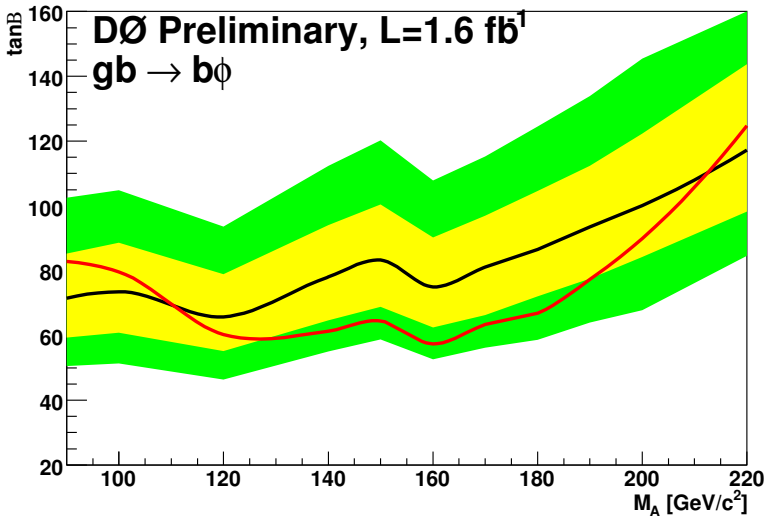


Figure 26: 95% CL exclusion limit in the $(m_A, \tan\beta)$ plane using the simple enhancement $2 \times 0.9 \times \tan\beta^2 \times (\sigma \times \mathrm{Br})_{SM}$ for the p20 analysis. The red curve is the observed limit. The black curve is the expected limit (in the no-signal hypothesis) and the bands correspond to $\pm 1\sigma$ and $\pm 2\sigma$ variations around the expectation. (The truncation of the $\pm 1\sigma$ and $\pm 2\sigma$ bands will be corrected.)

## 6.1 Exclusion limit within different MSSM scenarios

Radiative corrections at NNLO modify both the coupling and the mass relationships between the Higgs bosons. The effects of these corrections depend upon the overall (continuous) set of SUSY parameters so that it is nearly impossible to test every possible scenario. Typical benchmark scenarios have been defined [15] in terms of $M_{\mathrm{SUSY}}$, the mass scale of squarks, $\mu$, the Higgs sector bilinear coupling, $M_2$, the gaugino mass term, $A_t$, the trilinear coupling of the stop sector, $A_b$, the trilinear coupling of the sbottom sector and $m_{\tilde{g}}$ the gluino mass term. The most tested scenarios are:

1. The maximal-mixing or $m_h^{\mathrm{max}}$ scenario (the parameters are chosen such that the maximum possible Higgs-boson mass as a function of $\tan\beta$ is obtained):

$$
\begin{aligned}
&M_{\mathrm{SUSY}} = 1\,\mathrm{TeV}, \quad \mu = 200\,\mathrm{GeV}, \quad M_2 = 200\,\mathrm{GeV}, \\
&X_t^{\mathrm{OS}} = 2\,M_{\mathrm{SUSY}}\ \text{(FD calculation)}, \quad X_t^{\overline{\mathrm{MS}}} = \sqrt{6}\,M_{\mathrm{SUSY}}\ \text{(RG calculation)} \\
&A_b = A_t, \quad m_{\tilde{g}} = 0.8\,M_{\mathrm{SUSY}}\ . \qquad (4)
\end{aligned}
$$

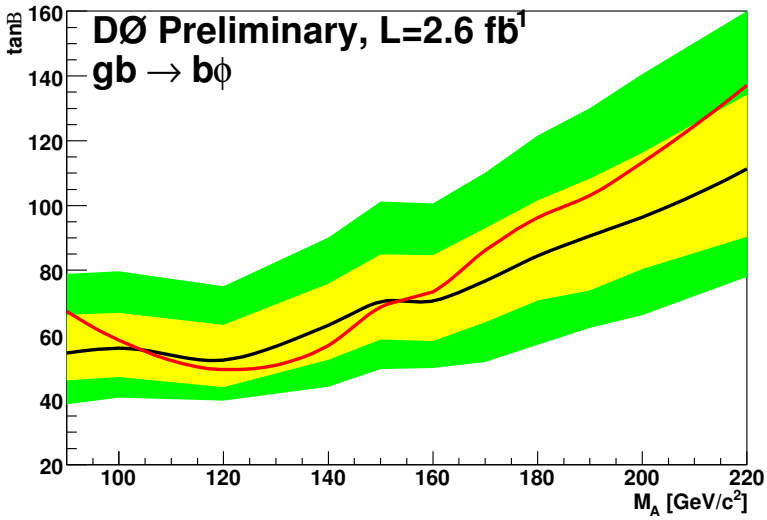


Figure 27: 95% CL exclusion limit in the $(m_A, \tan\beta)$ plane using the simple enhancement $2 \times 0.9 \times \tan\beta^2 \times (\sigma \times \mathrm{Br})_{SM}$ for the combined p17 and p20 analyses. The red curve is the observed limit. The black curve is the expected limit (in the no-signal hypothesis) and the bands correspond to $\pm 1\sigma$ and $\pm 2\sigma$ variations around the expectation. Some mass points are missing in this plot due to failed limit setting jobs.

2. The no-mixing scenario This benchmark scenario is the same as the $m_h^{\max}$ scenario, but with vanishing mixing in the stop sector and with a higher SUSY mass scale to avoid the LEP Higgs bounds:

$$M_{\mathrm{SUSY}} = 2\,\mathrm{TeV}, \quad \mu = 200\,\mathrm{GeV}, \quad M_2 = 200\,\mathrm{GeV},$$
$$X_t = 0\ (\mathrm{FD/RG\ calculation}), \quad A_b = A_t, \quad m_{\tilde{g}} = 0.8\,M_{\mathrm{SUSY}}\ . \qquad (5)$$

In addition results are very dependent upon $\mu$ so it is suggested in [16] to probe at least its two possible signs.
This analysis is most sensitive in the case of the maximal-mixing $\mu < 0$ scenario and the results interpreted in this scenario are below. An interpretation of the results in the other scenarios is currently in progress.
The exclusion limit for the maximal-mixing $\mu < 0$ case is displayed in Figs. 28 and 29 for the p20 and combined p17 and p20 analyses respectively. Figs. 30 and 31 show the 95% C.L. exclusion obtained with the p20 and combined p17 and p20 analyses respectively along with the exclusion limit from the LEP experiments in the $m_h^{\max}$ $\mu = -200$ scenario.

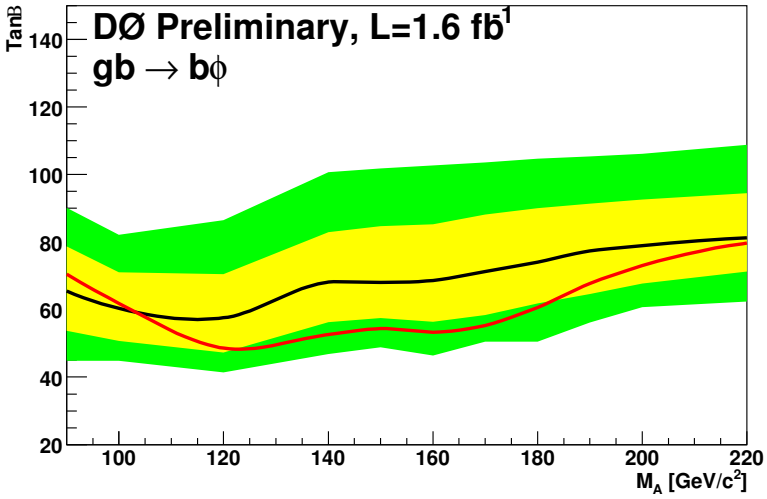


Figure 28: 95% CL exclusion limit in the $(m_A, \tan\beta)$ for maximal-mixing and $\mu < 0$ for the p20 analyses. The red curve is the observed limit. The black curve is the expected limit (in the no-signal hypothesis) and the bands correspond to $\pm 1\sigma$ and $\pm 2\sigma$ variations around the expectation.

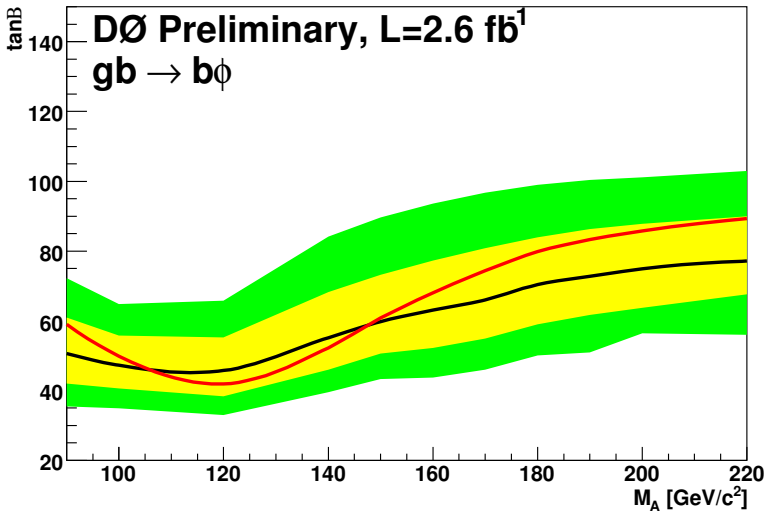


Figure 29: 95% CL exclusion limit in the $(m_A, \tan\beta)$ for maximal-mixing and $\mu < 0$ for the combined p17 and p20 analyses. The red curve is the observed limit. The black curve is the expected limit (in the no-signal hypothesis) and the bands correspond to $\pm 1\sigma$ and $\pm 2\sigma$ variations around the expectation.

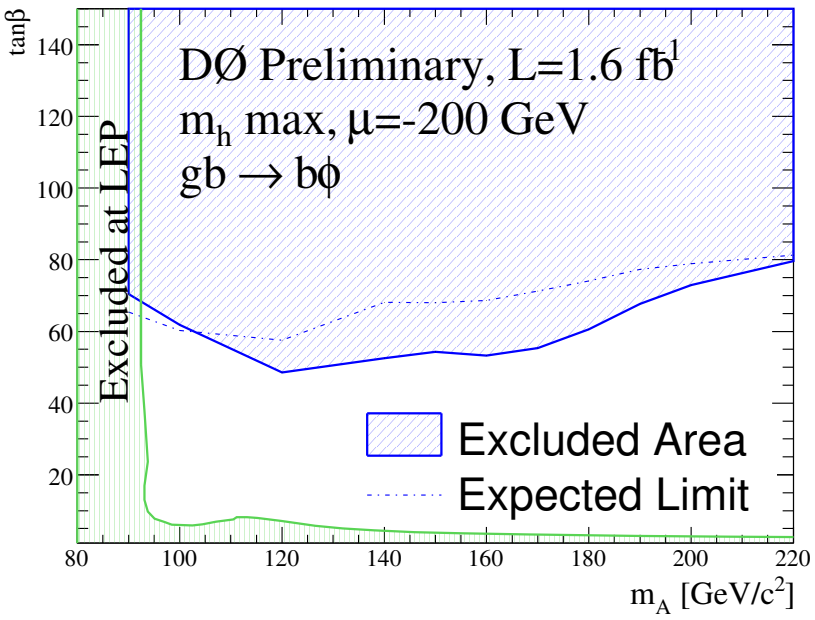


Figure 30: 95% CL exclusion limit in the $(m_A, \tan\beta)$ obtained with the p20 analysis for the $m_h^{\max}$, $\mu$=-200 GeV scenario. The exclusion limit obtained from the LEP experiments are also overlayed.

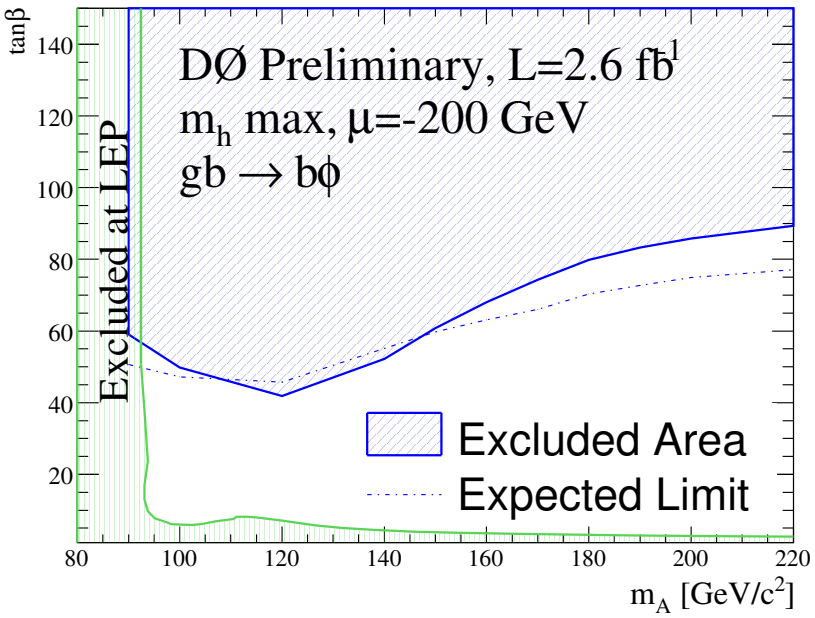


Figure 31: 95% CL exclusion limit in the $(m_A, \tan\beta)$ obtained with the combined p17 and p20 analyses for the $m_h^{\max}$ , $\mu$=-200 GeV scenario. The exclusion limit obtained from the LEP experiments are also overlayed.

# A Trigger

## A.1 L1 Jets

The L1 term requires one L1 jet with $p_T > 30$ GeV, two with $p_T > 15$ GeV and three with $p_T > 8$ GeV. The required turn-on curves are determined using muon triggered events from the TOPJETTRIG skim. The events are required to have exactly three offline jets with $p_T > 15$ GeV and $\eta < 2.5$. Events where any jet pairing have $dR < 1.0$ are vetoed. Figures 32, 33 and 34 show the turn-on curves when requiring a L1 jet with a $p_T > 8$, 15 and 30 GeV respectively.

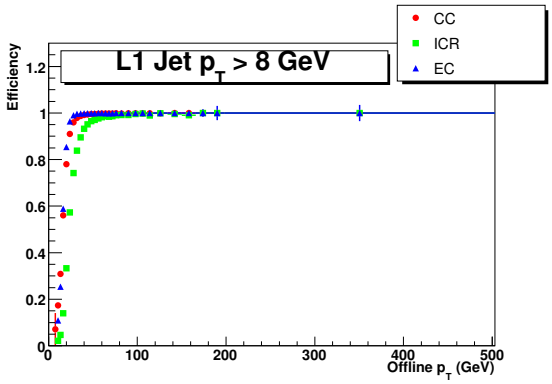


Figure 32: Level 1 Jet $p_T > 8$ GeV Turn on curve.

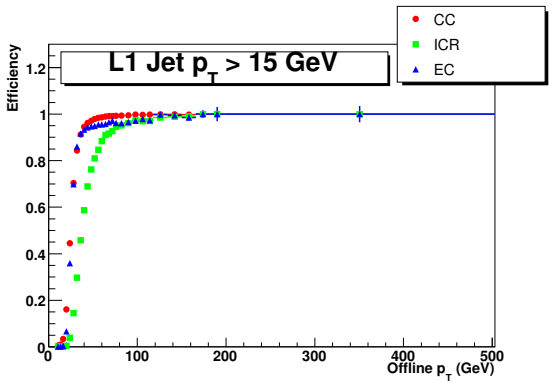


Figure 33: Level 1 Jet $p_T > 15$ GeV Turn on curve.

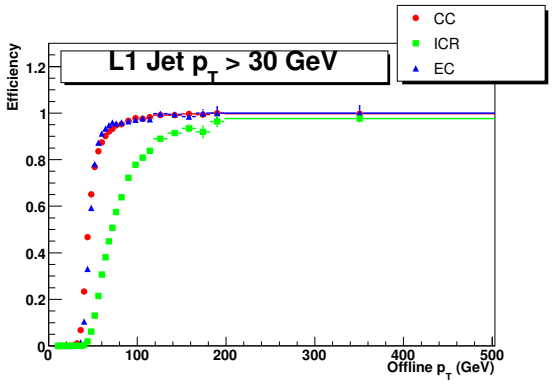


Figure 34: Level 1 Jet $p_T > 30$ GeV Turn on curve.

### A.1.1 L1 Noise Jets

Any L1 jet not matched to an offline jet within $dR < 0.5$ is considered a noise jet. The number of noise jets above each L1 jet $p_T$ threshold in each event is parameterised as a function of $H_T$. This 2D distribution is used to model the probability that $x$ noise jets are present in an event as a function of offline $H_T$. Figure 35 shows the probability of $x$ noise jets being present for two representative $H_T$ values. Figures 36 and 37 show the angular distibution of the L1 noise jets.

### A.1.2 L1 Closure

Closure tests are performed on events containing four and five jets. This sample is orthogonal to the sample on which the turn-on curves were determined. The probability for an event to pass the Level 1 jet condition is determined by calculating the combining the jet probabilities as outlined in [14]. Noise jets are added by combining the probability to have less than the required numbers of jets in the event, with the probability to have greater than or equal to the required number of noise jets:

$$\begin{aligned} P(Pass3L1jets) = P(\geq 3jets) + P(= 2jets) \times P(\geq 1noisejet) + \\ + P(= 1jet) \times P(\geq 2noisejets) \\ + P(= 0jets) \times P(\geq 3noisejets) \end{aligned}$$

where $P(\geq xjets)$ refers to the probability to have $x$ or more jets present in the event and $P(= xjets)$ refers to the probability to have exactly $x$ jets present in the event. Figure 38 shows the measured and predicted trigger rates for the L1 trigger simulation. The ratio of the predicted and measured trigger rates is shown in Fig. 39.

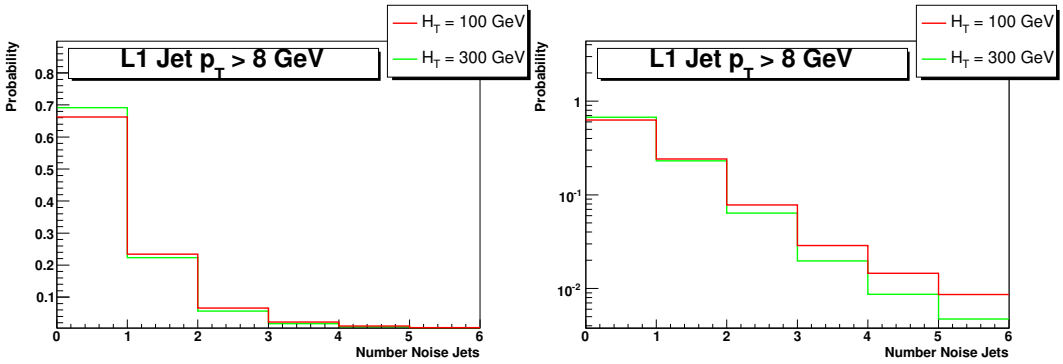


(a) $p_T > 8$ GeV

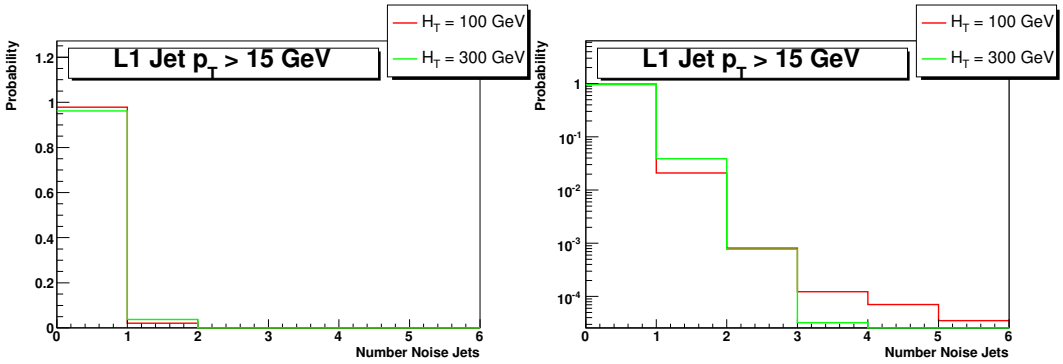


(b) $p_T > 15$ GeV

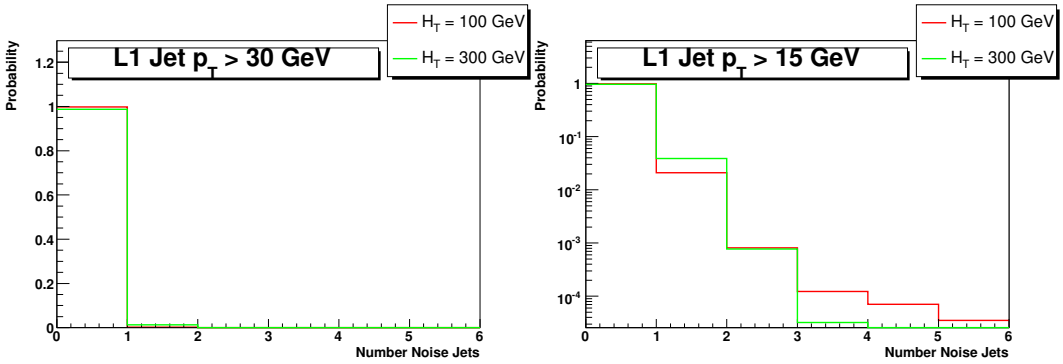


(c) $p_T > 30$ GeV

Figure 35: Probability for 0–5 L1 Noise jets for each trigger $p_T$ threshold for two representative $H_T$ values. The plots on the right are on a logarithmic scale.

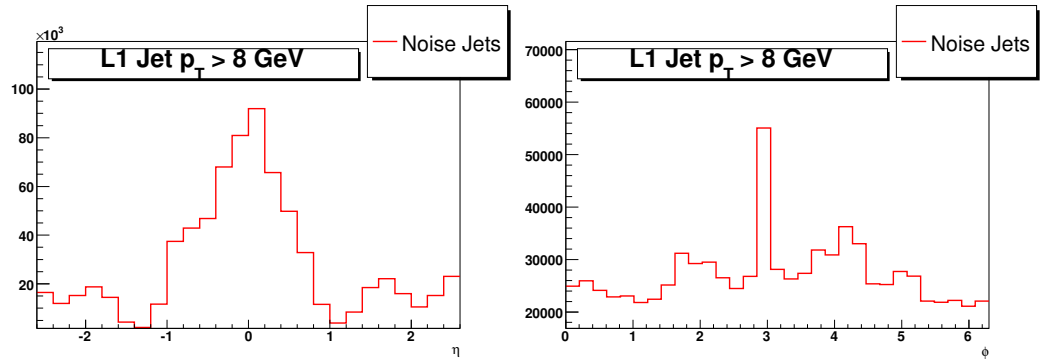


(a) $p_T > 8$ GeV

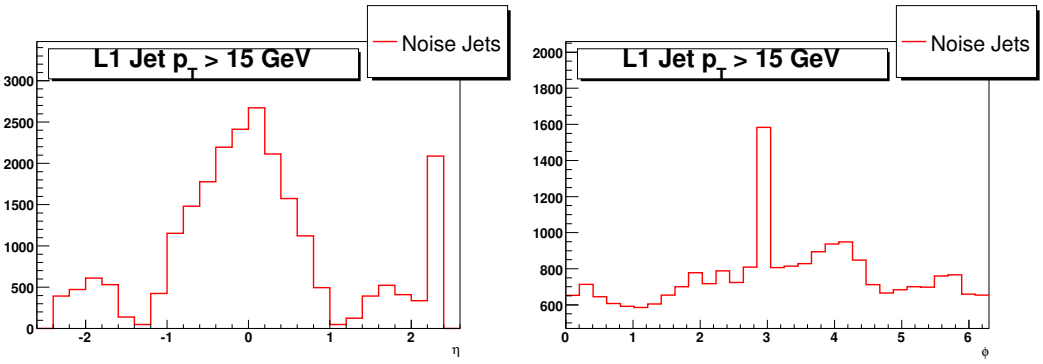


(b) $p_T > 15$ GeV

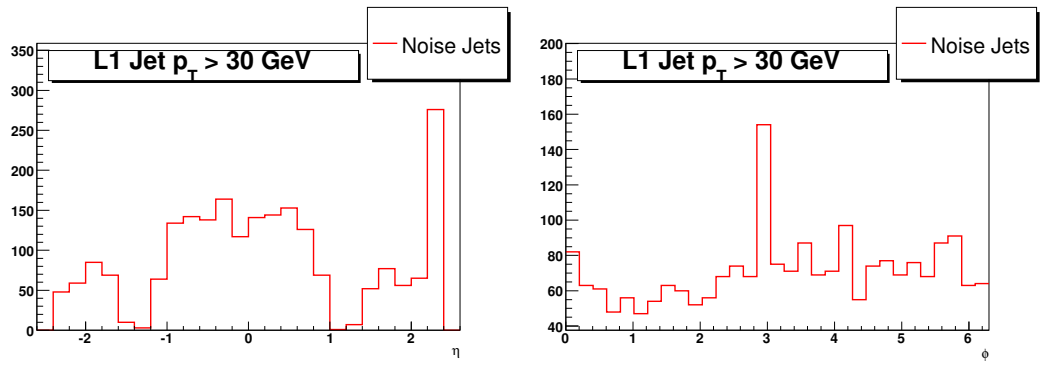


(c) $p_T > 30$ GeV

Figure 36: Distriubtion of the L1 noise jets as a function of $\eta$ (left) and $\phi$ (right).

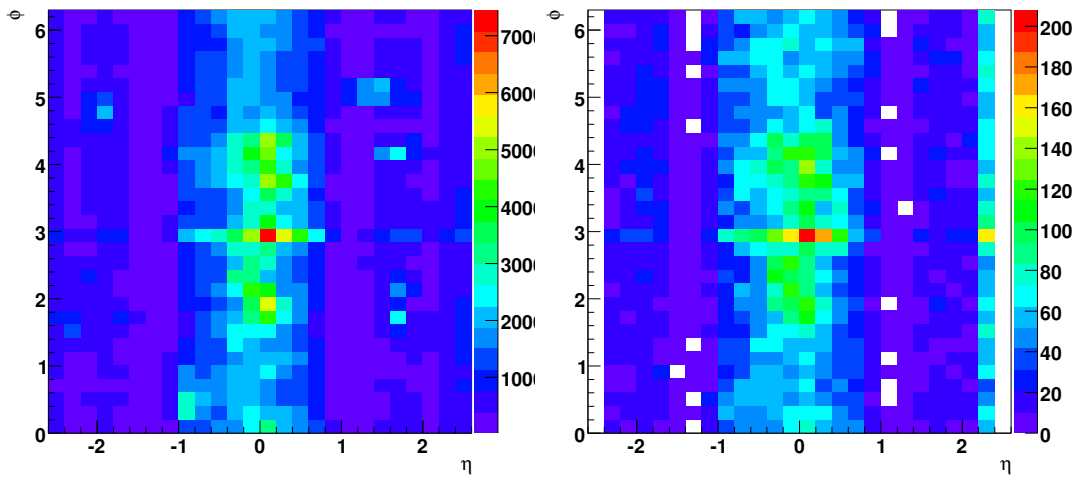


(a) $p_T > 8$ GeV

(b) $p_T > 15$ GeV

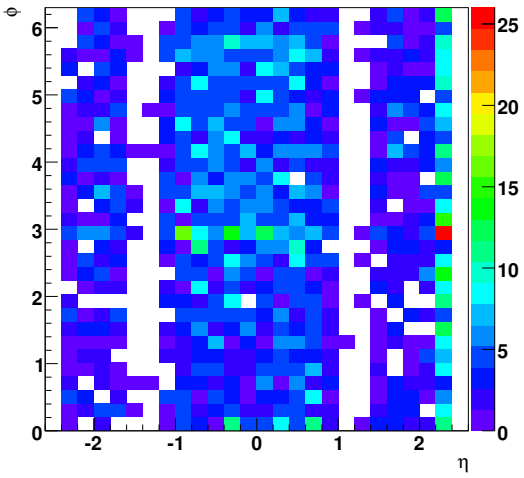


(c) $p_T > 30$ GeV

Figure 37: Distriubtion of the L1 noise jets in the $\eta$-$\phi$ plane.

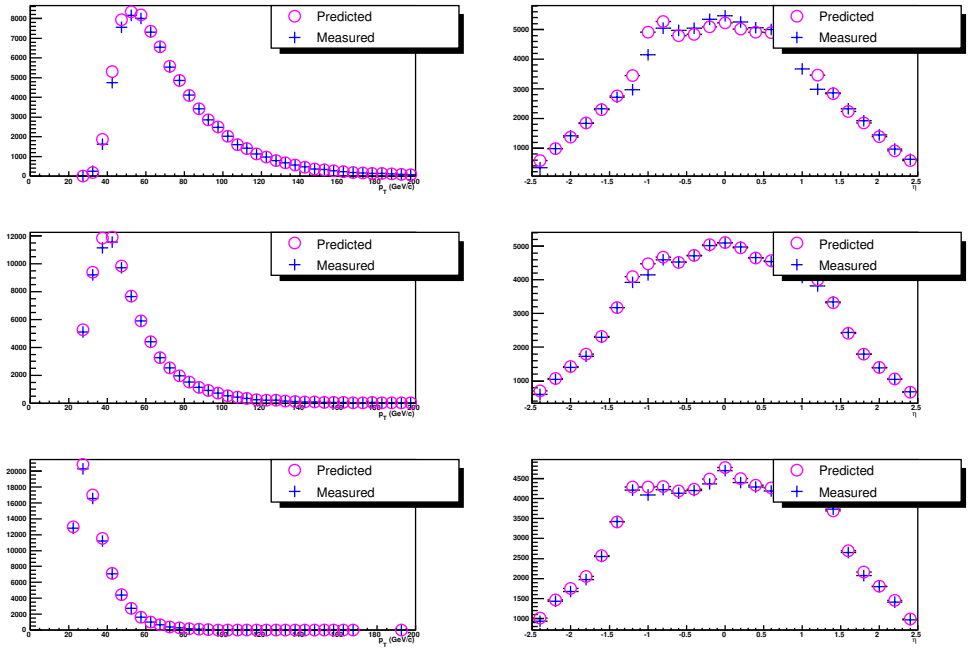


Figure 38: The predicted and measured $p_T$ (left) and $\eta$ (right) distributions for the leading (top), 2nd (middle) and 3rd (bottom) jets in 4 and 5 jets events after requiring that the L1 trigger term has fired.

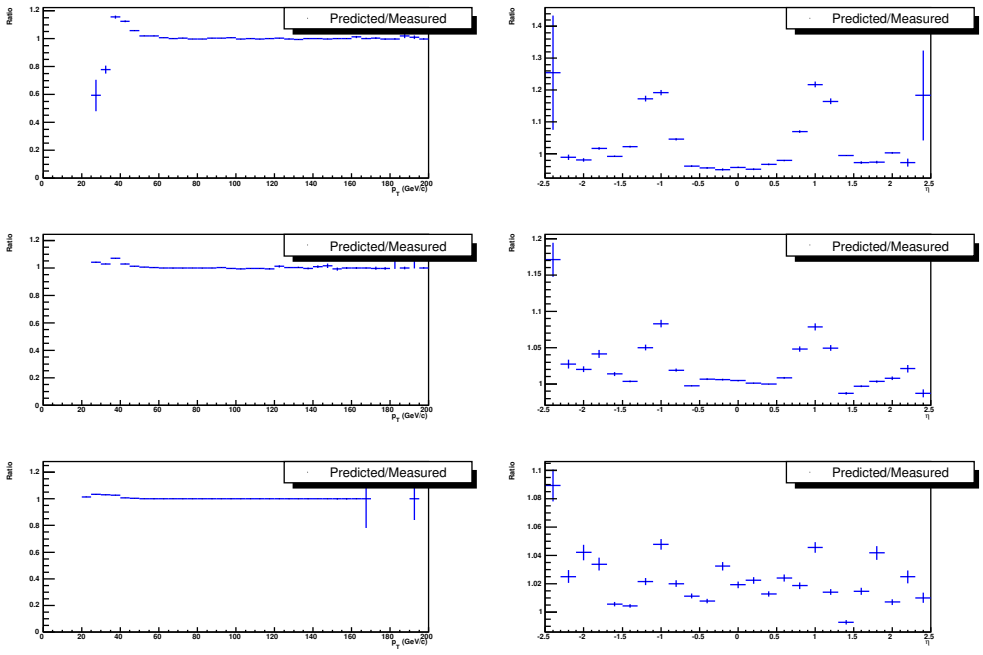


Figure 39: Ratio of the predicted and measured $p_T$ (left) and $\eta$ (right) distributions for the leading (top), 2nd (middle) and 3rd (bottom) jets in 4 and 5 jets events after requiring that the L1 trigger term has fired.

## A.2 Level 2

The L2 trigger consists of an OR of four terms. Only two are currently parameterised and included in the analysis:

*Top*: 3 jets with $p_T$ >8 GeV, 2 jets with $p_T$ >15 GeV, 1 jet with $p_T$ >30 GeV and $H_T$ >100 GeV

$ME_T$: 3 jets with $p_T$ >8 GeV, 2 jets with $p_T$ >15 GeV, 1 jet with $p_T$ >30 GeV, $H_T$ >75 GeV and $MH_T$ > 10 GeV.

The OR of these two terms is calculated by determining the efficiency of the $ME_T$ term with respect to the case when the *Top* term has not fired. This allows the total Level 2 efficiency to be calculated using the following formula:

$$P(L2Fired) = P(Top) + (1 - P(Top)) \times P(ME_T|!Top) \quad (6)$$

where P(x) corresponds to the probability of either L2, the $ME_T$ term or the $TOP$ term firing. The same data sample as the L1 trigger determination was used for L2, with the added requirement that the L1 trigger term has fired.

### A.2.1 L2 Jet

In the Run IIb trigger the L1 and L2 jet finding algorithms are very similar. The L2 jet requirements are also a subset of the L1 requirements. This means that the probability of the L2 jet terms firing, if the L1 term has fired, is effectively unity. A parametrisation for the L2 jet terms is therefore not explicitly calculated and the probability to pass these term is taken as unity. Figure 40 shows the probability to pass the L2 jet term given that the L1 trigger has already fired.

### A.2.2 L2 Top

The turn-on curve for $L2H_T$ >100 GeV is shown in Fig. 41.

### A.2.3 L2 $ME_T$ Term

The turn-on curves for the $L2ME_T$ trigger terms are calculated with respect to the L2 *Top* trigger term not firing. The only L2 *Top* trigger requirement which could not have fired and yet still allow the $ME_T$ trigger to fire is if $H_T$ <100 GeV. The $MH_T$ >10 GeV and $H_T$ >75 GeV turn-on curves are shown in Figs. 42 and 43 respectively.

### A.2.4 L2 Closure

Closure tests are performed on events containing four and five jets. This sample is orthogonal to the sample on which the turn-on curves were determined. The probability for an event to pass the Level 2 *Top* term is first calculated using the $H_T$ distribution. This is then combined with the probability for the $MET$ trigger $MH_T$

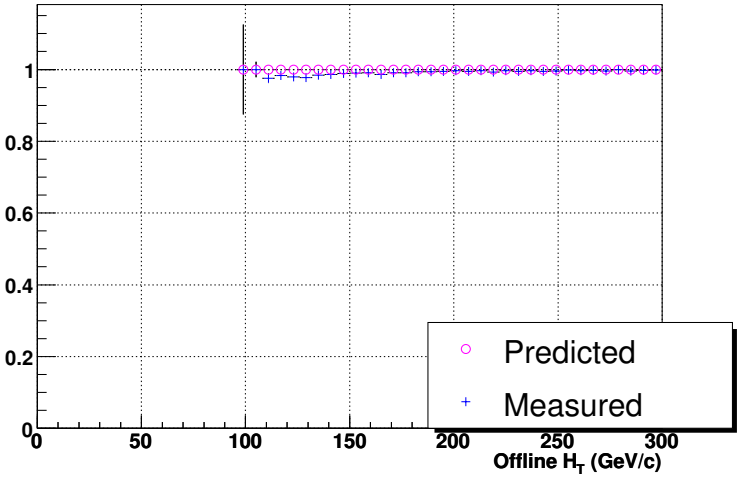


Figure 40: The probability that the L2 trigger jet term has fired given that the L1 trigger has fired as a function of offline $H_T$.

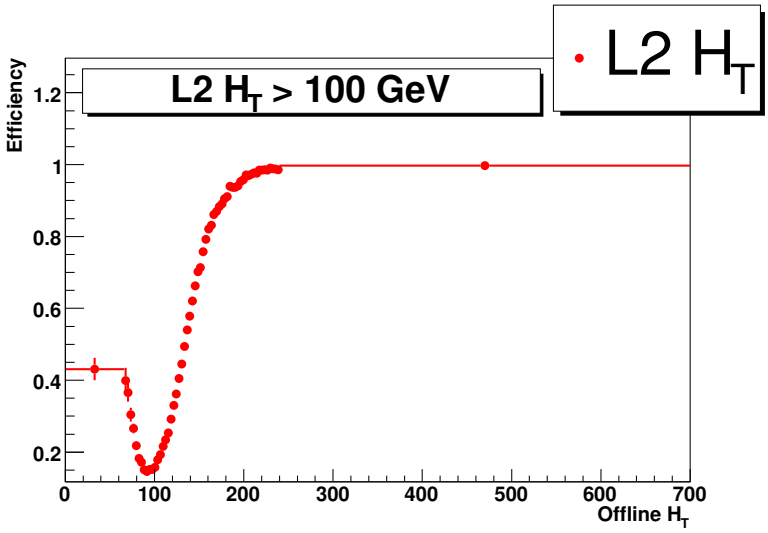


Figure 41: Level 2 $H_T > 100$ GeV turn-on curve.

and $H_T$ terms to have fired given that the *Top* trigger term did not fire. Figure 44 shows the actually and predicted trigger rates for the L1 trigger simulation. The ratio of the predicted and measured trigger rates is shown in Fig. 45.

## A.3 L3 Jets

The turn-on curves for Level 3 jets are determined on the mu-inclusive skim on events that have passed the L1 and L2 requirements for the Higgs trigger (JT2_3JT15L_IP_VX). The events are required to pass a muon trigger to avoid biases from the trigger selec-

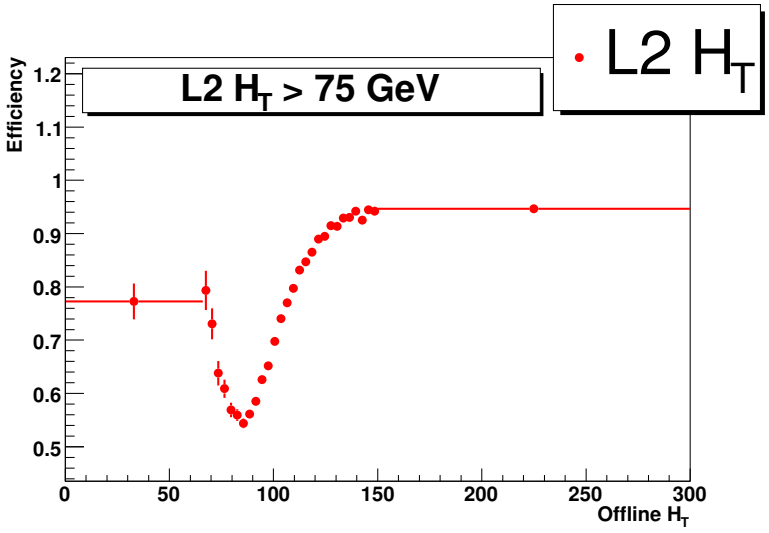


Figure 42: Level 2 $H_T$ > 75 GeV turn-on curve calculated for events where $L2H_T$ <100 GeV.

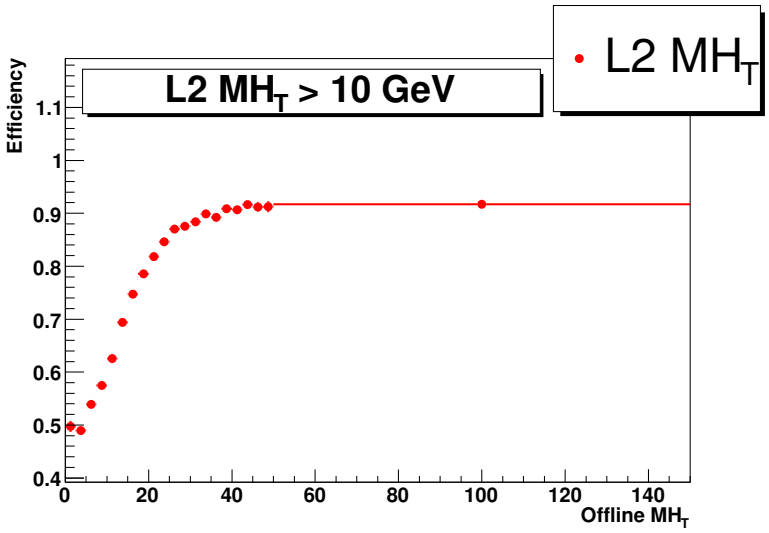


Figure 43: Level 2 $MH_T$ > 10 GeV turn-on curve calculated for events where $L2H_T$ <100 GeV.

tion and the Level 3 jet tool (SC5JET_9) must have run. Furthermore the events are required to contain exactly three jets and all jets must have a JES corrected $p_T$ > 10 GeV. All plots in this section are made using the higgs_hb version p21-br-10. Figures 46 and 47 show the turn on curves for a Level 3 $p_T$ cut of 15 and 25 GeV. The closure tests are discussed in section A.4.

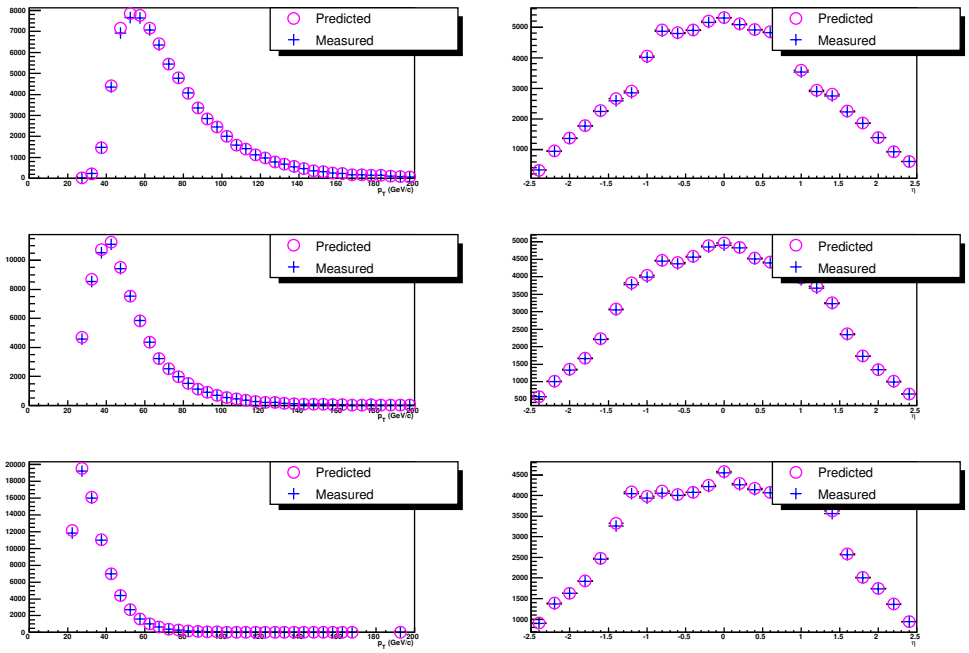


Figure 44: The predicted and measured $p_T$ (left) and $\eta$ (right) distributions for the leading (top), 2nd (middle) and 3rd (bottom) jets in 4 and 5 jets events which have passed the L1 and L2 trigger requirements.

### A.3.1 L3 Noise Jets

The effect of noise jets, i.e. L3 jets that cannot be matched to a reco jet is determined as a function of the number of jets in the event and sum of all jet $p_T$. The results are shown in figs. 48 and 49.

## A.4 Closure Tests

Closure tests are done on events containing three, four or five jets separately, the latter two samples being orthogonal to the sample the turn on curves where determined on. Noise jets are incorporated as an additional jet which fires the triggers according to figs. 48, 49. The probability for an event to pass the Level 3 jet condition (two jets $p_T > 25$ GeV, plus an additional jet with $p_T > 15$ GeV) is determined by calculating the probability for the three 'fail' scenarios: 1) All jets fail the 25 GeV trigger. 2) Exactly one jet fires the 25 GeV trigger, all others fail. 3) Exactly two jets fire the 25 GeV trigger, but all other jets fail the 15 GeV trigger. This takes into account that a jet passing the $p_T > 25$ GeV cut, will automatically also fire the 15 GeV trigger. Figures 50 and 51 show probability for an event to pass the trigger cuts for 3,4 and 5 jets events, with and without the inclusion of noise jets.

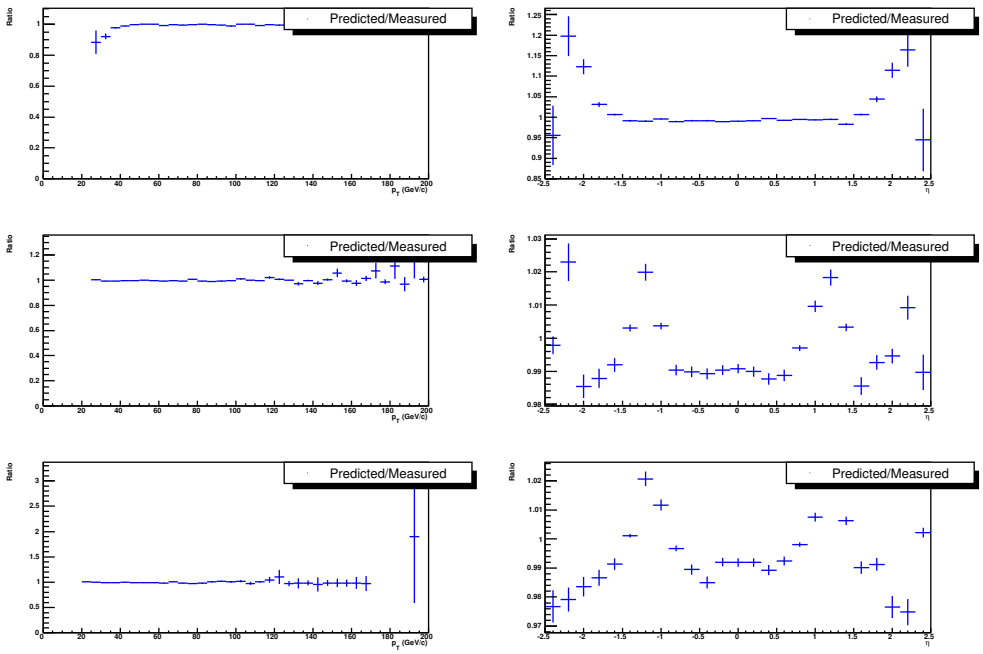


Figure 45: Ratio of the predicted and measured $p_T$ (left) and $\eta$ (right) distributions for the leading (top), 2nd (middle) and 3rd (bottom) jets in 4 and 5 jets events which have passed the L1 and L2 trigger requirements.

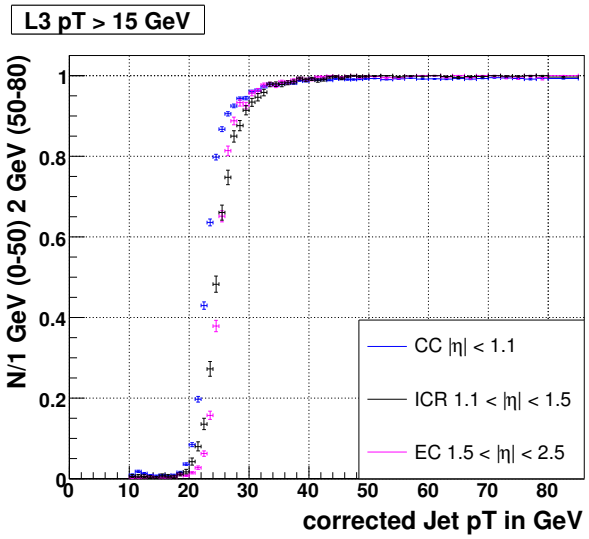


Figure 46: Level 3 15 GeV Turn on curve.

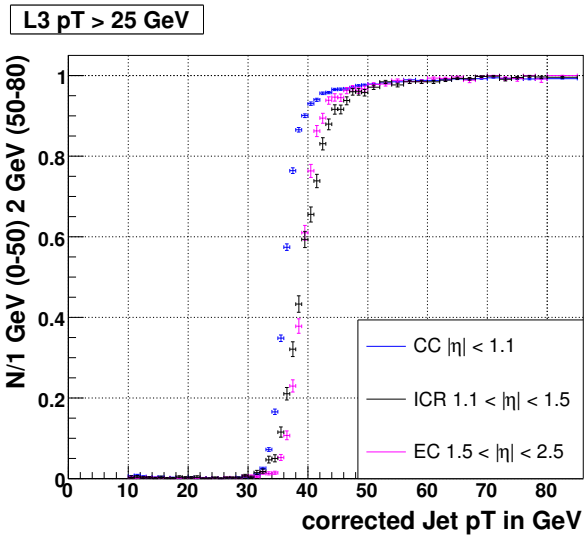


Figure 47: Level 3 25 GeV Turn on curve.

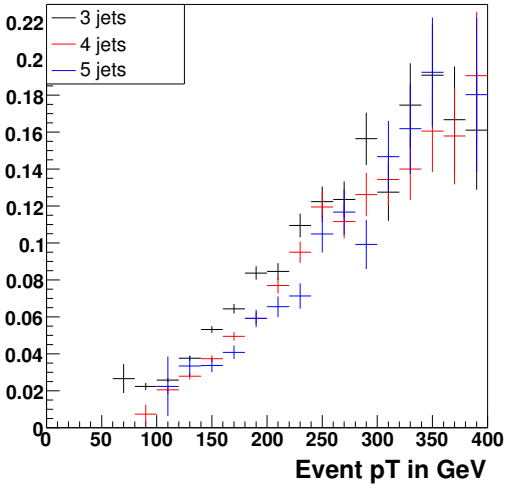


Figure 48: Probability for a given number of jets to fire a 15 GeV Level3 jet trigger as a function of event $p_T$.

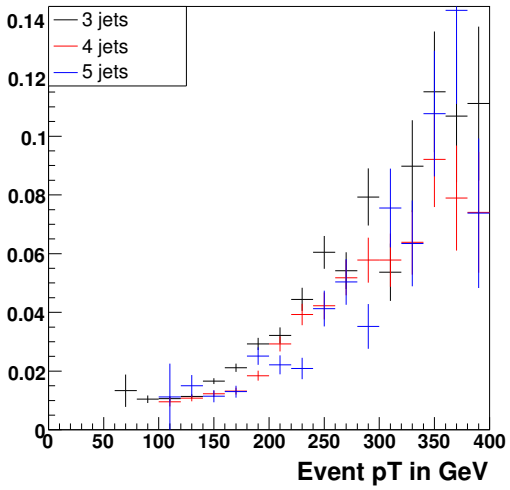


Figure 49: Probability for a given number of jets to fire a 25 GeV Level 3 jet trigger as a function of event $p_T$.

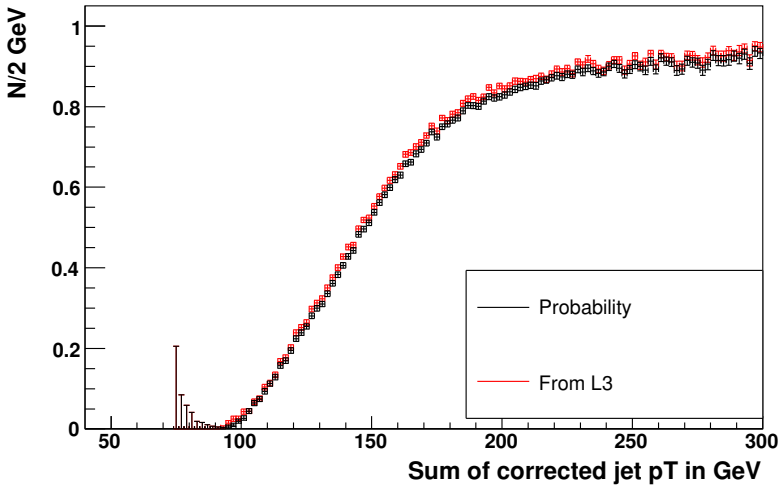


Figure 50: Closure plot for 3 to 5 jets events (excluding noise jets).

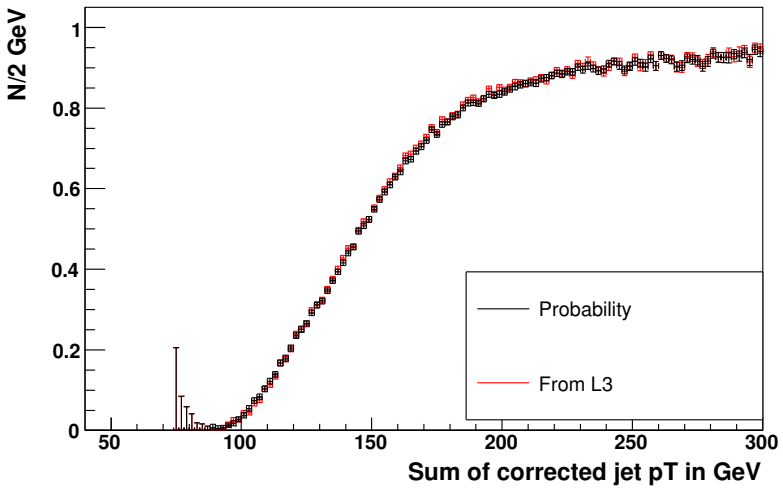


Figure 51: Closure plot for 3 to 5 jets events (including noise jets).

## A.5 IP Tagger at Level 3

For double tagged samples, the IP tag tool (IPTag6_JT10) has no turn-on curve and is flat over the whole range of $H_T$ (see fig. 52 (a)) when measured for events that have passed the Level1, Level2 and Level 3 jet conditions. For untagged samples (see fig. 52 (b)) there is a hint of a turn on at low $H_T$.

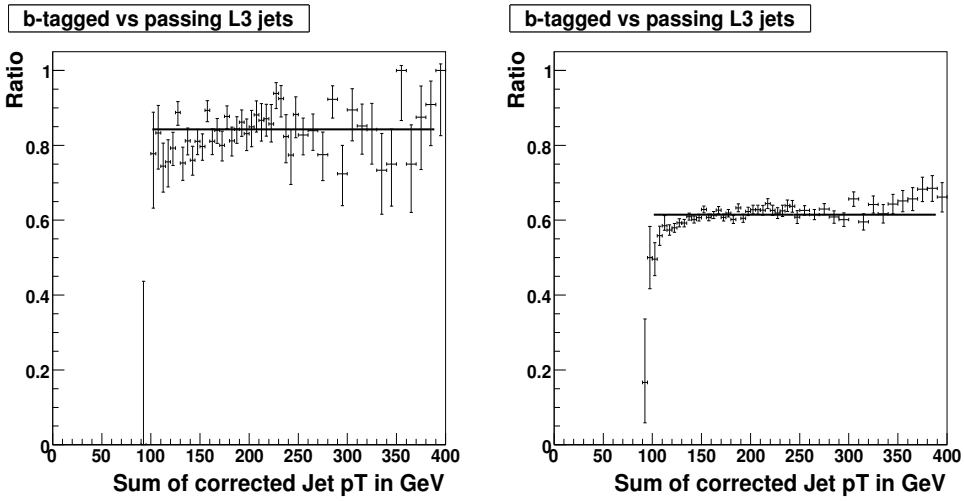


(a) 2 $b$-tags.

(b) Untagged.

Figure 52: (a) Ratio of events passing L3 jet and L3 $b$-tag (Level3 Event $b$-tag $< 0.05$ for runs up to run 223343, 0.4 thereafter) vs events passing the Level3 jet condition only. The selected events had 3-5 jets with a JES corrected $p_T$ of at least 20 GeV and two offline NN (TIGHT) $b$-tags. (b) Ratio of events passing L3 jet and L3 $b$-tag vs events passing the Level3 jet condition only. No offline $b$-tags were required.

# B Data Background Comparison

## B.1 Low Mass Likelihood

Figures 53 - 61 show comparison plots between data and the predicted background for the 3, 4 and 5 jet channels for a Higgs mass of 120 GeV.

### B.1.1 3 jet events

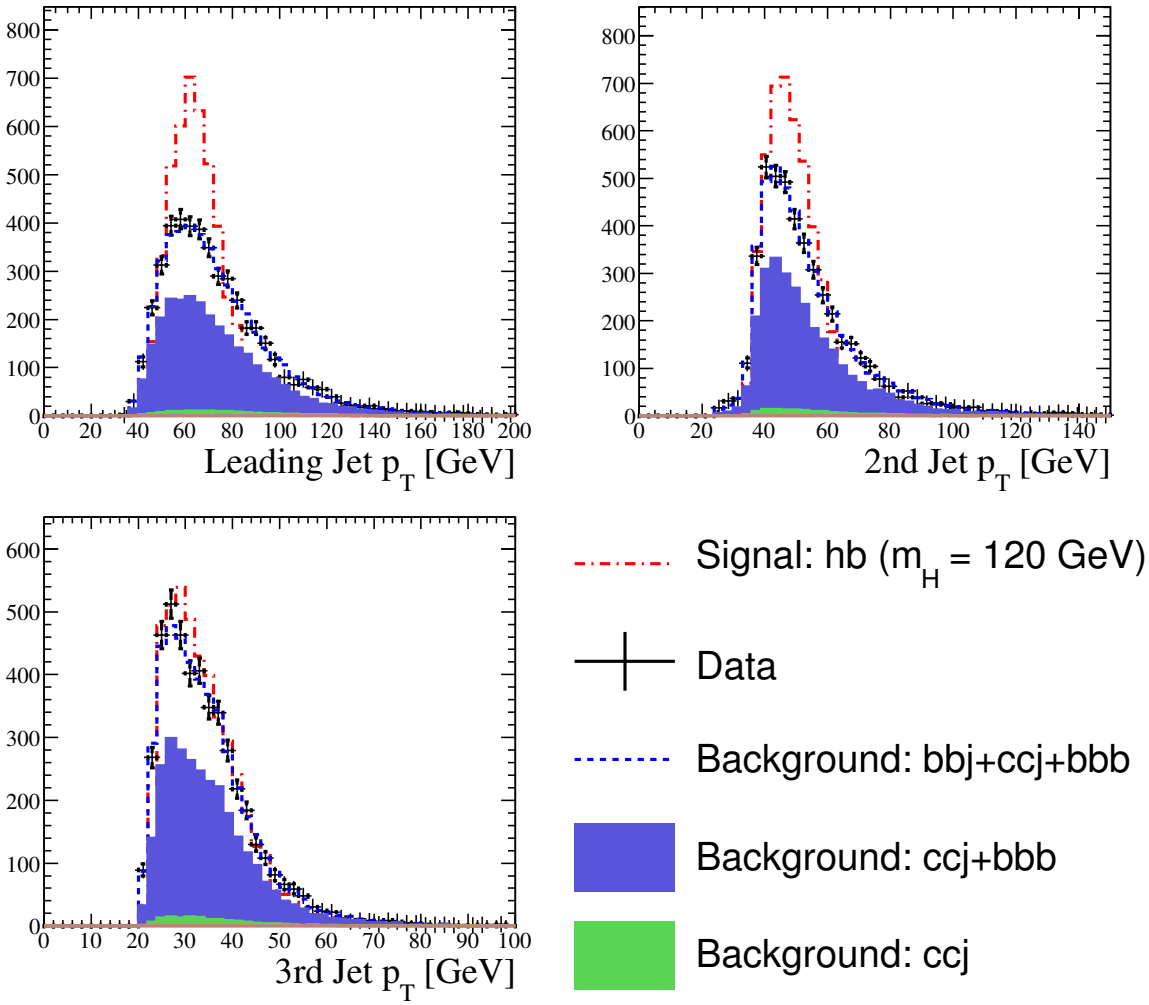


Figure 53: Data predicted background comparison for 3 jets, 3 $b$-tag sample with a 120 GeV Higgs Sample used as signal. Shown is jet $p_T$ for the three jets with the highest $p_T$ in the event.

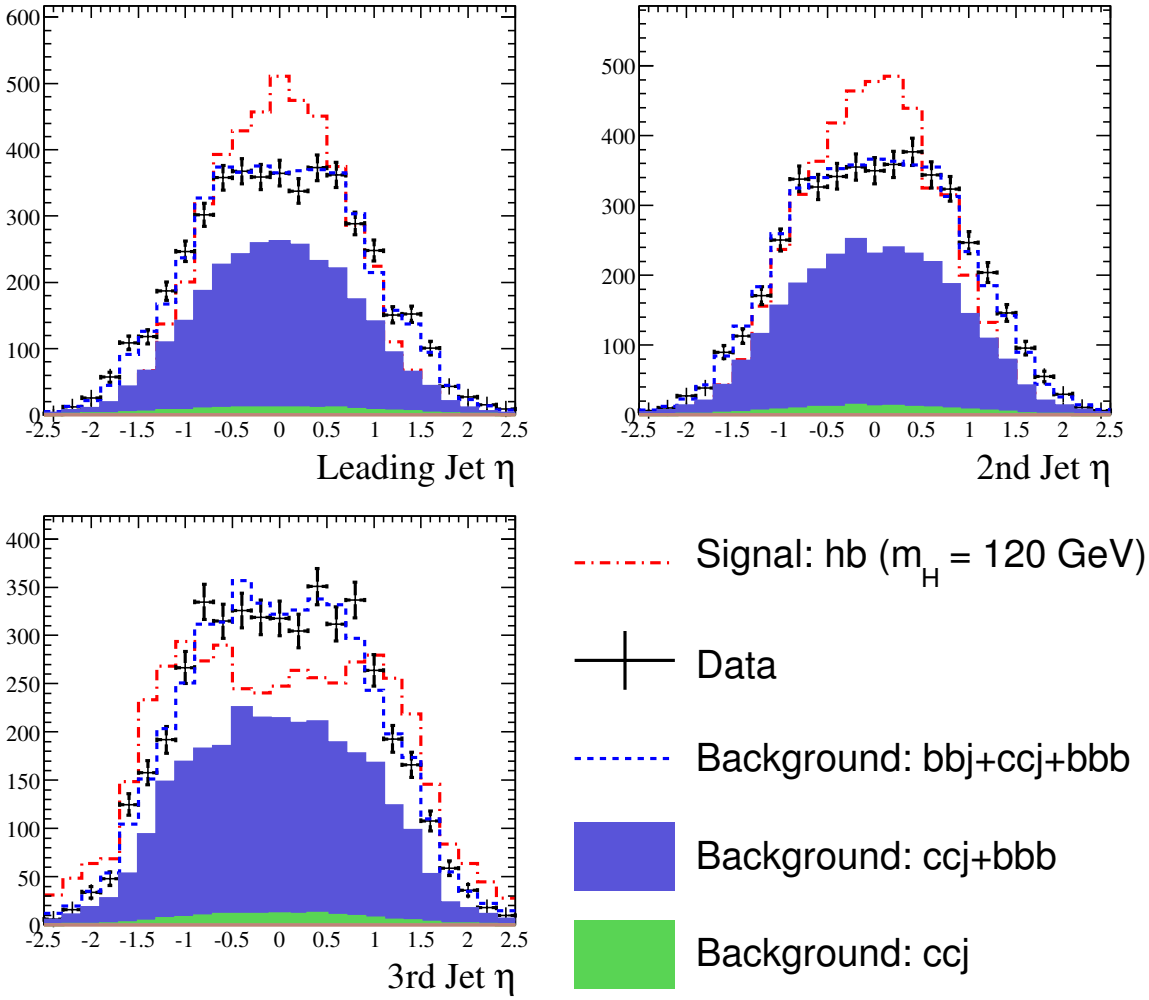


Figure 54: Data predicted background comparison for 3 jets, 3 $b$-tag sample with a 120 GeV Higgs Sample used as signal. Shown is jet $\eta$ for the three jets with the highest $p_T$ in the event.

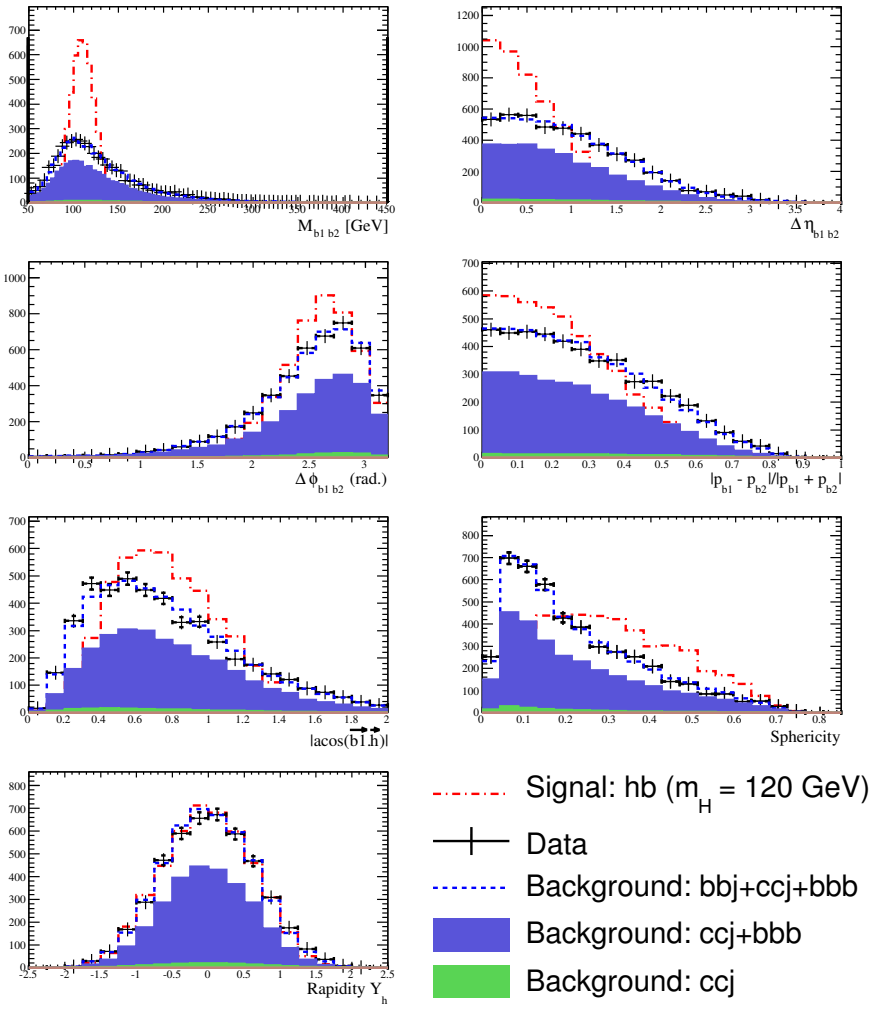


Figure 55: Data predicted background comparison for 3 jets, 3 $b$-tag sample with a 120 GeV Higgs Sample used as signal. Shown are the variables used to determine the signal likelihood (see table 13).

### B.1.2 4 jet events

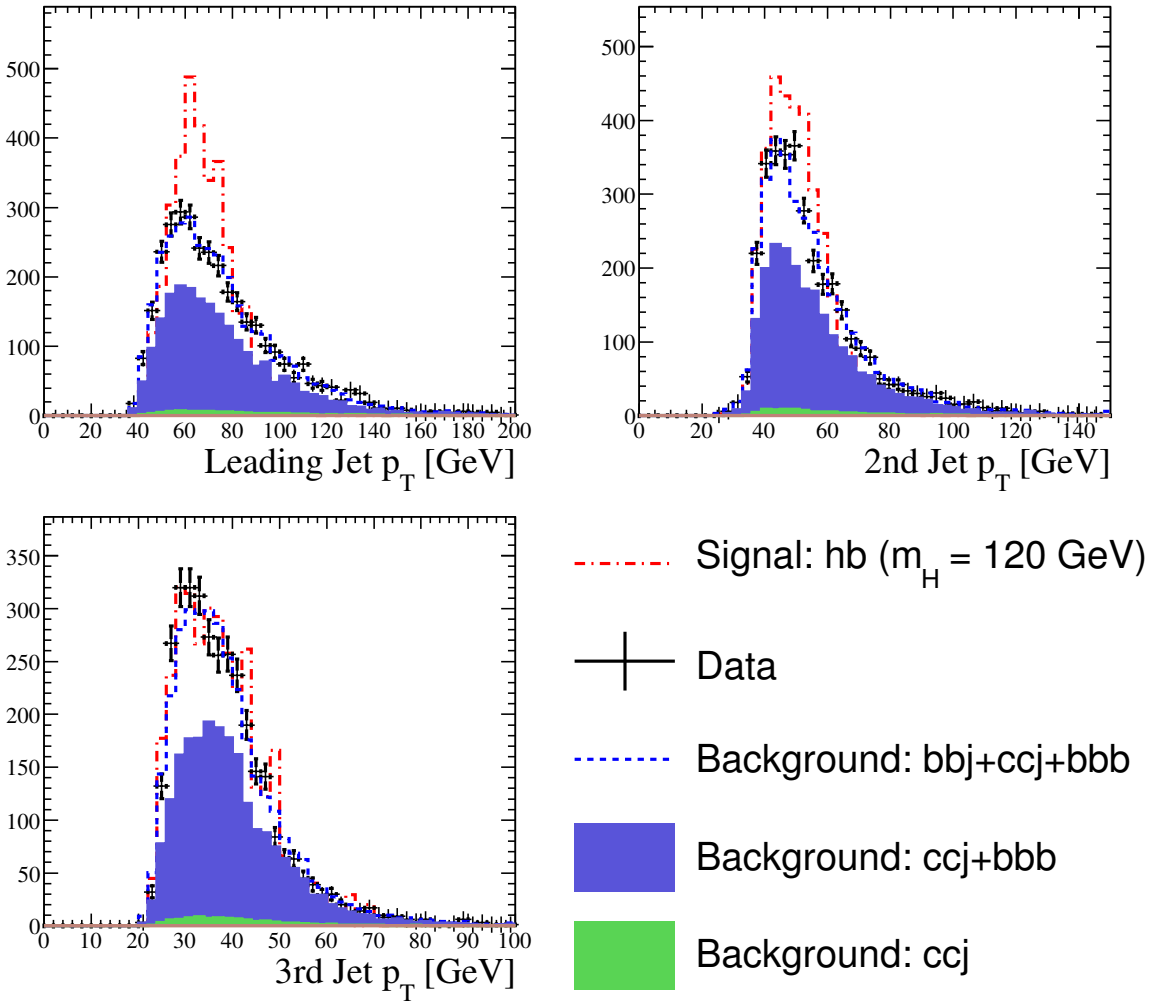


Figure 56: Data predicted background comparison for 4 jets, 3 $b$-tag sample with a 120 GeV Higgs Sample used as signal. Shown is jet $p_T$ for the three jets with the highest $p_T$ in the event.

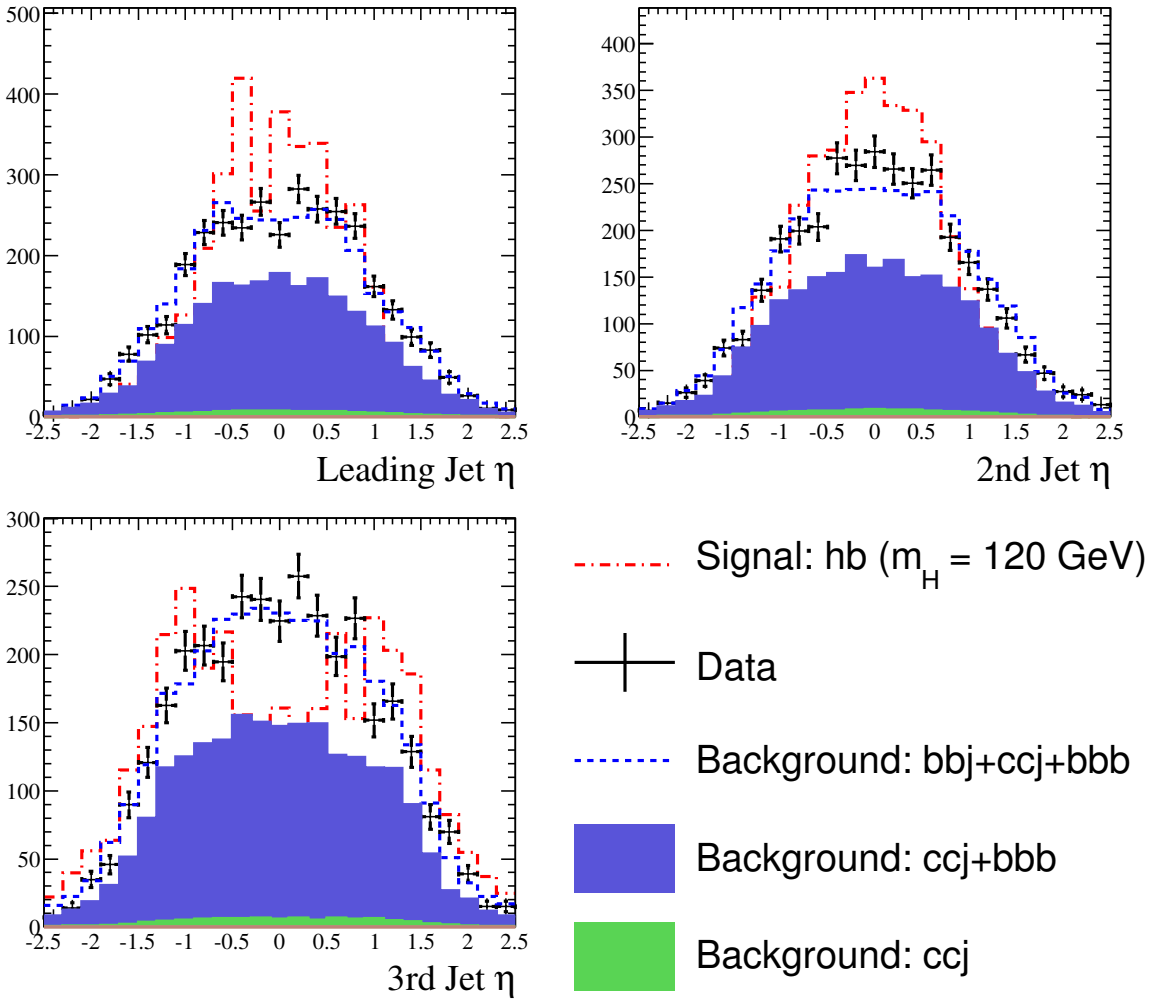


Figure 57: Data predicted background comparison for 4 jets, 3 $b$-tag sample with a 120 GeV Higgs Sample used as signal. Shown is jet $\eta$ for the three jets with the highest $p_T$ in the event.

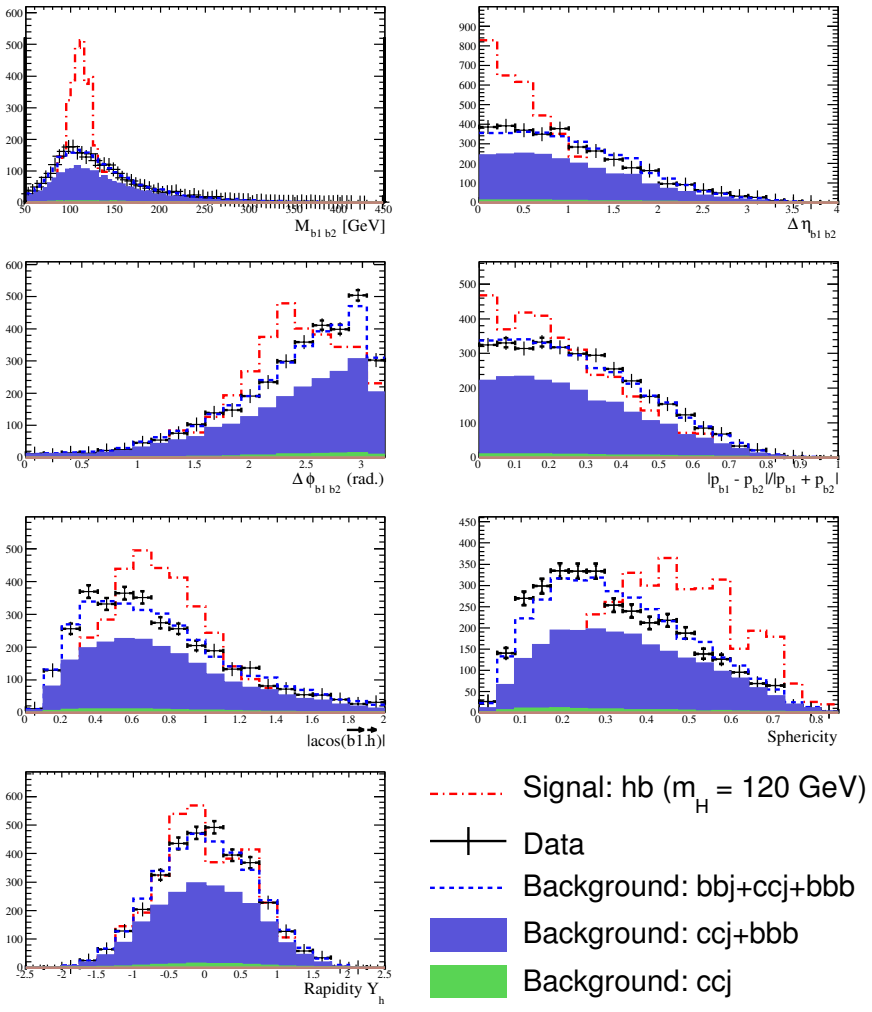


Figure 58: Data predicted background comparison for 4 jets, 3 $b$-tag sample with a 120 GeV Higgs Sample used as signal. Shown are the variables used to determine the signal likelihood (see table 13).

### B.1.3 5 jet events

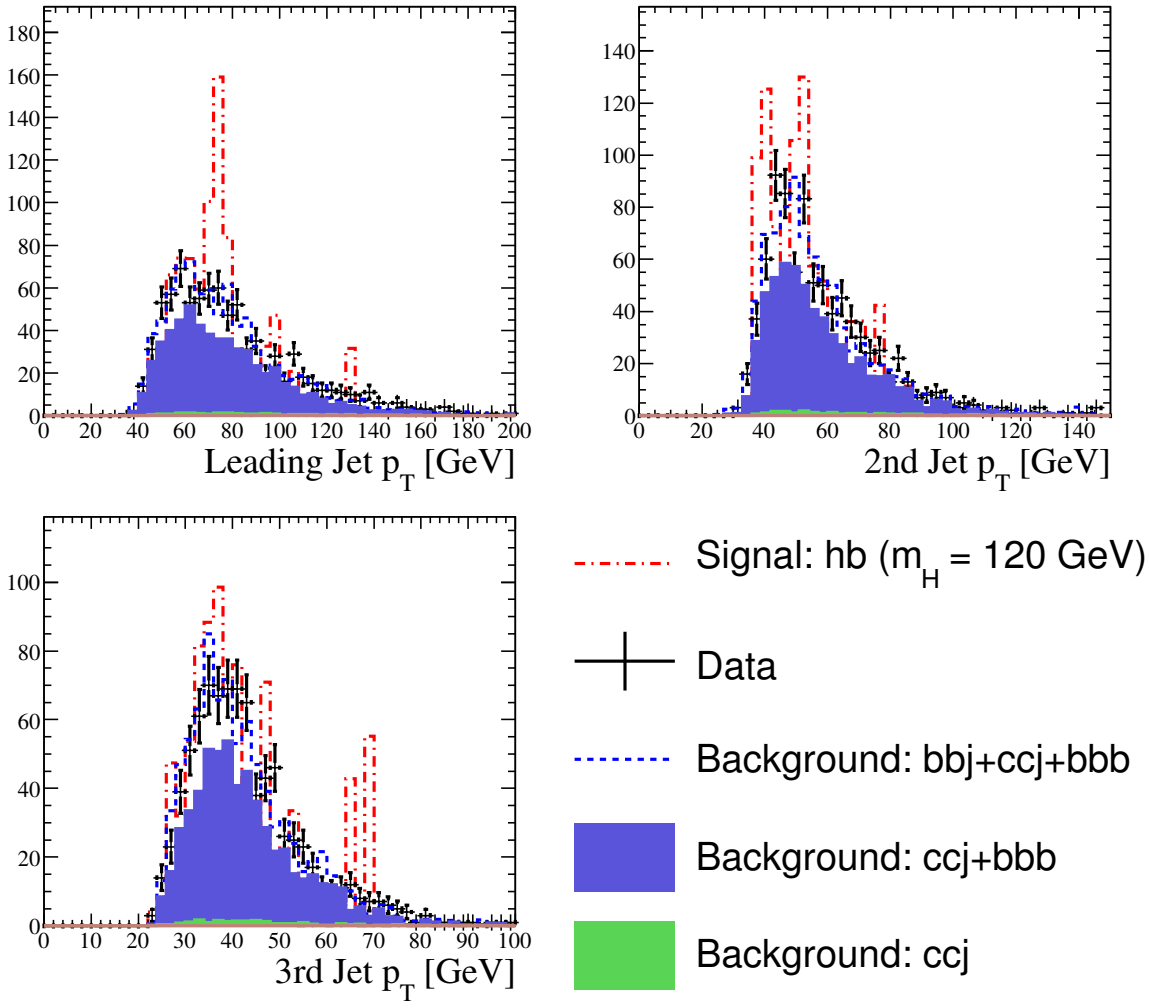


Figure 59: Data predicted background comparison for 5 jets, 3 $b$-tag sample with a 120 GeV Higgs Sample used as signal. Shown is jet $p_T$ for the three jets with the highest $p_T$ in the event.

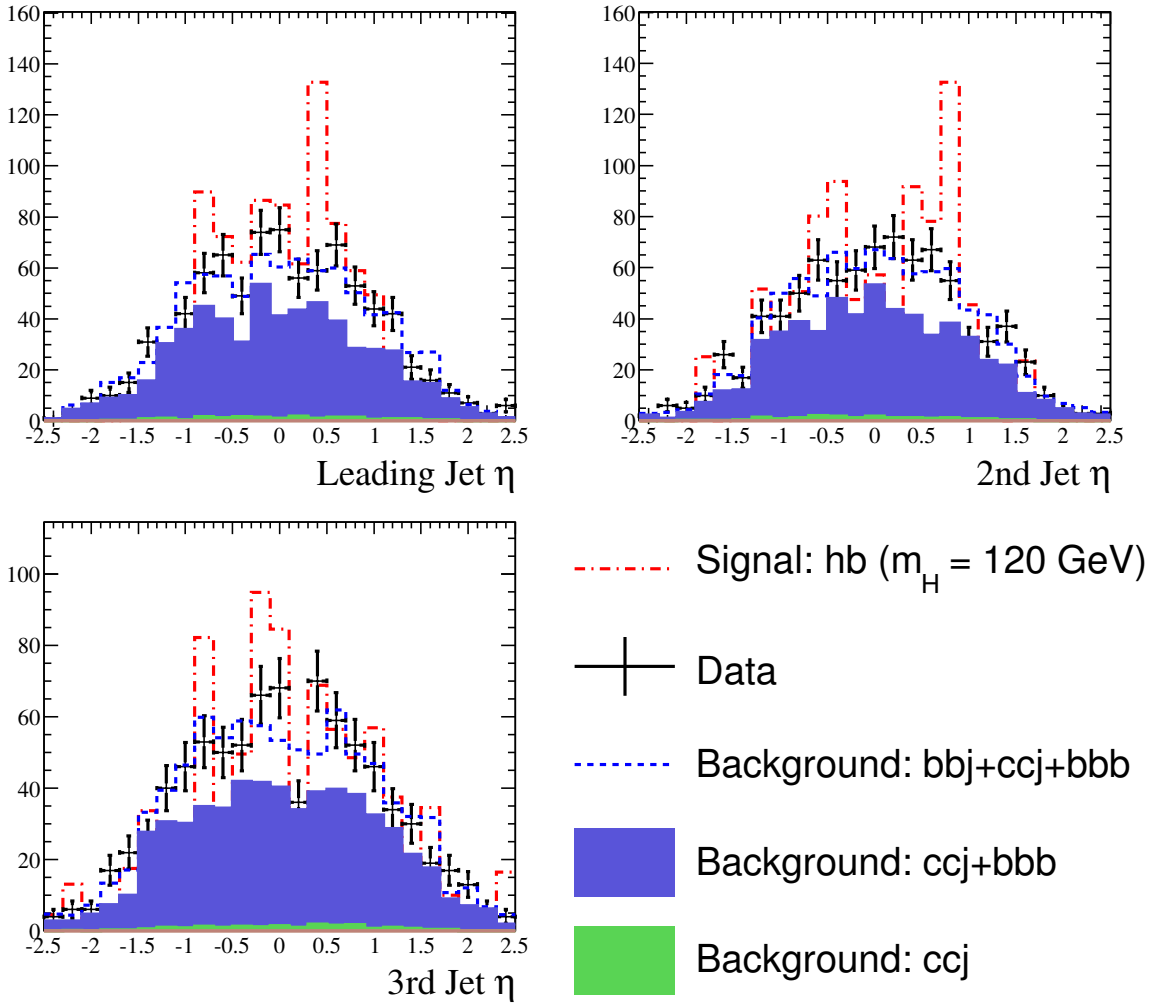


Figure 60: Data predicted background comparison for 5 jets, 3 $b$-tag sample with a 120 GeV Higgs Sample used as signal. Shown is jet $\eta$ for the three jets with the highest $p_T$ in the event.

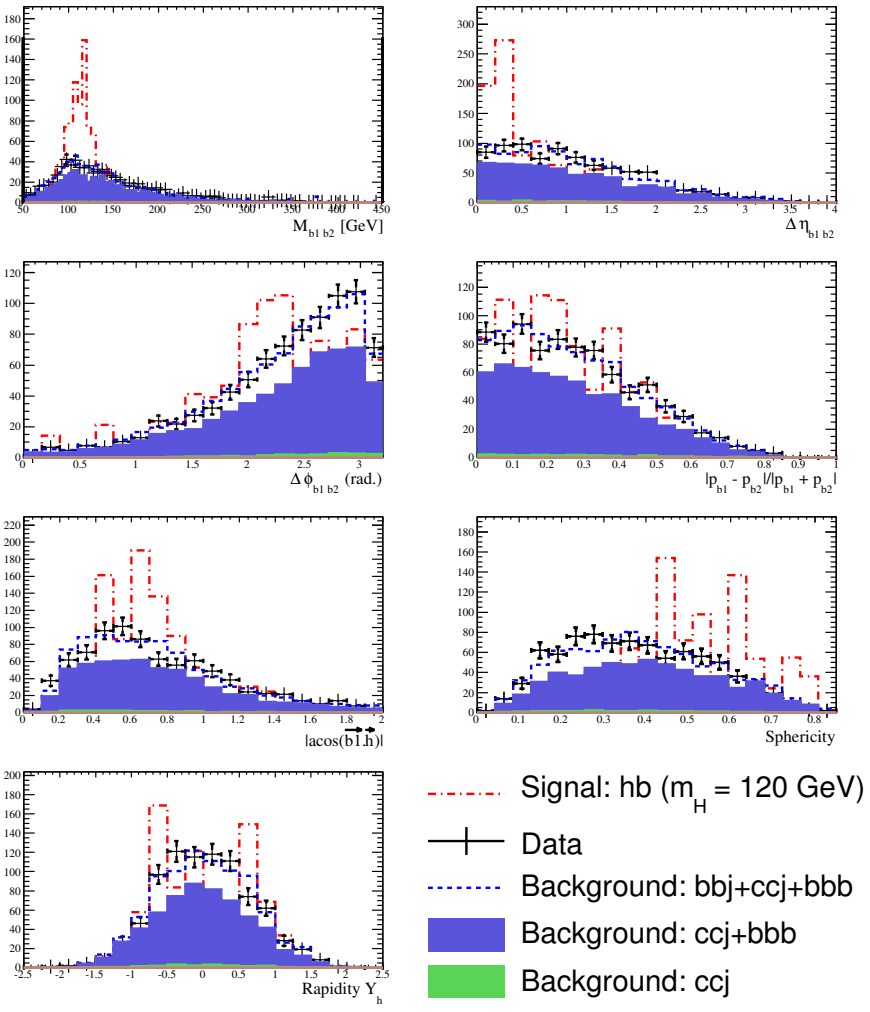


Figure 61: Data predicted background comparison for 5 jets, 3 $b$-tag sample with a 120 GeV Higgs Sample used as signal. Shown are the variables used to determine the signal likelihood (see table 13).

## B.2 High Mass Likelihood

Figures 62 - 67 show comparison plots between data and the predicted background for the 4 and 5 jet channels for the 180 GeV mass point.

### B.2.1 4 jet events

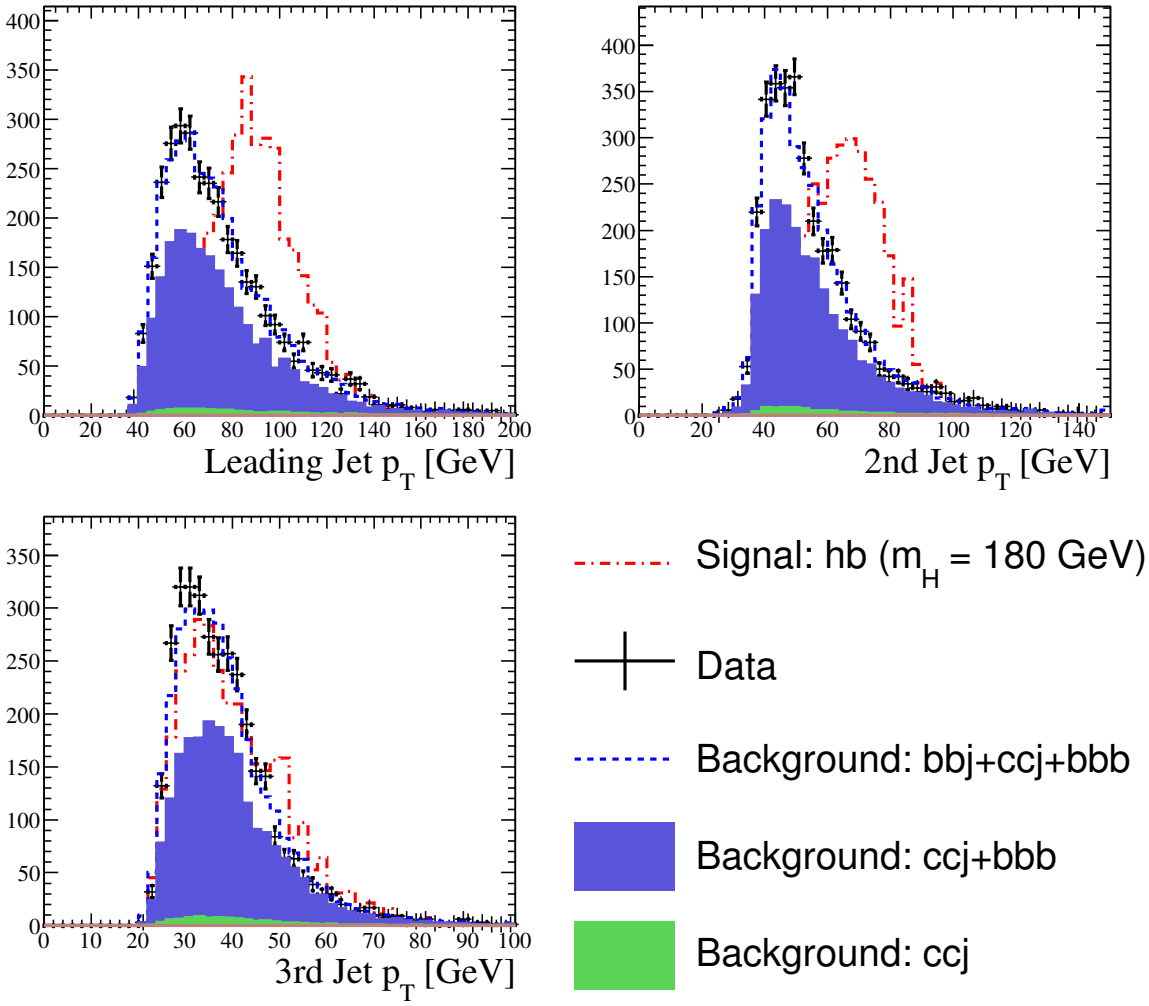


Figure 62: Data predicted background comparison for 4 jets, 3 $b$-tag sample with a 180 GeV Higgs Sample used as signal. Shown is jet $p_T$ for the three jets with the highest $p_T$ in the event.

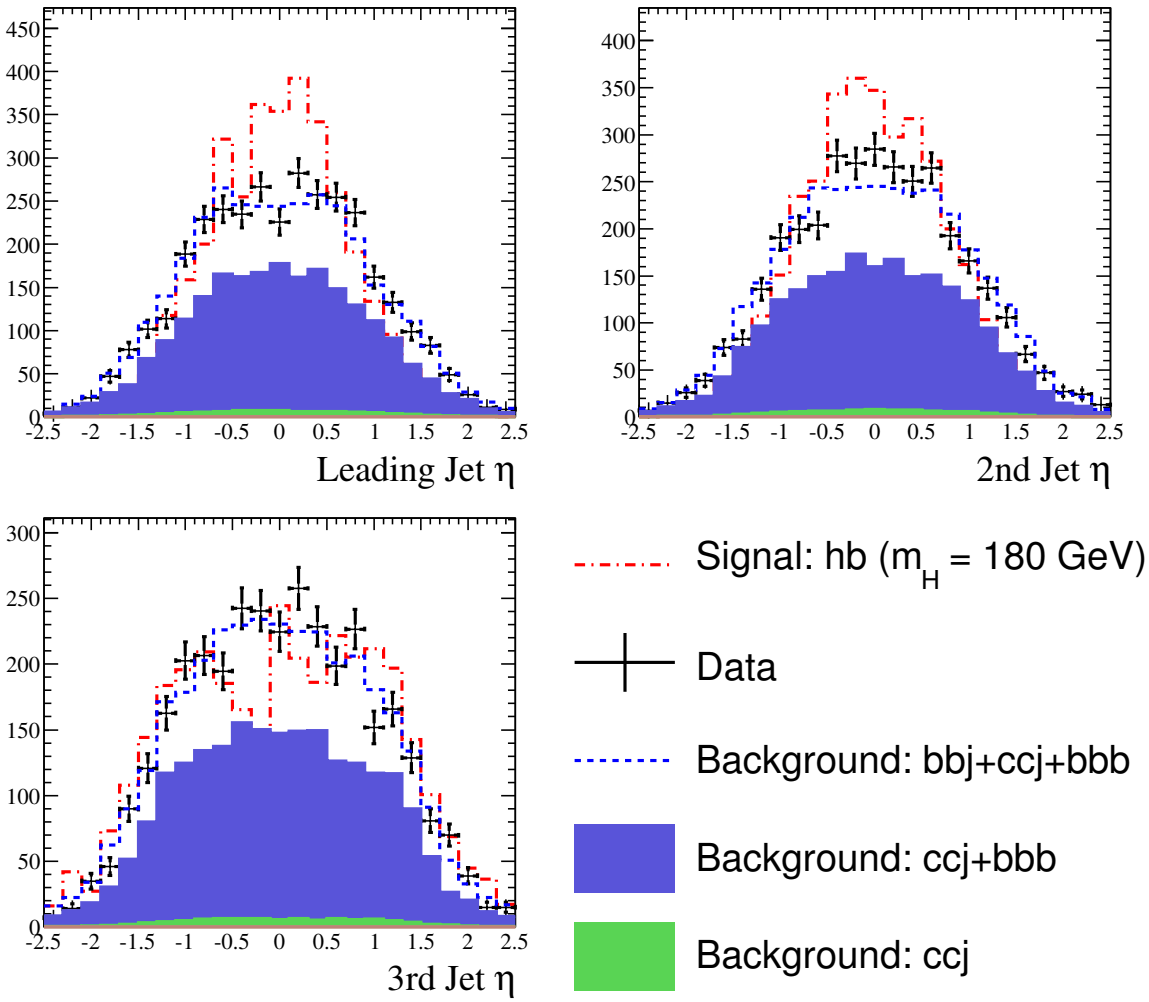


Figure 63: Data predicted background comparison for 4 jets, 3 $b$-tag sample with a 180 GeV Higgs Sample used as signal. Shown is jet $\eta$ for the three jets with the highest $p_T$ in the event.

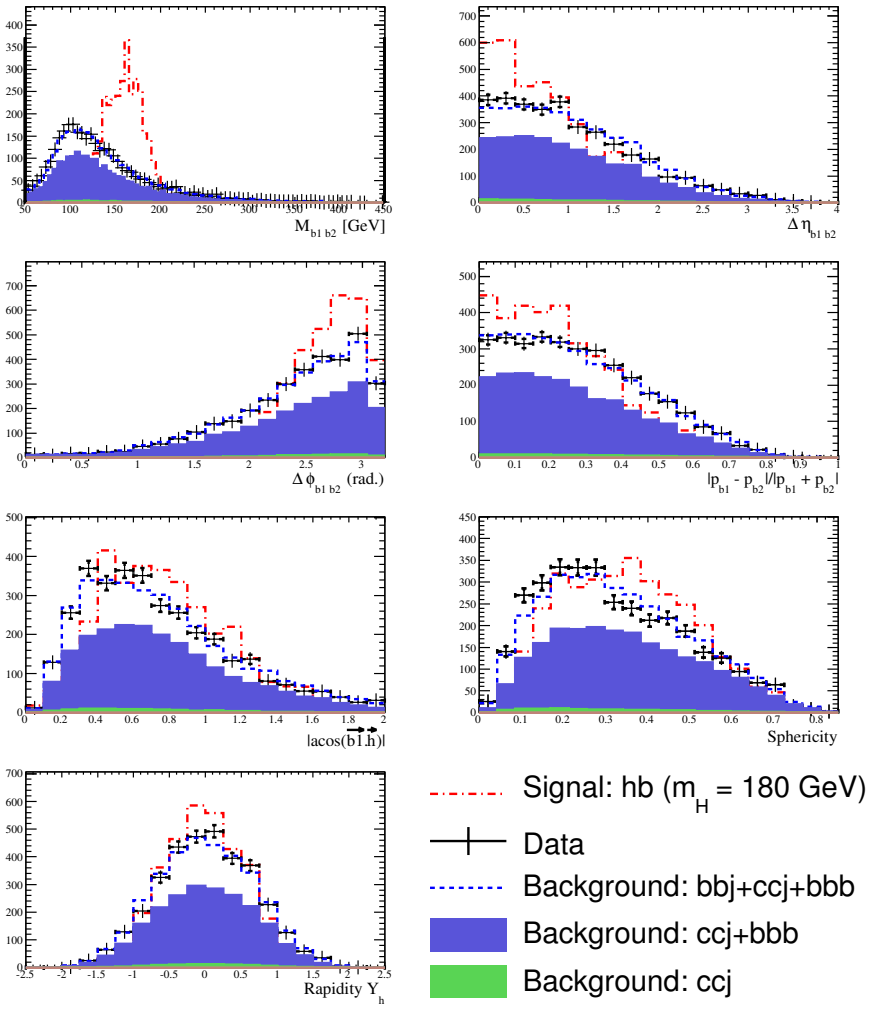


Figure 64: Data predicted background comparison for 4 jets, 3 $b$-tag sample with a 180 GeV Higgs Sample used as signal. Shown are the variables used to determine the signal likelihood (see table 13).

### B.2.2 5 jet events

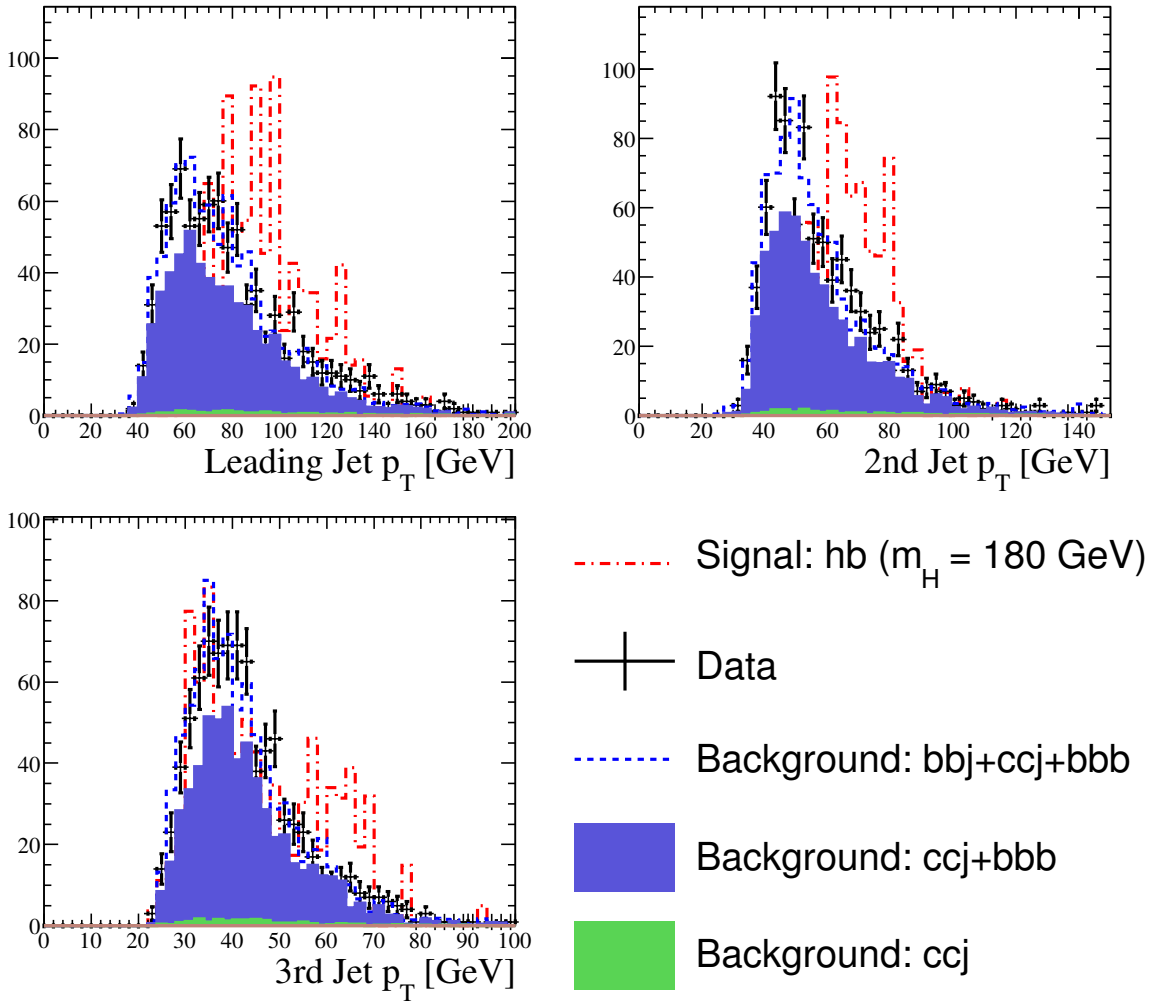


Figure 65: Data predicted background comparison for 5 jets, 3 $b$-tag sample with a 180 GeV Higgs Sample used as signal. Shown is jet $p_T$ for the three jets with the highest $p_T$ in the event.

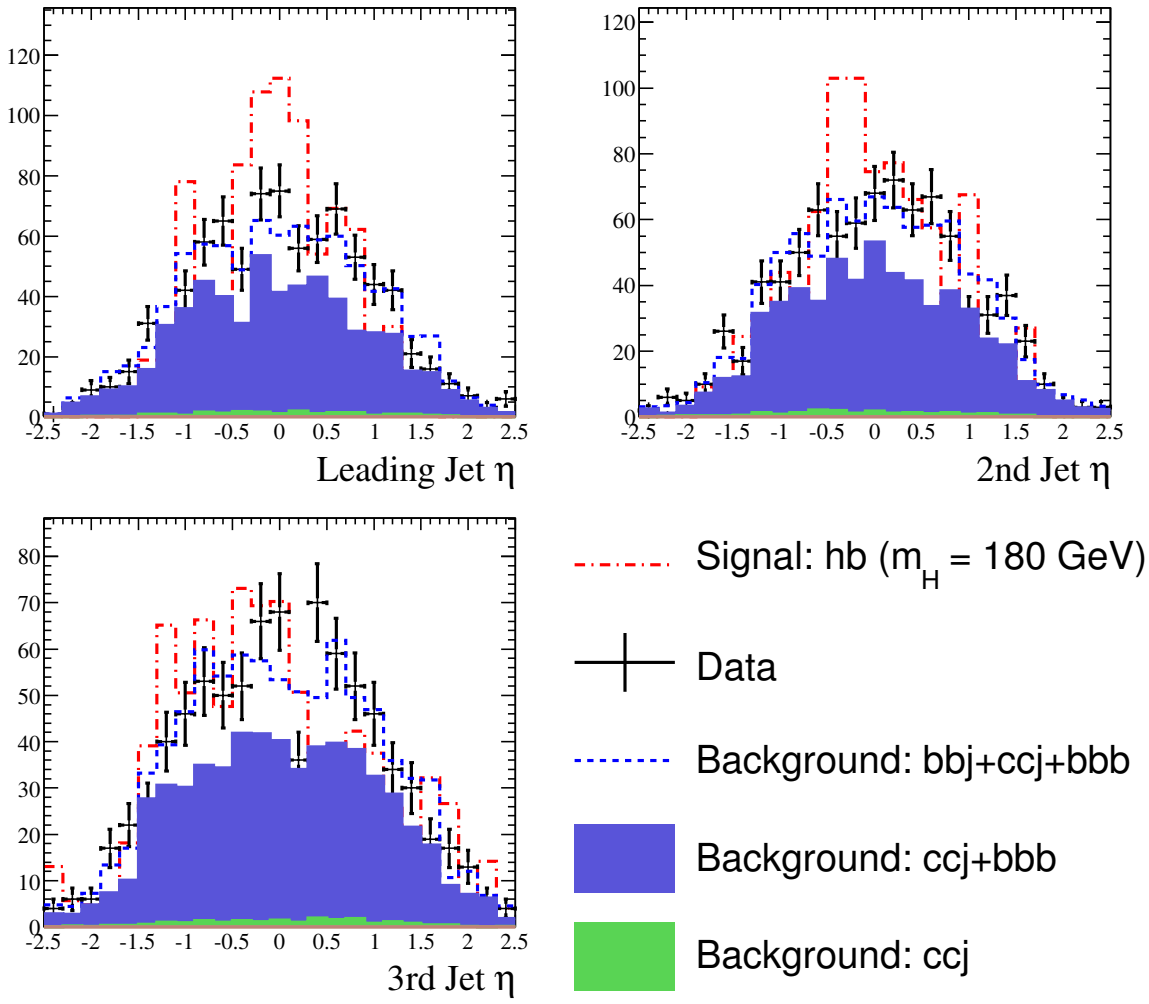


Figure 66: Data predicted background comparison for 5 jets, 3 $b$-tag sample with a 180 GeV Higgs Sample used as signal. Shown is jet $\eta$ for the three jets with the highest $p_T$ in the event.

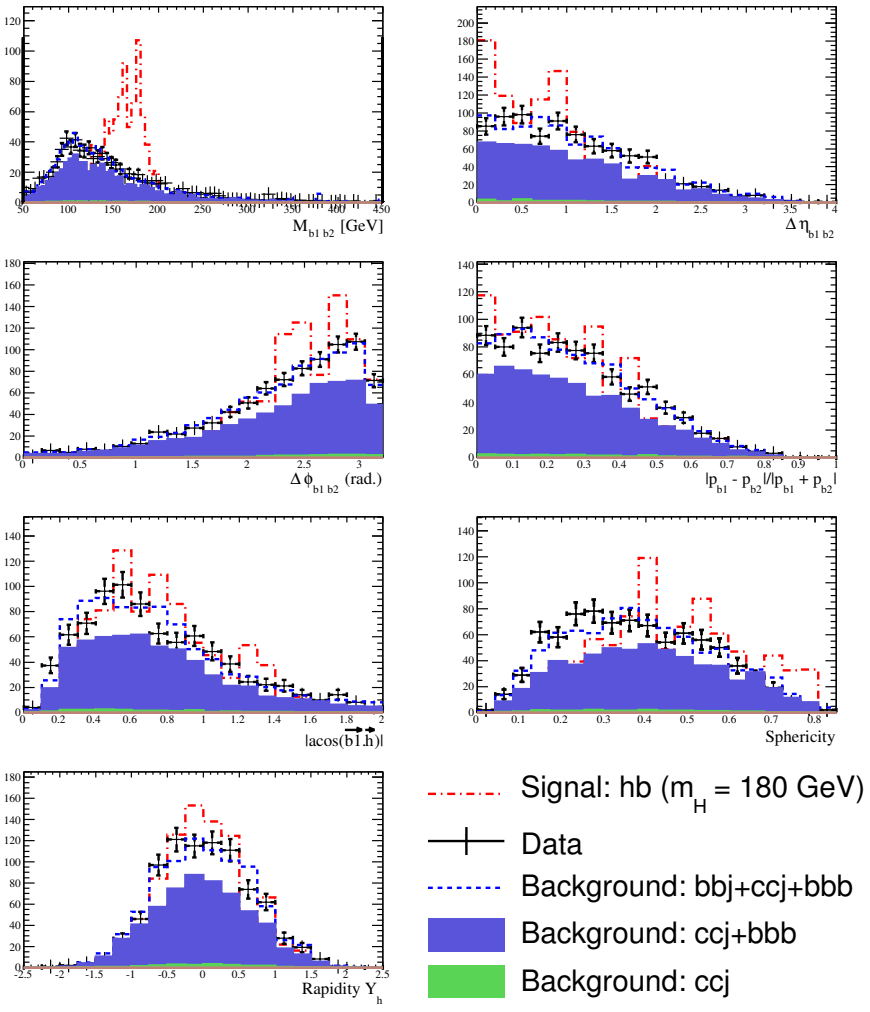


Figure 67: Data predicted background comparison for 5 jets, 3 $b$-tag sample with a 180 GeV Higgs Sample used as signal. Shown are the variables used to determine the signal likelihood (see table 13).

# C Data Monte Carlo Comparison

## C.1 Low Likelihood Sample

### C.1.1 Three jet, two tag sample

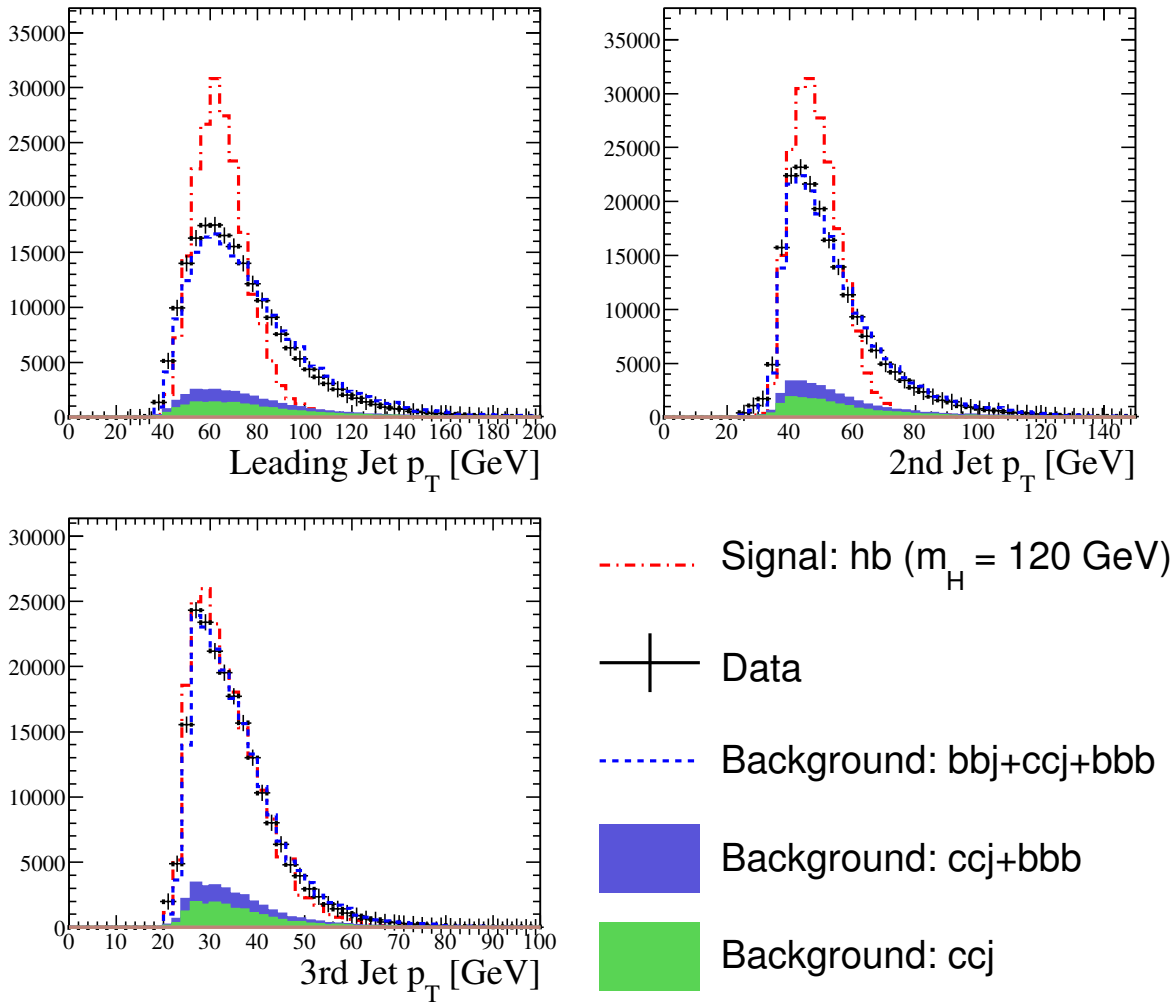


Figure 68: Data Monte Carlo comparison for 3 jets, 2 $b$-tag sample with a 120 GeV Higgs Sample used as signal. Shown is jet $p_T$ for the three jets with the highest $p_T$ in the event.

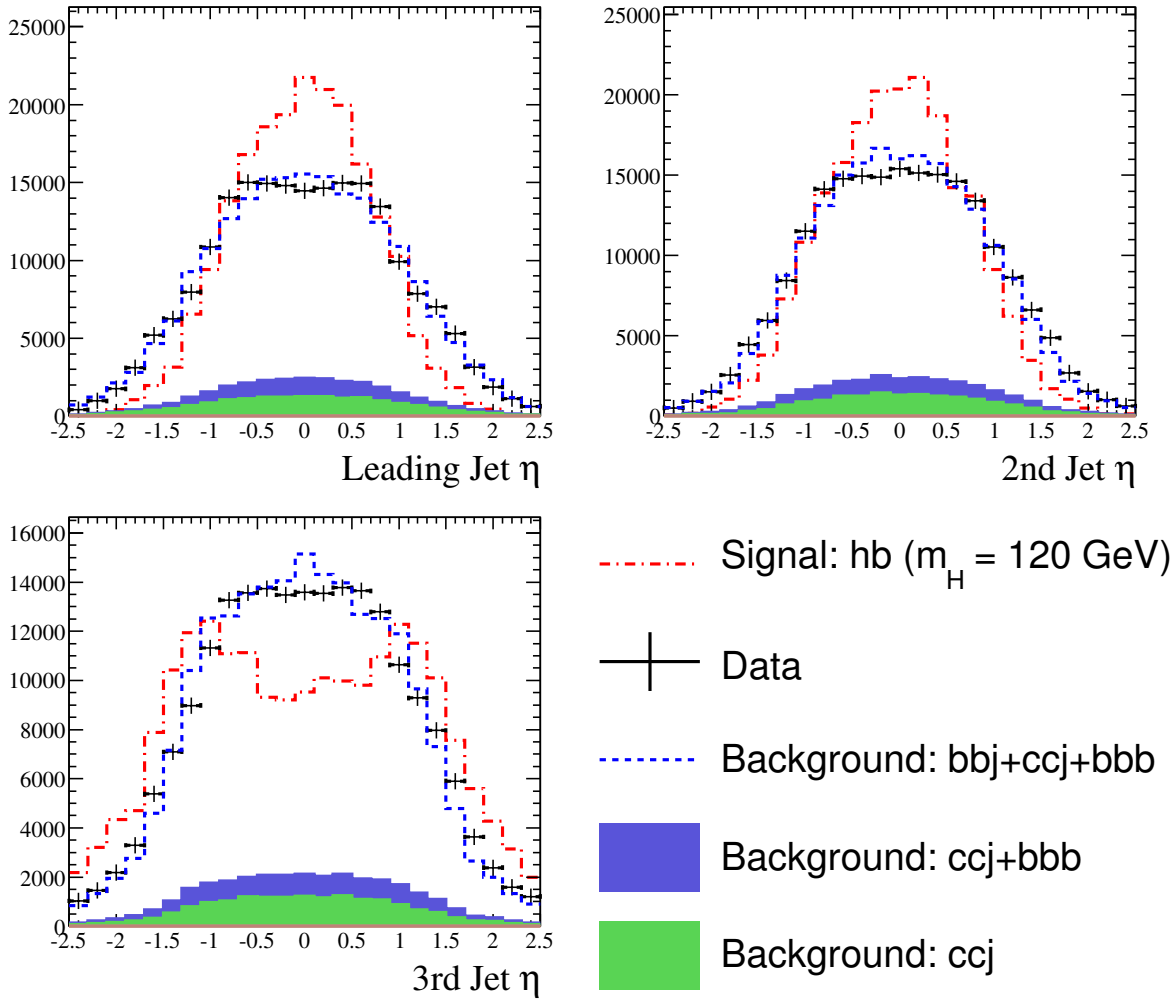


Figure 69: Data Monte Carlo comparison for 3 jets, 2 $b$-tag sample with a 120 GeV Higgs Sample used as signal. Shown is jet $\eta$ for the three jets with the highest $p_T$ in the event.

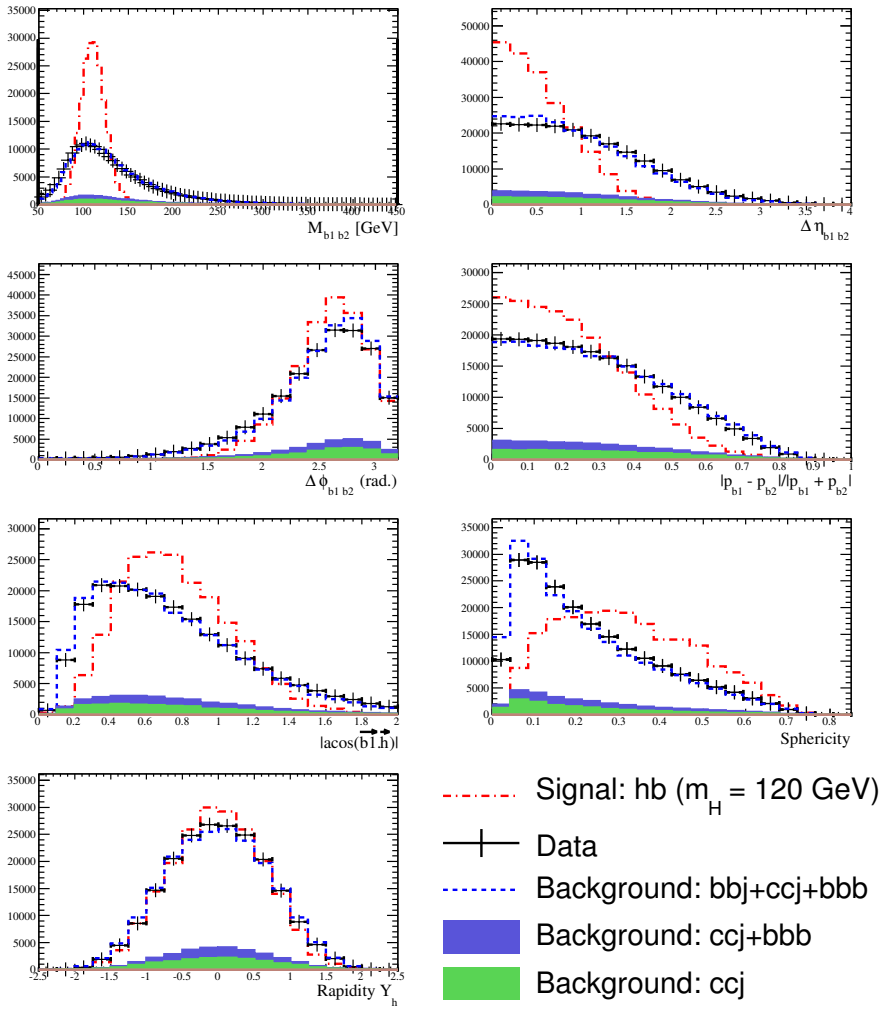


Figure 70: Data Monte Carlo comparison for 3 jets, 2 $b$-tag sample with a 120 GeV Higgs Sample used as signal. Shown are the variables used to determine the signal likelihood (see table 13).

### C.1.2 Four jet, two tag sample

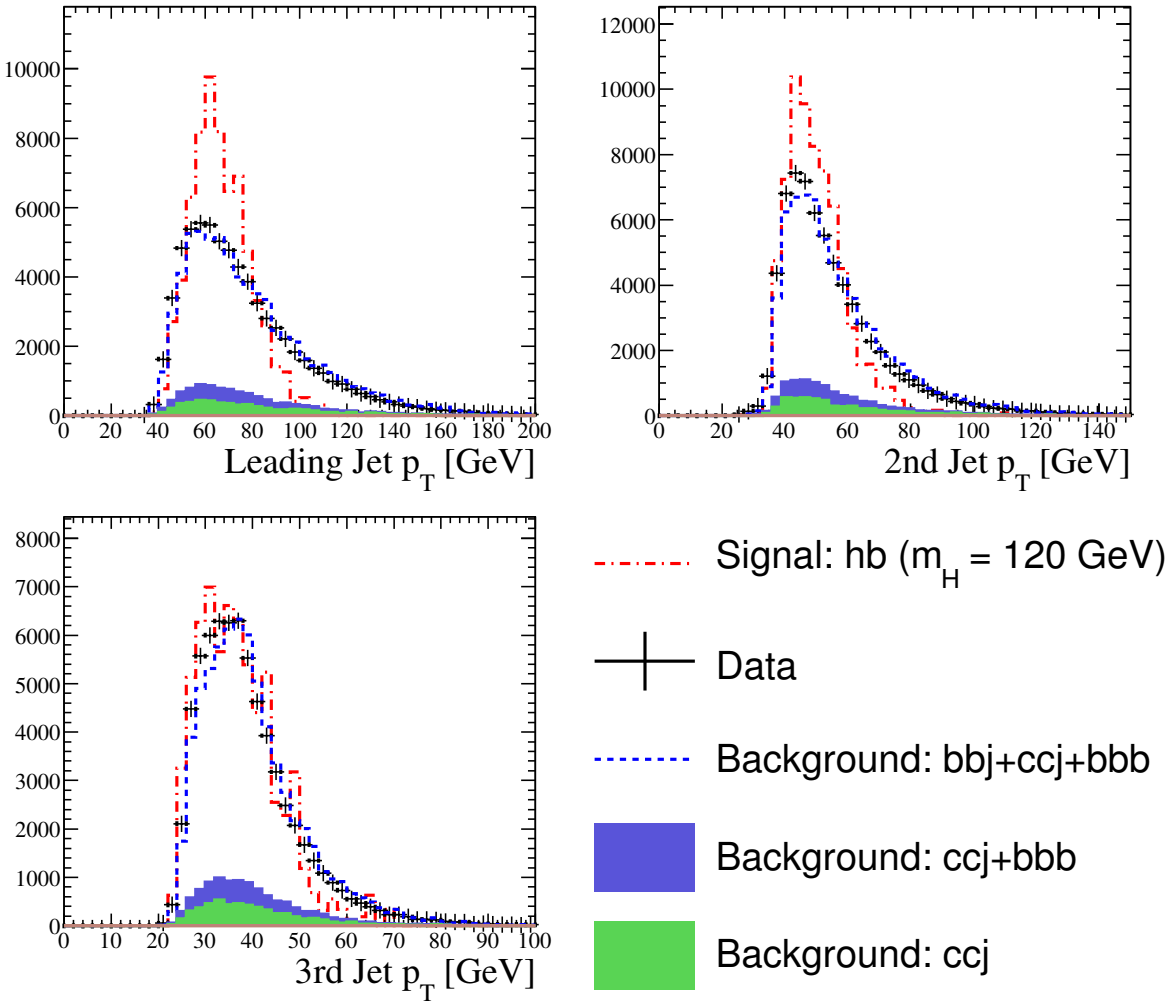


Figure 71: Data Monte Carlo comparison for 4 jets, 2 $b$-tag sample with a 120 GeV Higgs Sample used as signal. Shown is jet $p_T$ for the three jets with the highest $p_T$ in the event.

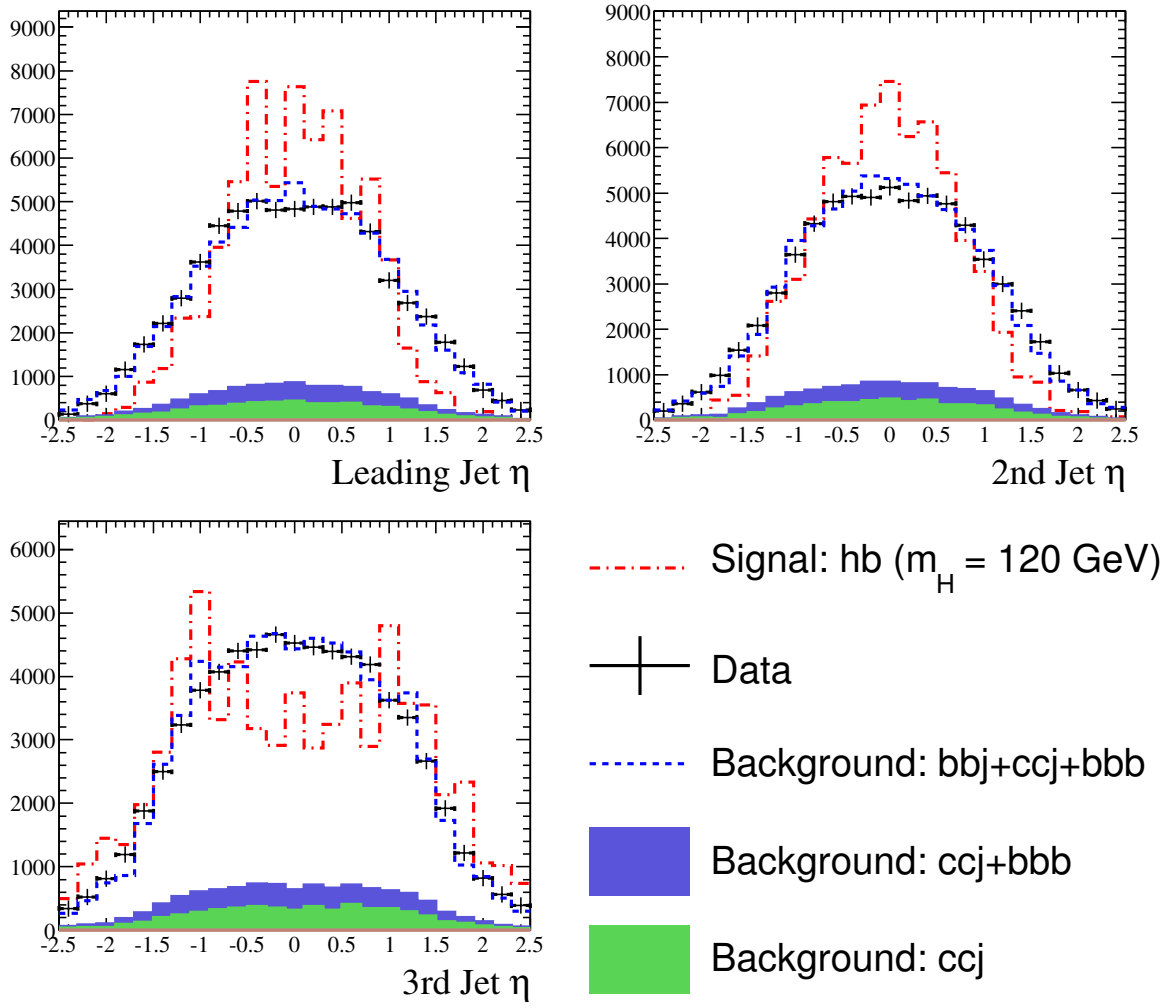


Figure 72: Data Monte Carlo comparison for 4 jets, 2 $b$-tag sample with a 120 GeV Higgs Sample used as signal. Shown is jet $\eta$ for the three jets with the highest $p_T$ in the event.

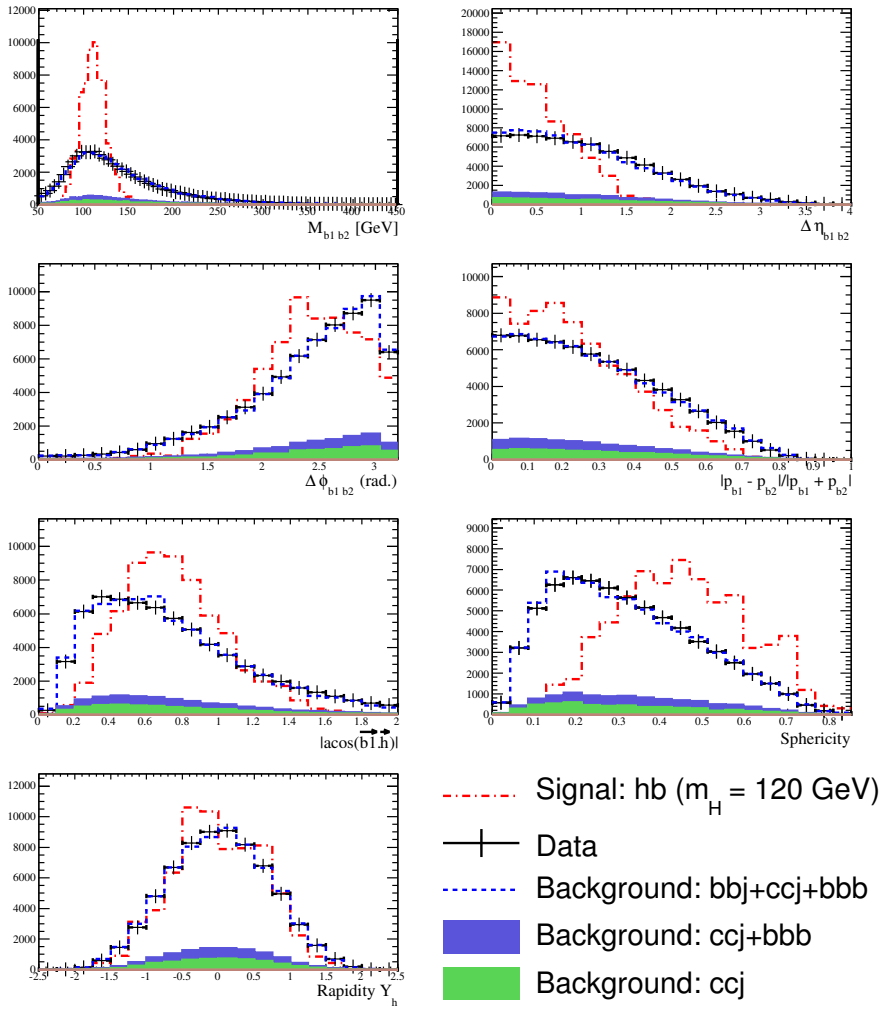


Figure 73: Data Monte Carlo comparison for 4 jets, 2 $b$-tag sample with a 120 GeV Higgs Sample used as signal. Shown are the variables used to determine the signal likelihood (see table 13).

### C.1.3 Five jet, two tag sample

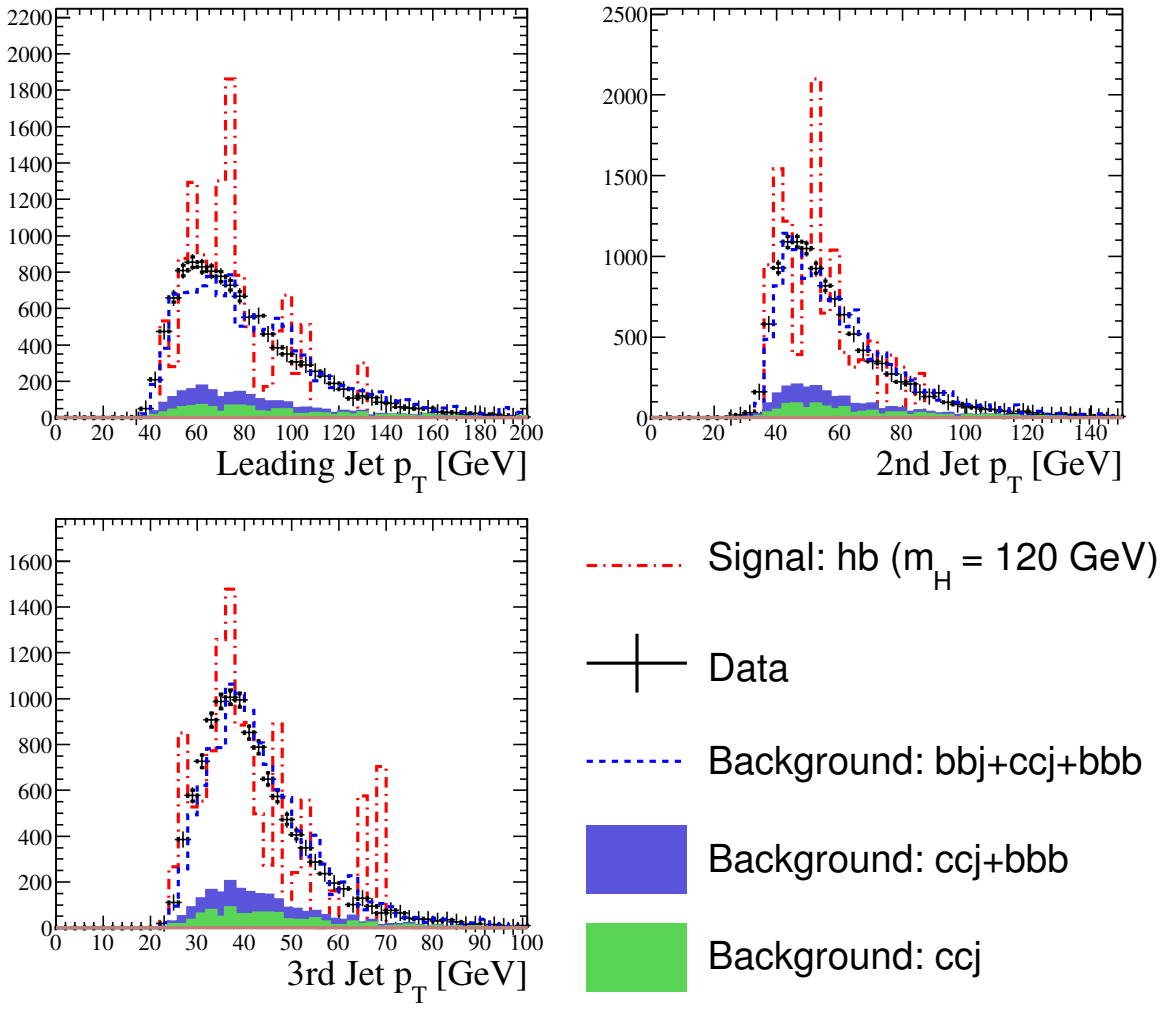


Figure 74: Data Monte Carlo comparison for 5 jets, 2 $b$-tag sample with a 120 GeV Higgs Sample used as signal. Shown is jet $p_T$ for the three jets with the highest $p_T$ in the event.

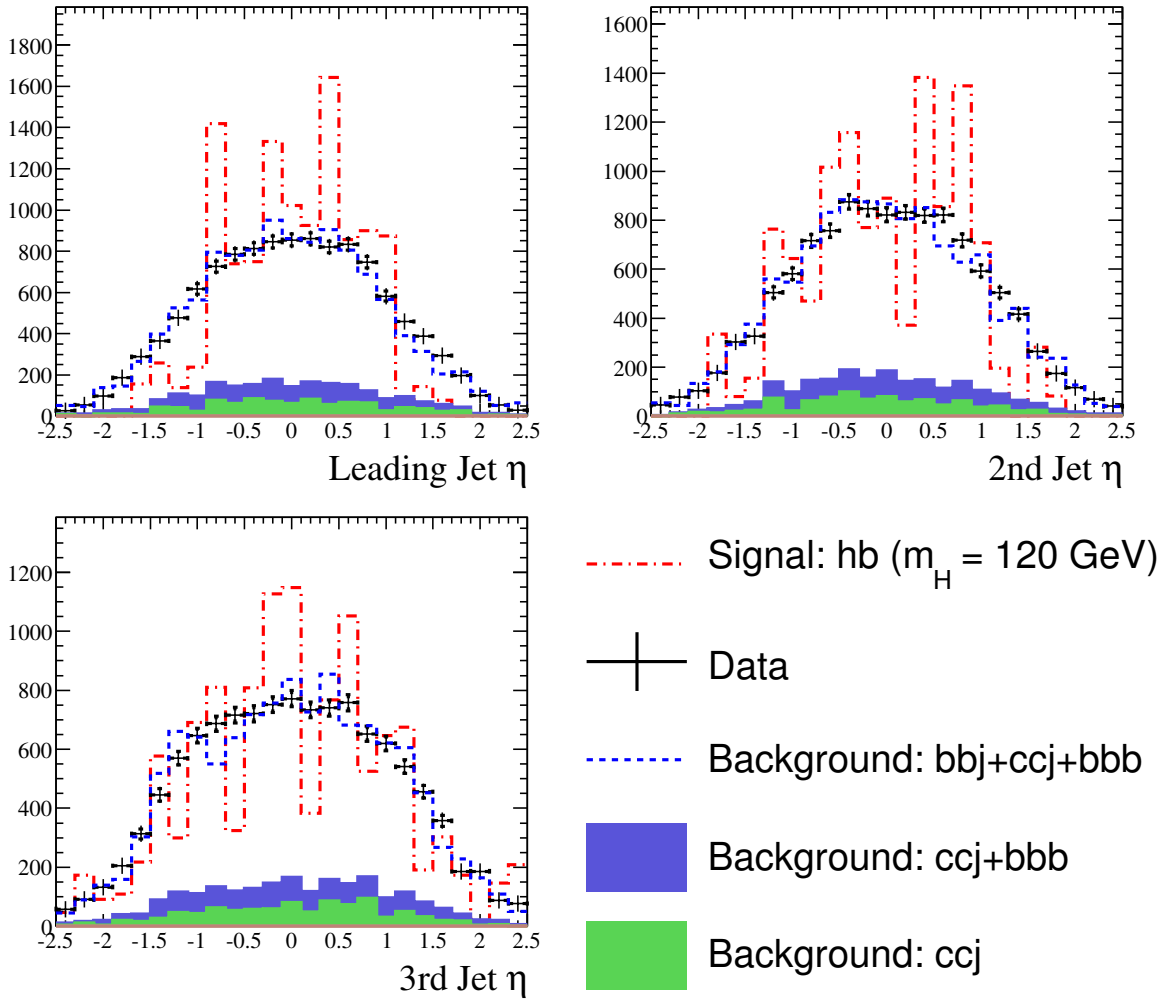


Figure 75: Data Monte Carlo comparison for 5 jets, 2 $b$-tag sample with a 120 GeV Higgs Sample used as signal. Shown is jet $\eta$ for the three jets with the highest $p_T$ in the event.

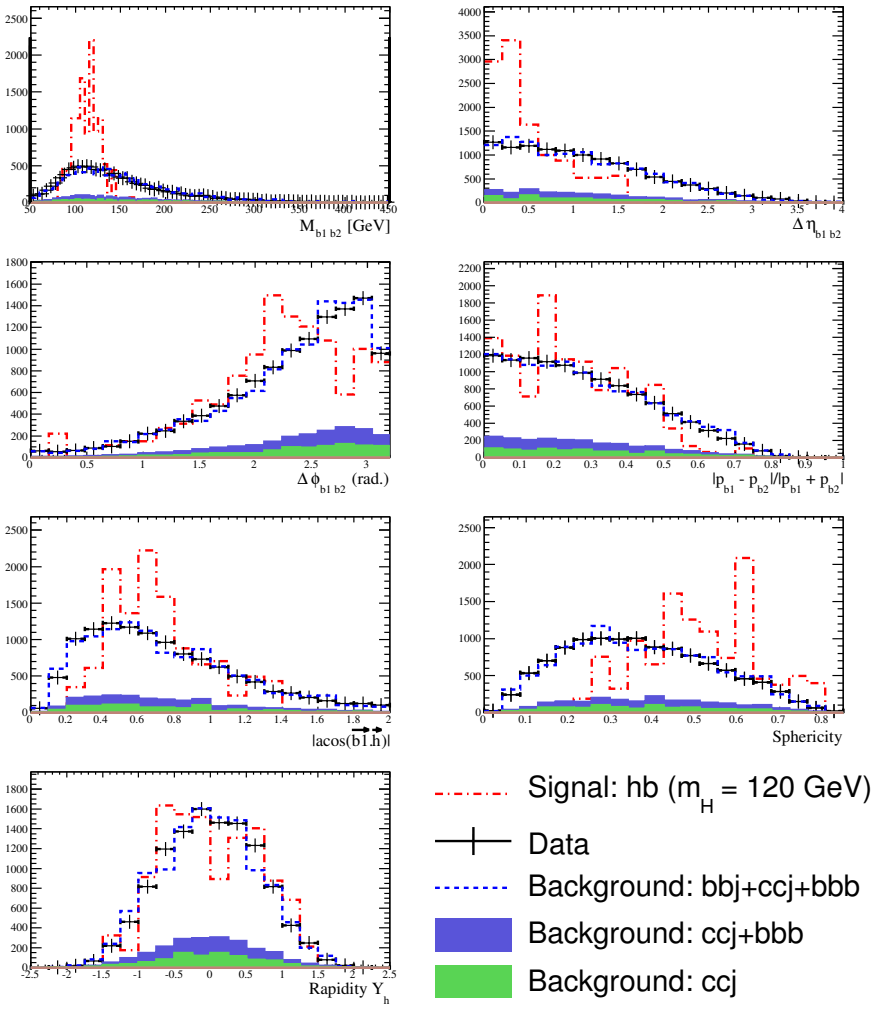


Figure 76: Data Monte Carlo comparison for 5 jets, 2 $b$-tag sample with a 120 GeV Higgs Sample used as signal. Shown are the variables used to determine the signal likelihood (see table 13).

### C.1.4 Three jet, three tag sample

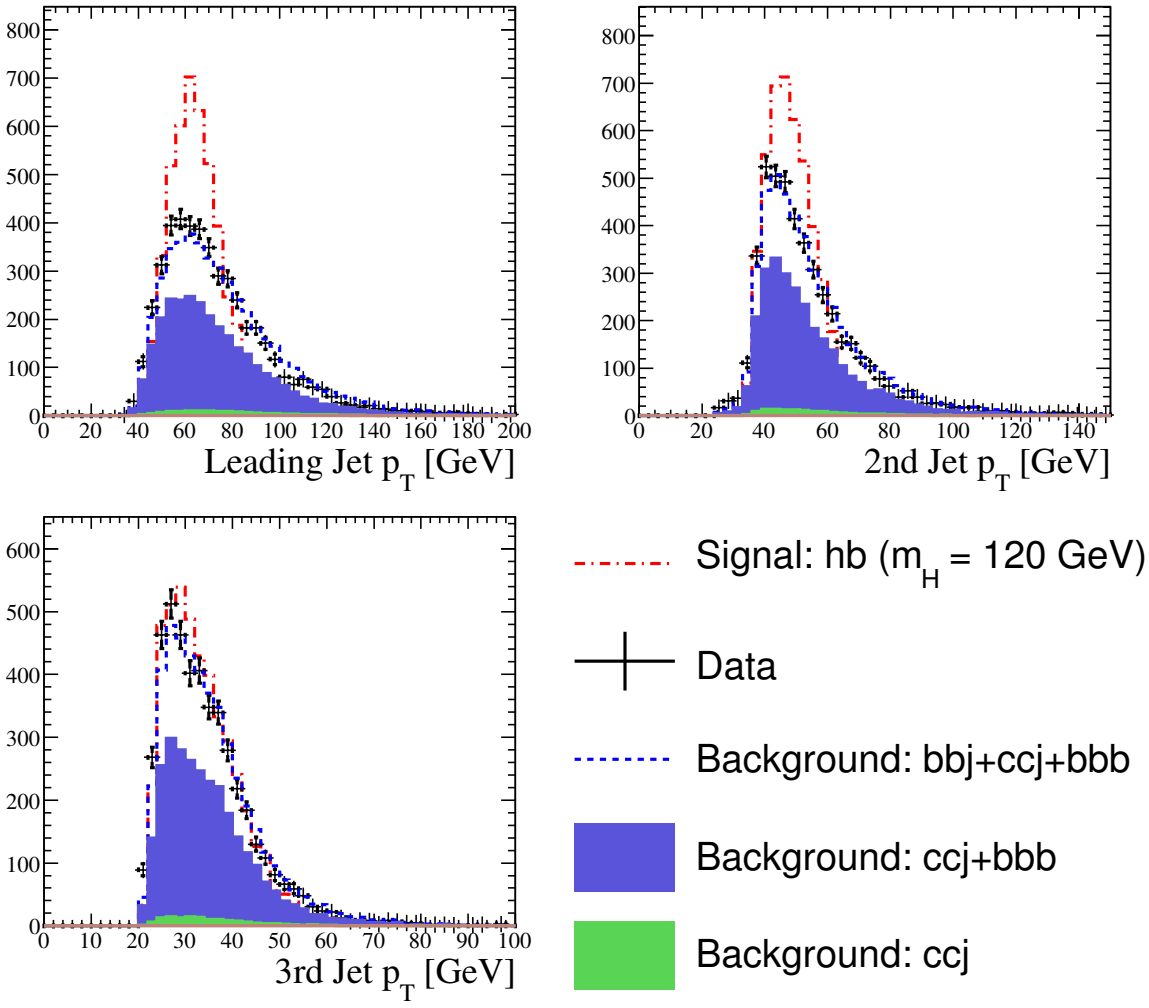


Figure 77: Data Monte Carlo comparison for 3 jets, 3 $b$-tag sample with a 120 GeV Higgs Sample used as signal. Shown is jet $p_T$ for the three jets with the highest $p_T$ in the event.

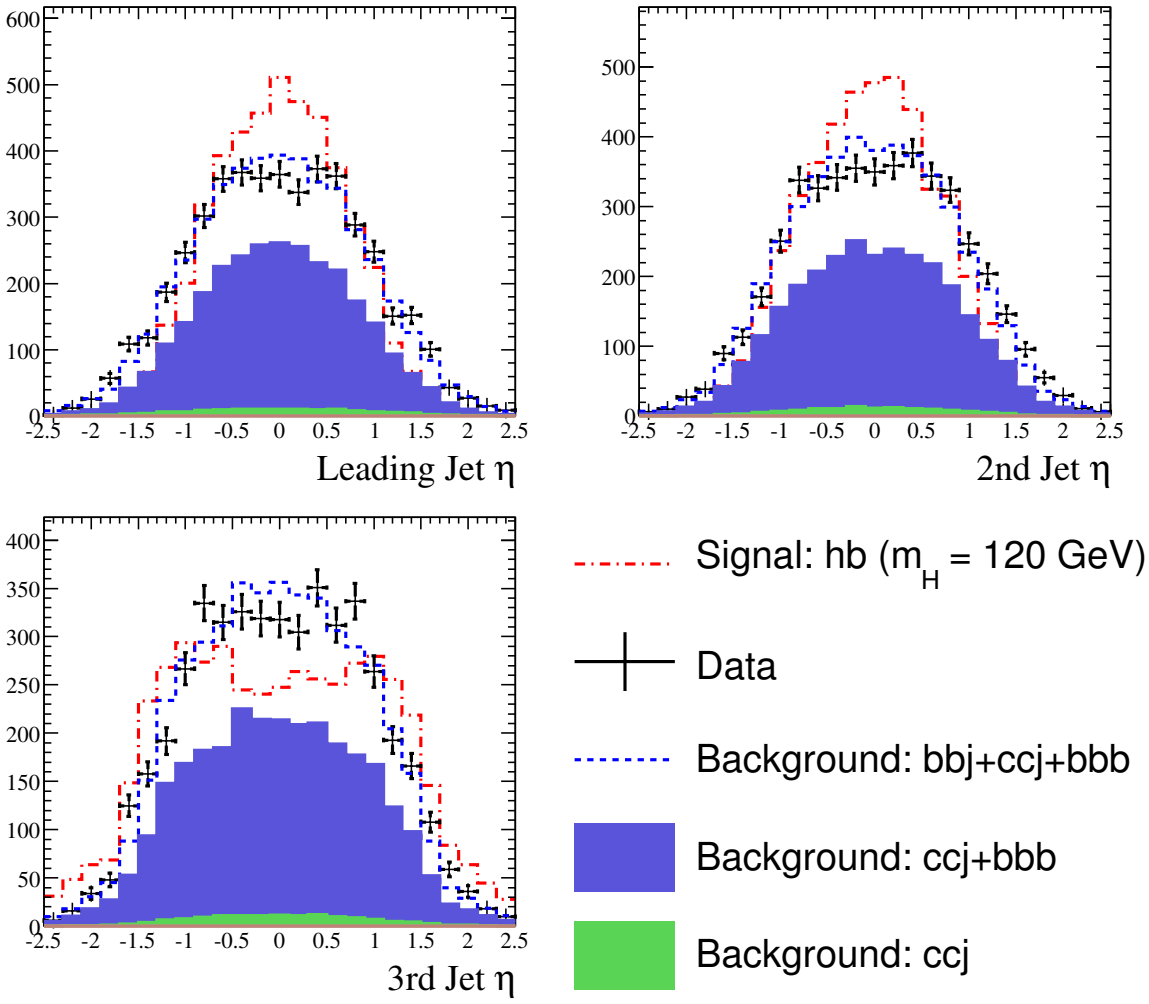


Figure 78: Data Monte Carlo comparison for 3 jets, 3 $b$-tag sample with a 120 GeV Higgs Sample used as signal. Shown is jet $\eta$ for the three jets with the highest $p_T$ in the event.

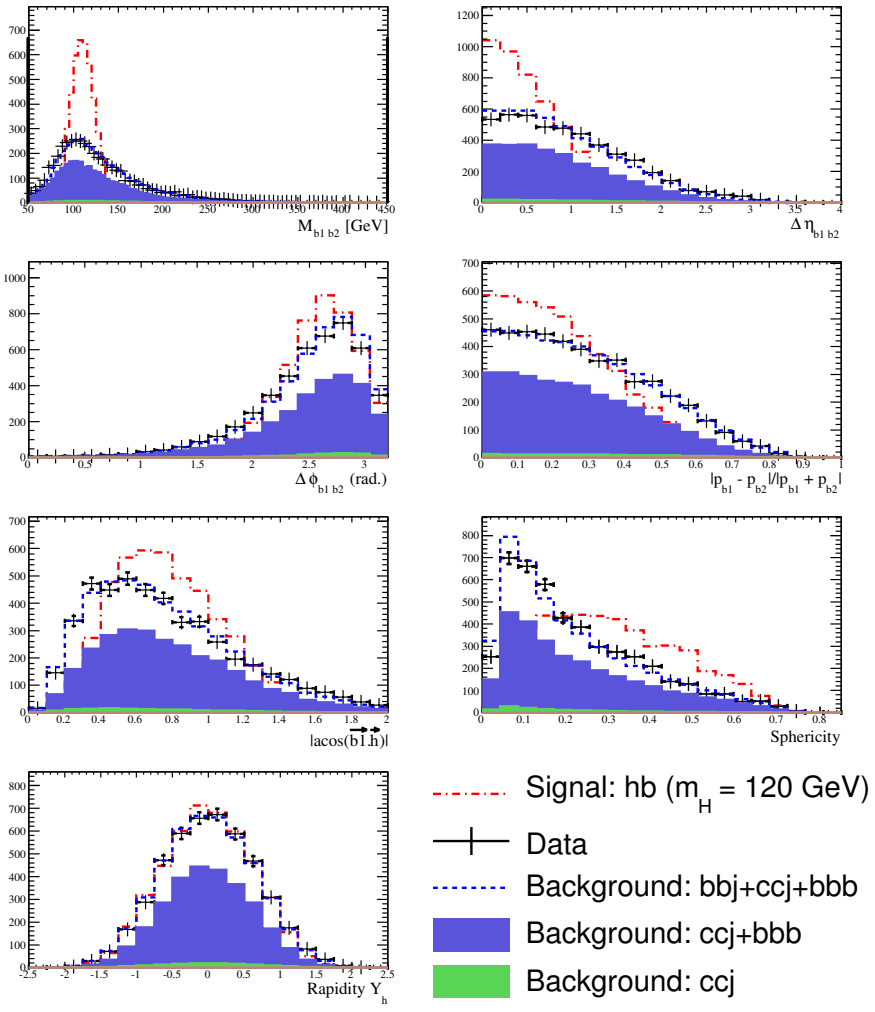


Figure 79: Data Monte Carlo comparison for 3 jets, 3 $b$-tag sample with a 120 GeV Higgs Sample used as signal. Shown are the variables used to determine the signal likelihood (see table 13).

### C.1.5 Four jet, three tag sample

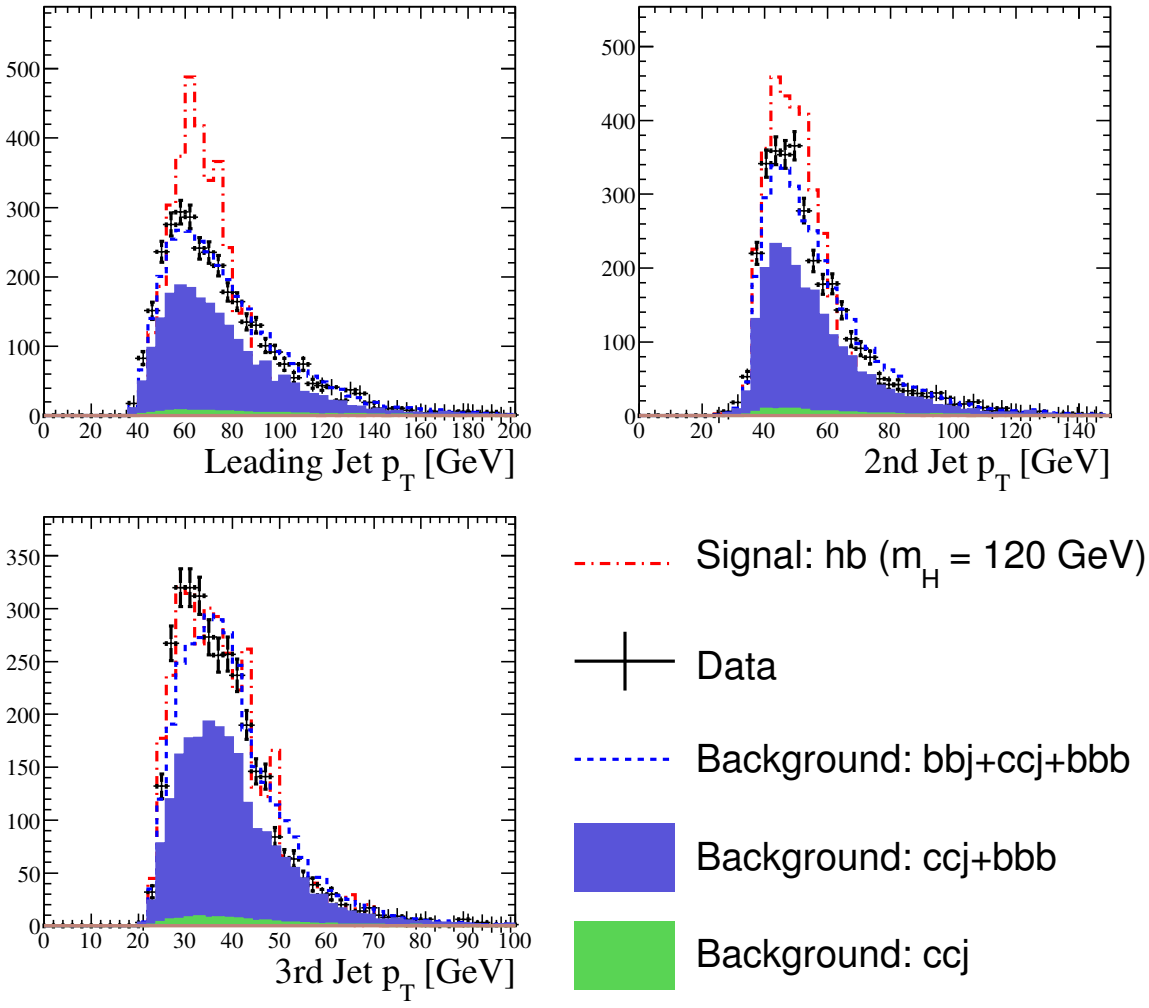


Figure 80: Data Monte Carlo comparison for 4 jets, 3 $b$-tag sample with a 120 GeV Higgs Sample used as signal. Shown is jet $p_T$ for the three jets with the highest $p_T$ in the event.

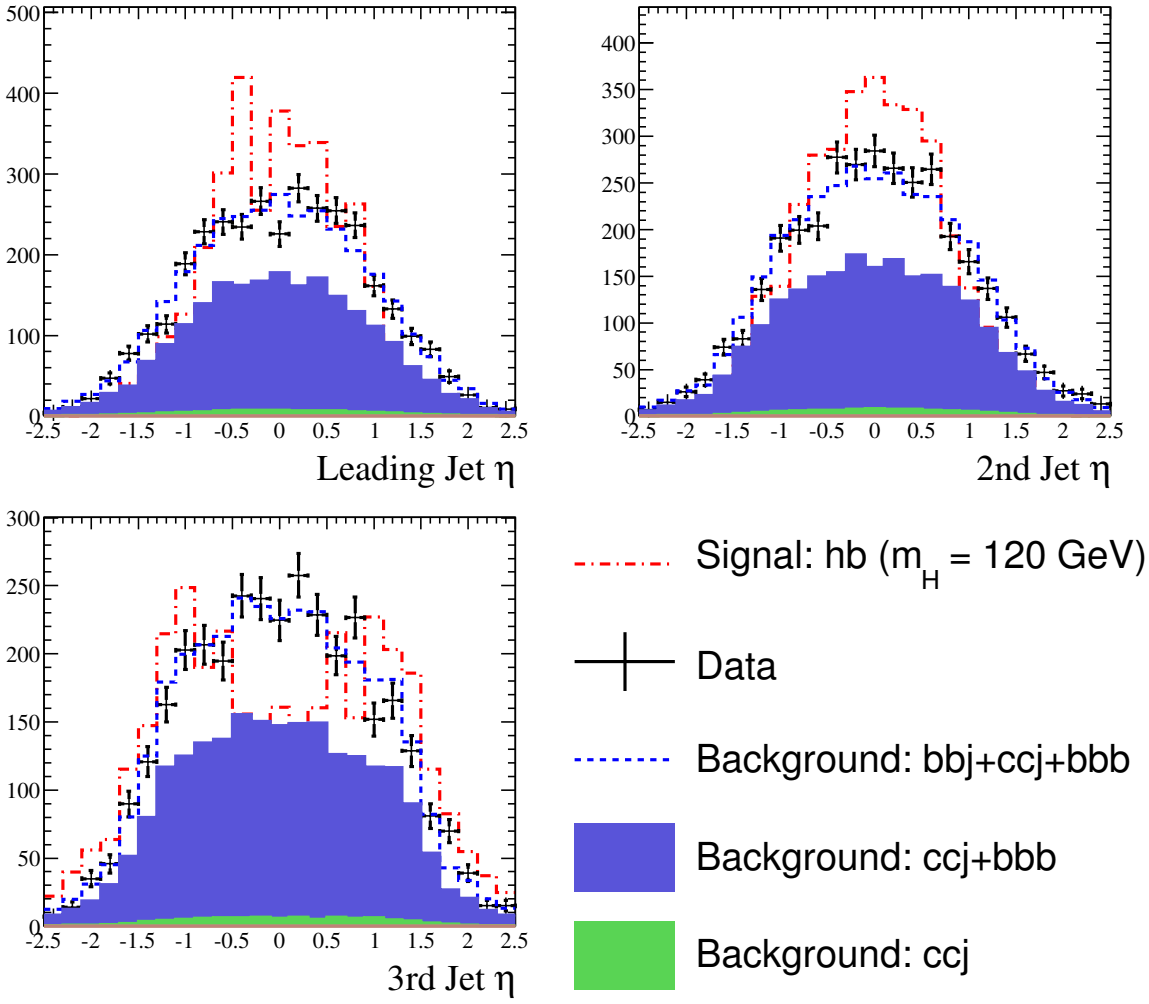


Figure 81: Data Monte Carlo comparison for 4 jets, 3 $b$-tag sample with a 120 GeV Higgs Sample used as signal. Shown is jet $\eta$ for the three jets with the highest $p_T$ in the event.

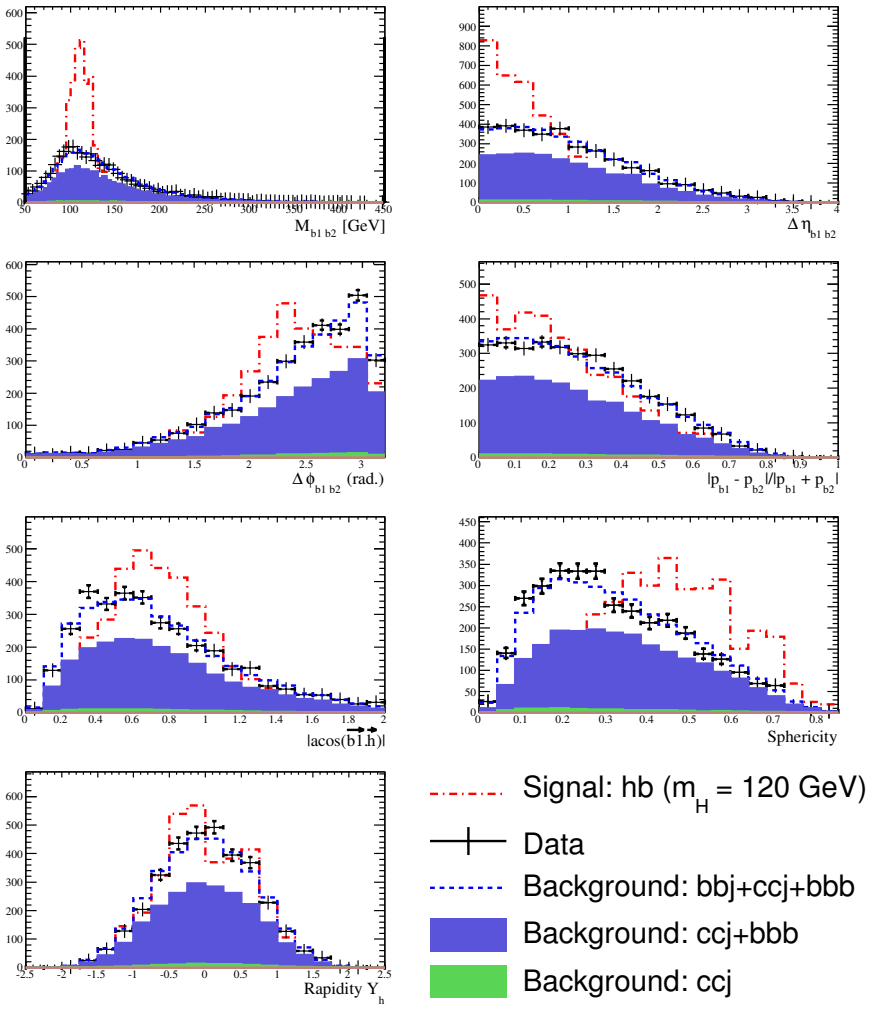


Figure 82: Data Monte Carlo comparison for 4 jets, 3 $b$-tag sample with a 120 GeV Higgs Sample used as signal. Shown are the variables used to determine the signal likelihood (see table 13).

### C.1.6 Five jet, three tag sample

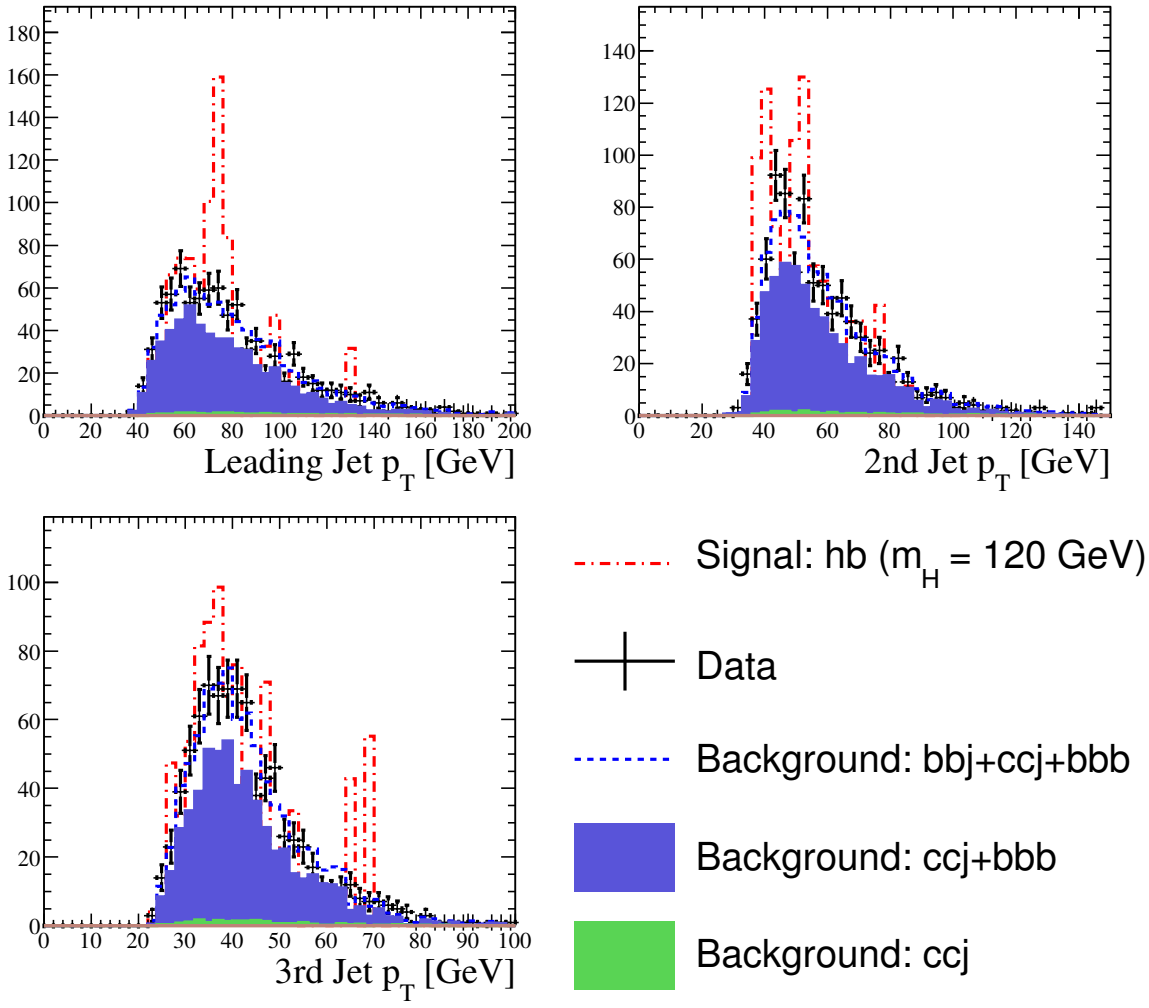


Figure 83: Data Monte Carlo comparison for 5 jets, 3 $b$-tag sample with a 120 GeV Higgs Sample used as signal. Shown is jet $p_T$ for the three jets with the highest $p_T$ in the event.

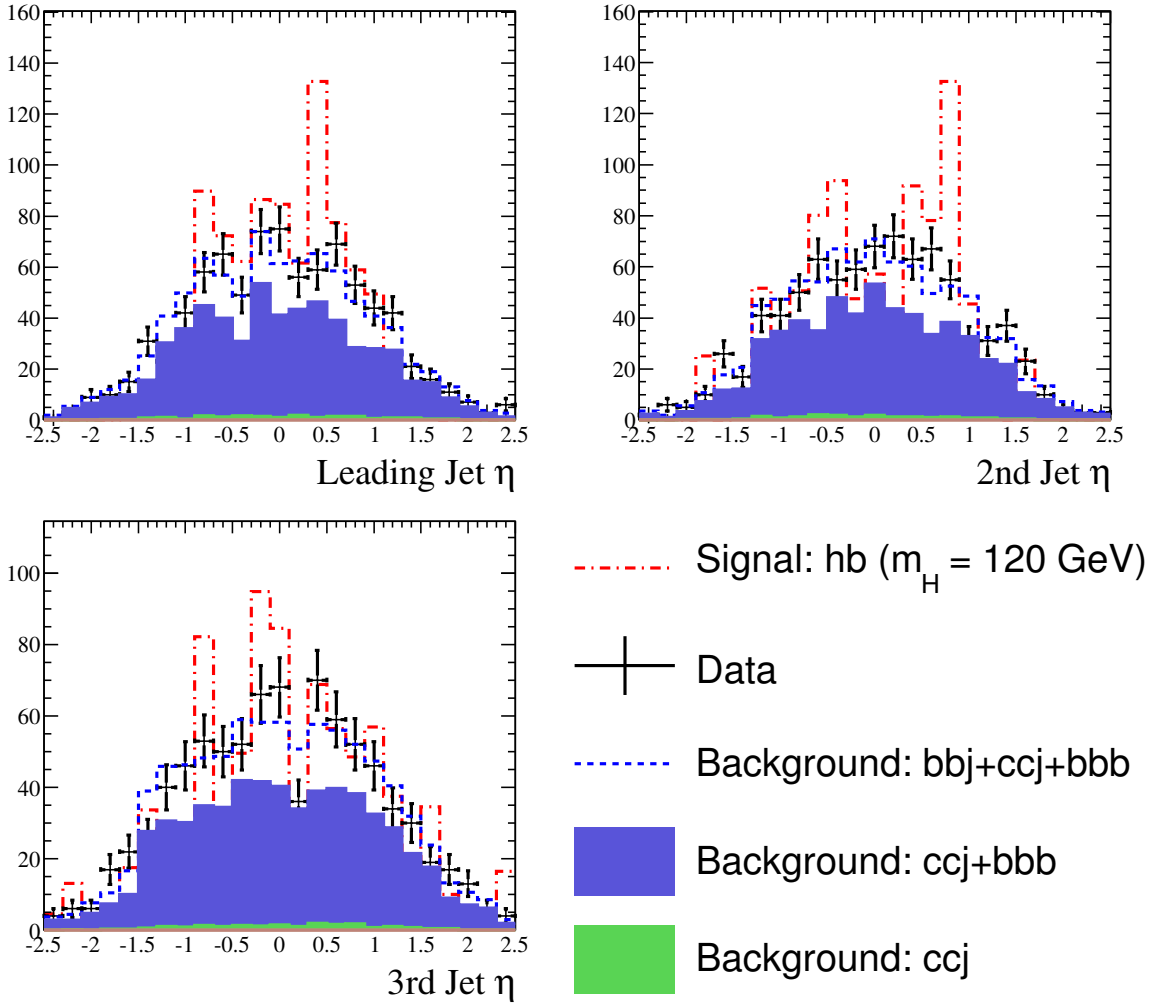


Figure 84: Data Monte Carlo comparison for 5 jets, 3 $b$-tag sample with a 120 GeV Higgs Sample used as signal. Shown is jet $\eta$ for the three jets with the highest $p_T$ in the event.

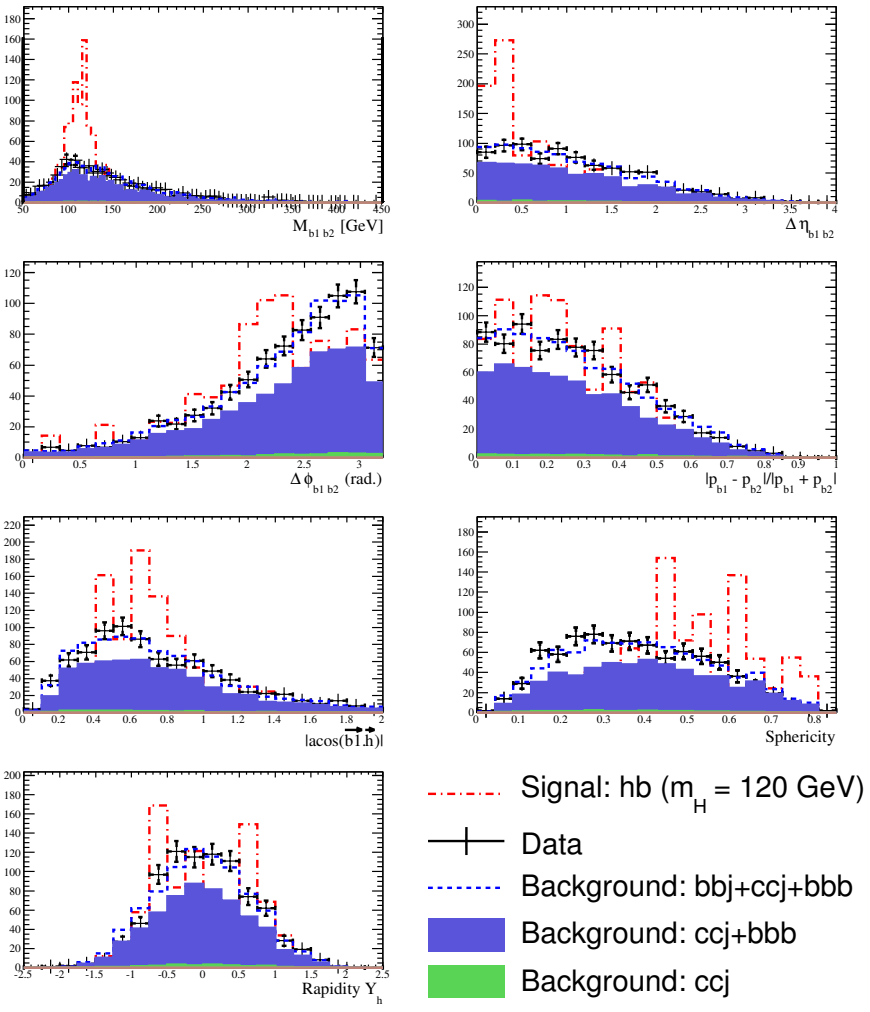


Figure 85: Data Monte Carlo comparison for 5 jets, 3 $b$-tag sample with a 120 GeV Higgs Sample used as signal. Shown are the variables used to determine the signal likelihood (see table 13).

## C.2 High Likelihood Sample

### C.2.1 Three jet, two tag sample

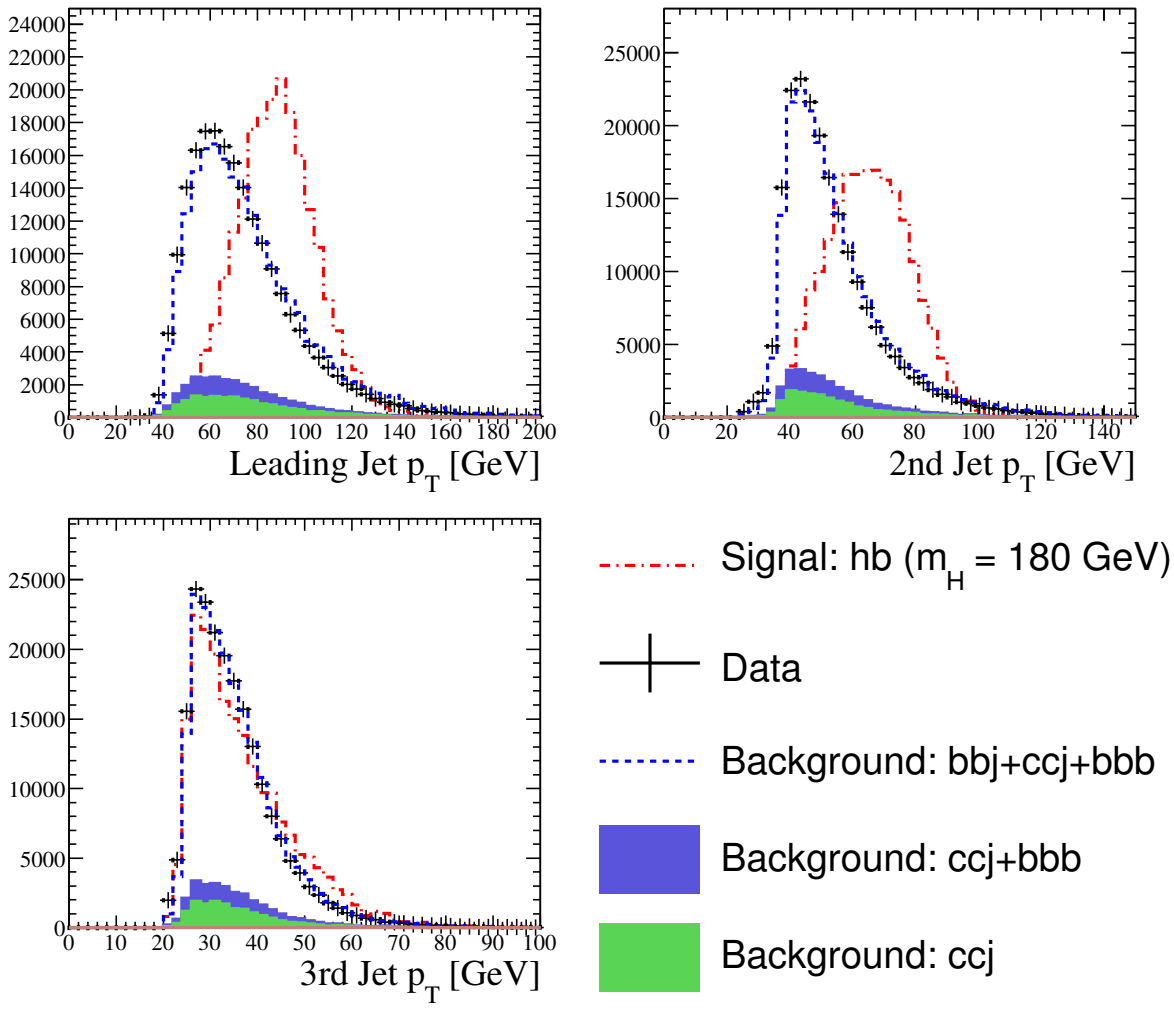


Figure 86: Data Monte Carlo comparison for 3 jets, 2 $b$-tag sample with a 180 GeV Higgs Sample used as signal. Shown is jet $p_T$ for the three jets with the highest $p_T$ in the event.

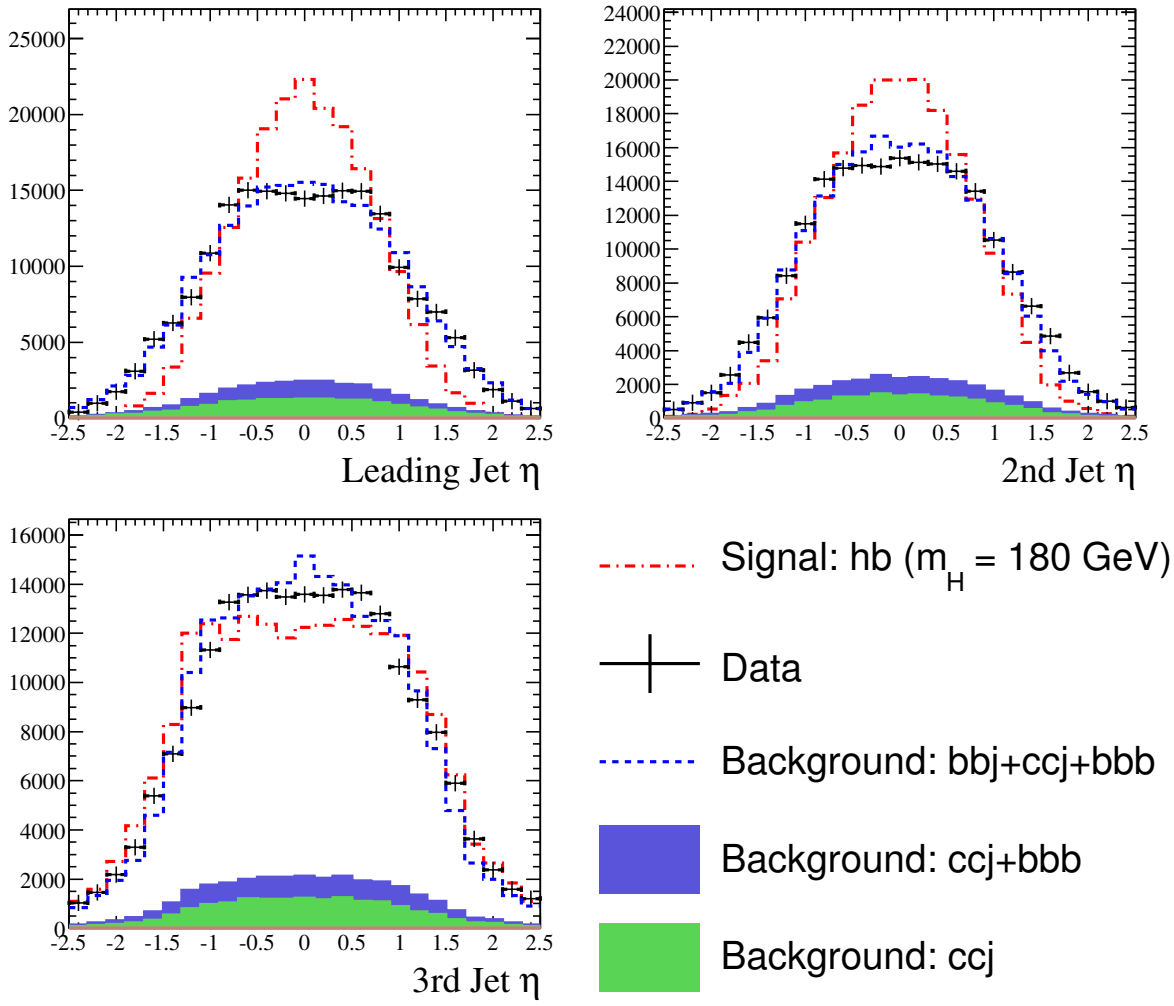


Figure 87: Data Monte Carlo comparison for 3 jets, 2 $b$-tag sample with a 180 GeV Higgs Sample used as signal. Shown is jet $\eta$ for the three jets with the highest $p_T$ in the event.

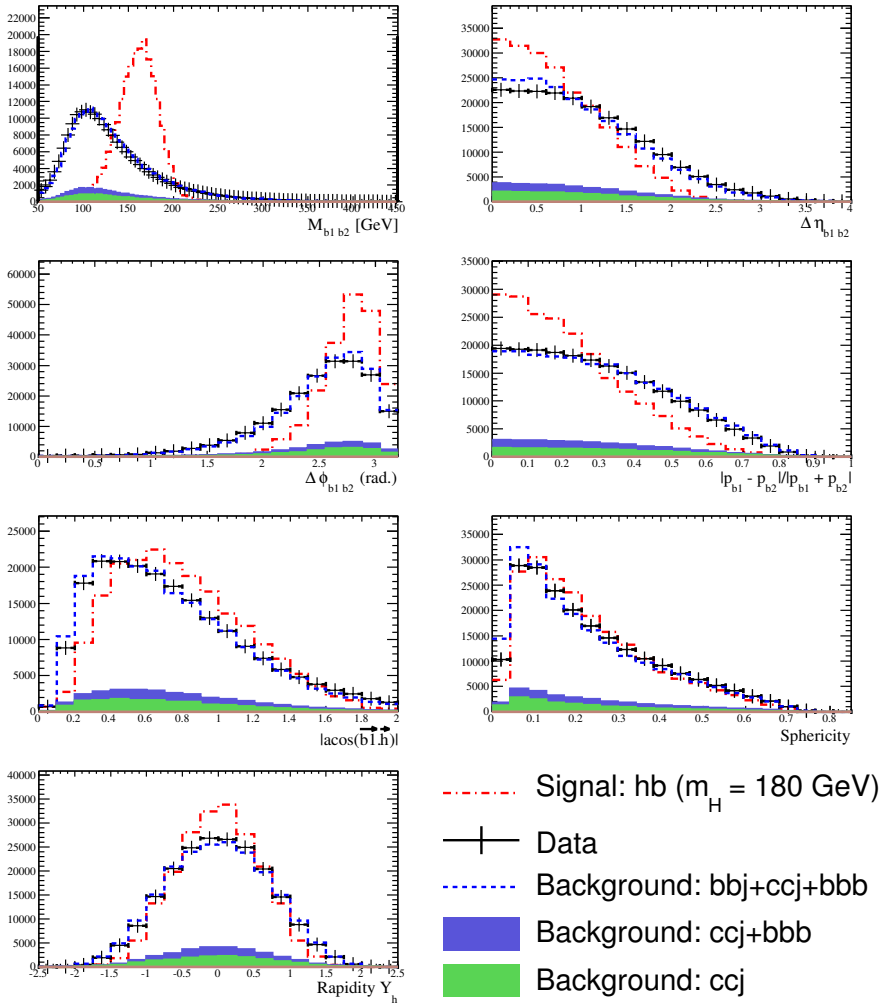


Figure 88: Data Monte Carlo comparison for 3 jets, 2 $b$-tag sample with a 180 GeV Higgs Sample used as signal. Likelihood.

### C.2.2 Four jet, two tag sample

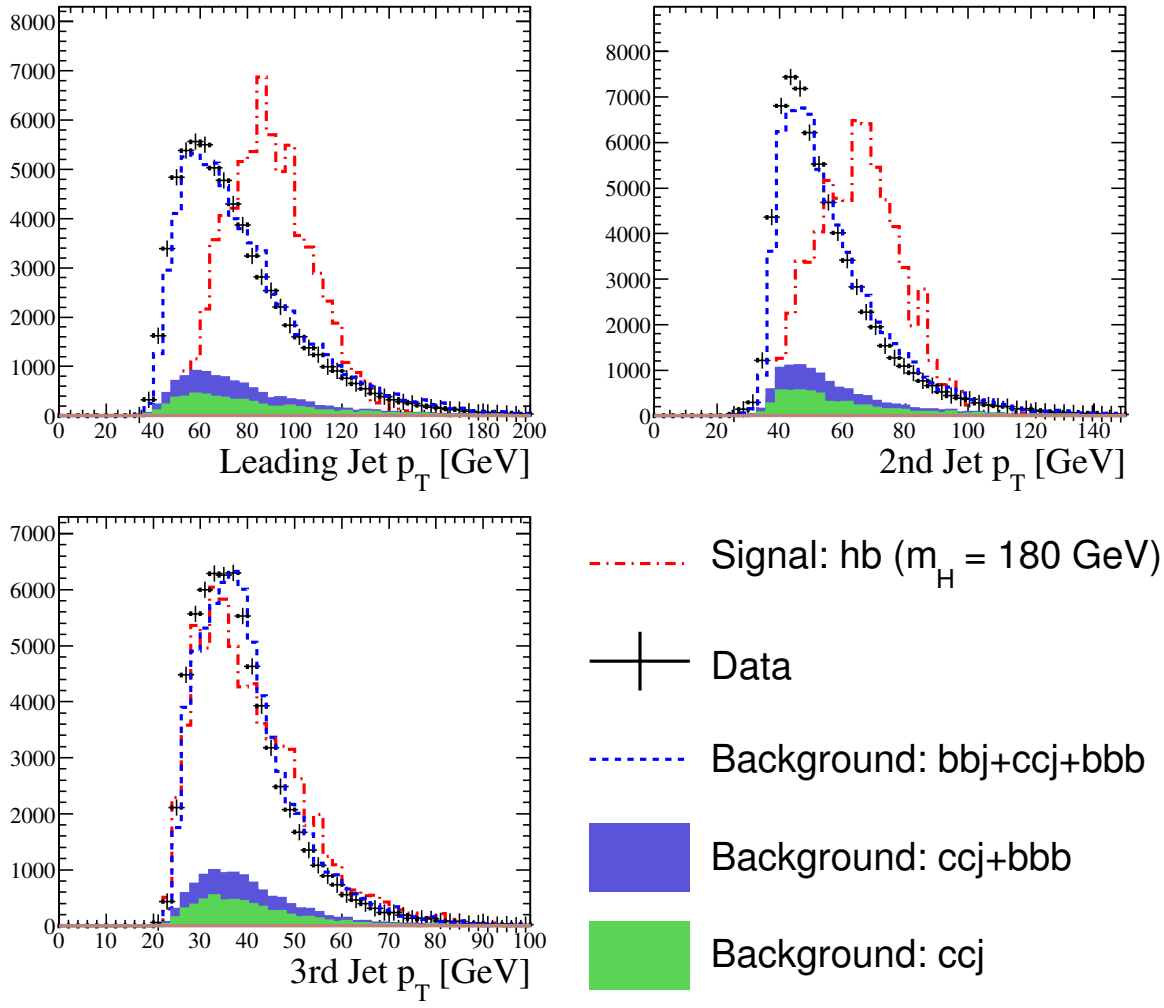


Figure 89: Data Monte Carlo comparison for 4 jets, 2 $b$-tag sample with a 180 GeV Higgs Sample used as signal. Shown is jet $p_T$ for the three jets with the highest $p_T$ in the event.

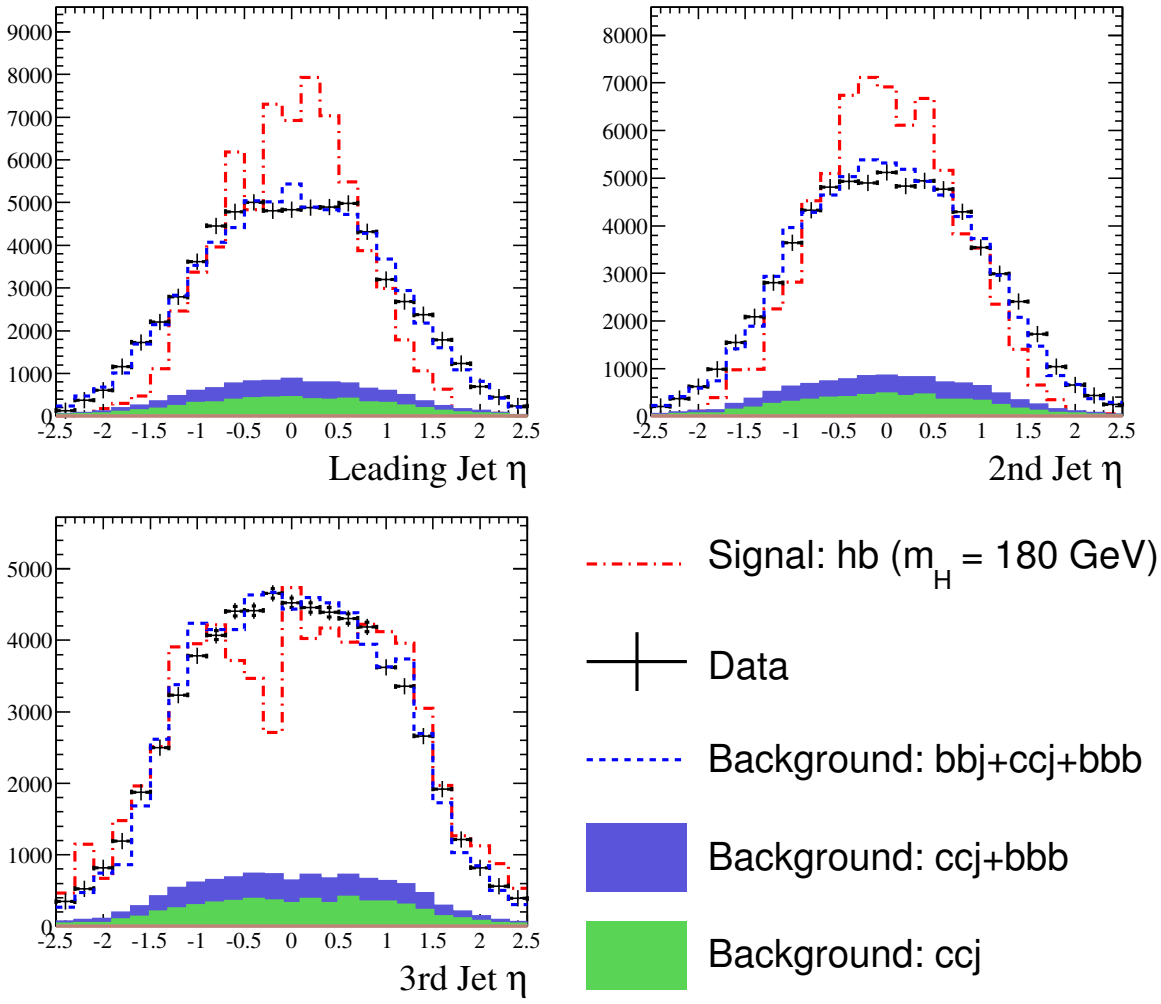


Figure 90: Data Monte Carlo comparison for 4 jets, 2 $b$-tag sample with a 180 GeV Higgs Sample used as signal. Shown is jet $\eta$ for the three jets with the highest $p_T$ in the event.

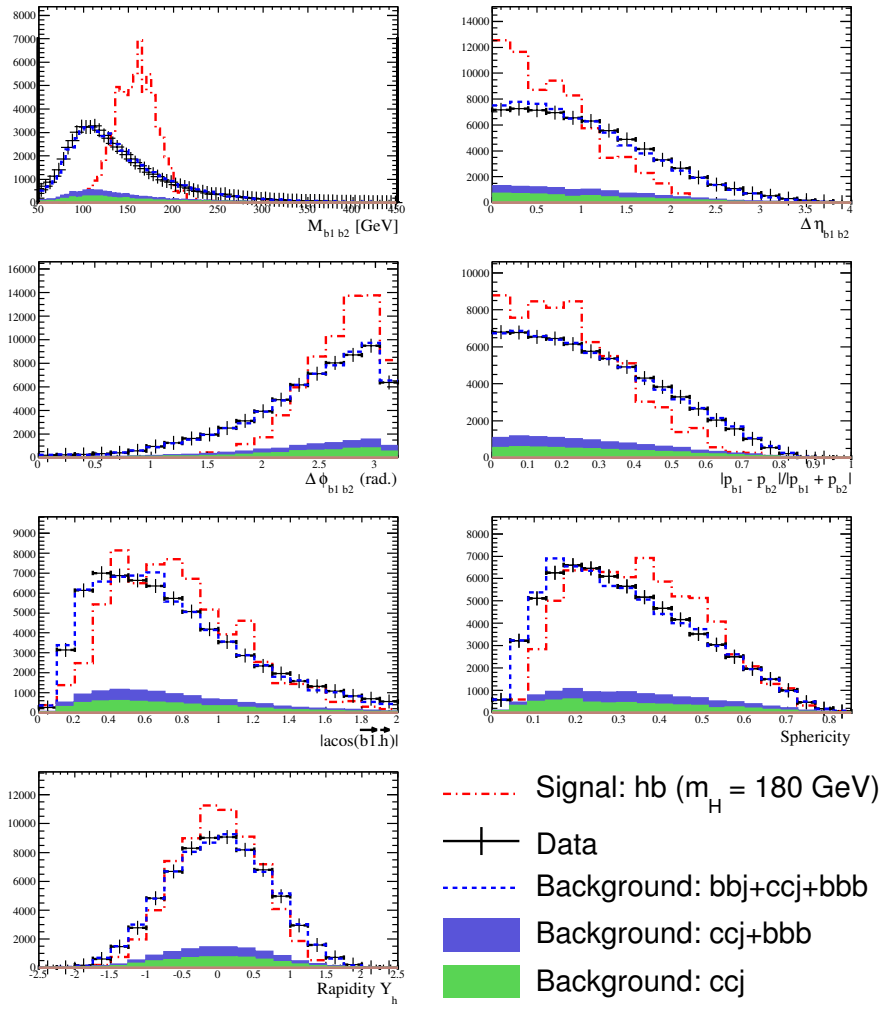


Figure 91: Data Monte Carlo comparison for 4 jets, 2 $b$-tag sample with a 180 GeV Higgs Sample used as signal. Shown are the variables used to determine the signal likelihood (see table 13).

### C.2.3 Five jet, two tag sample

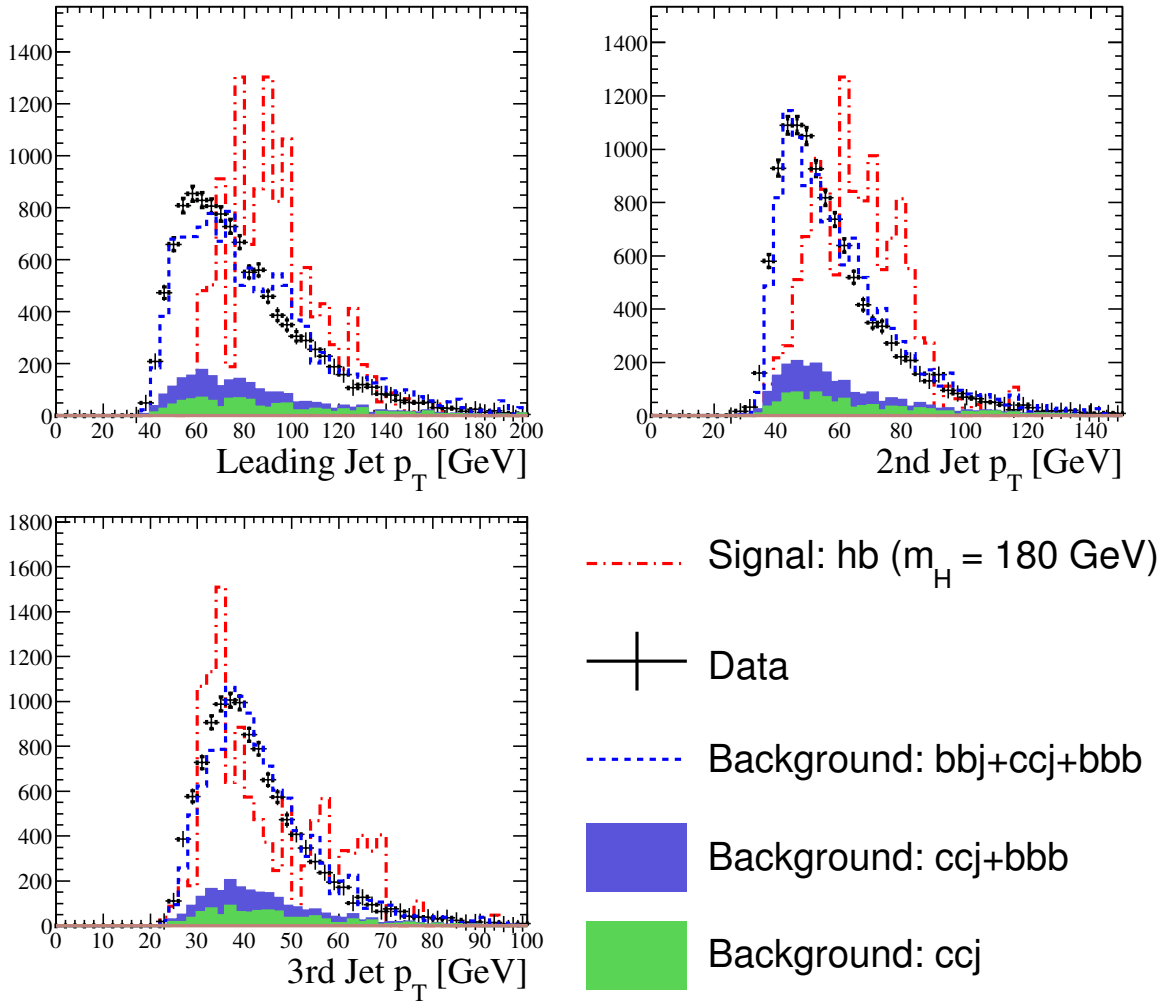


Figure 92: Data Monte Carlo comparison for 5 jets, 2 $b$-tag sample with a 180 GeV Higgs Sample used as signal. Shown is jet $p_T$ for the three jets with the highest $p_T$ in the event.

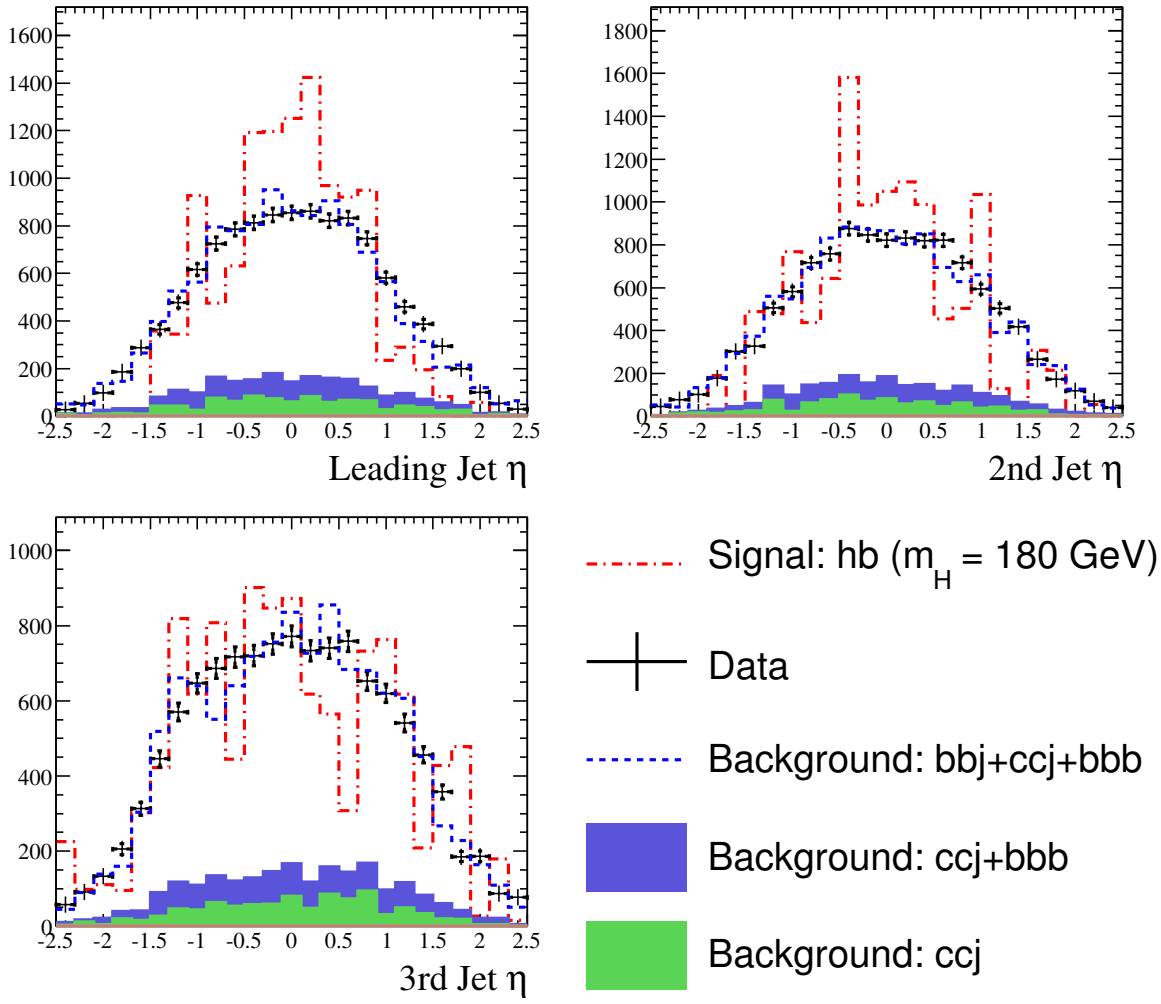


Figure 93: Data Monte Carlo comparison for 5 jets, 2 $b$-tag sample with a 180 GeV Higgs Sample used as signal. Shown is jet $\eta$ for the three jets with the highest $p_T$ in the event.

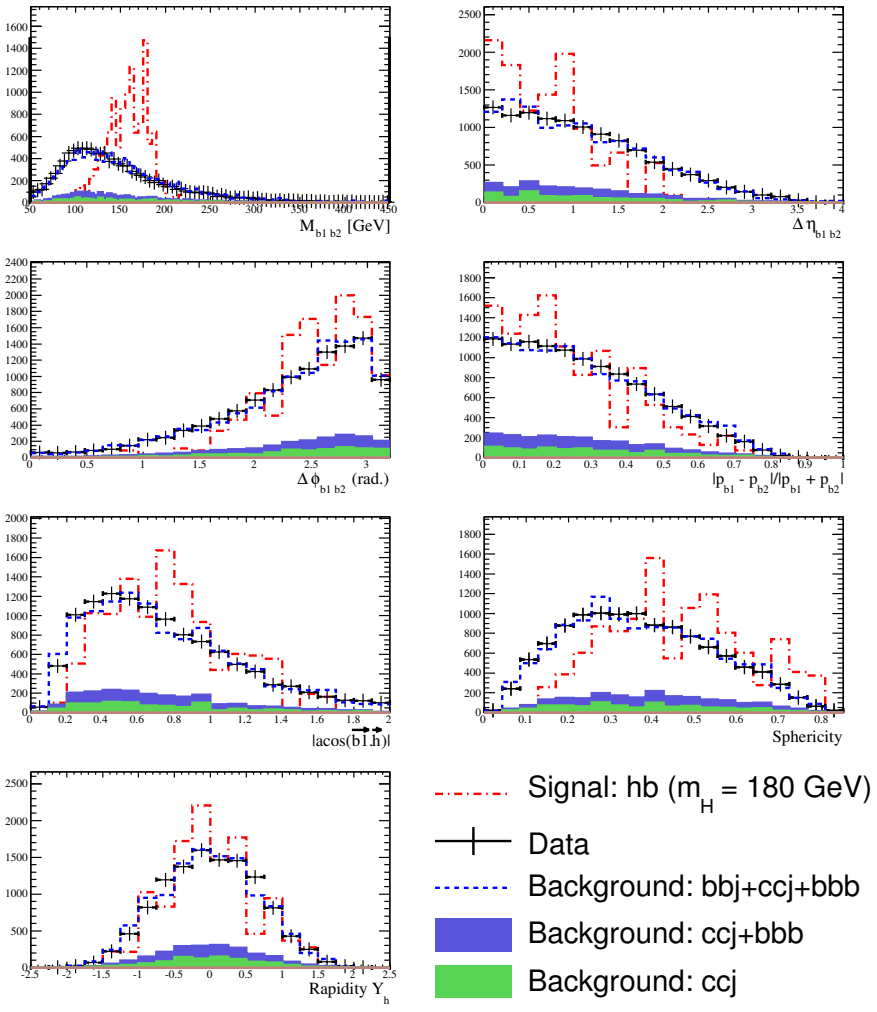


Figure 94: Data Monte Carlo comparison for 5 jets, 2 $b$-tag sample with a 180 GeV Higgs Sample used as signal. Shown are the variables used to determine the signal likelihood (see table 13).

### C.2.4 Three jet, three tag sample

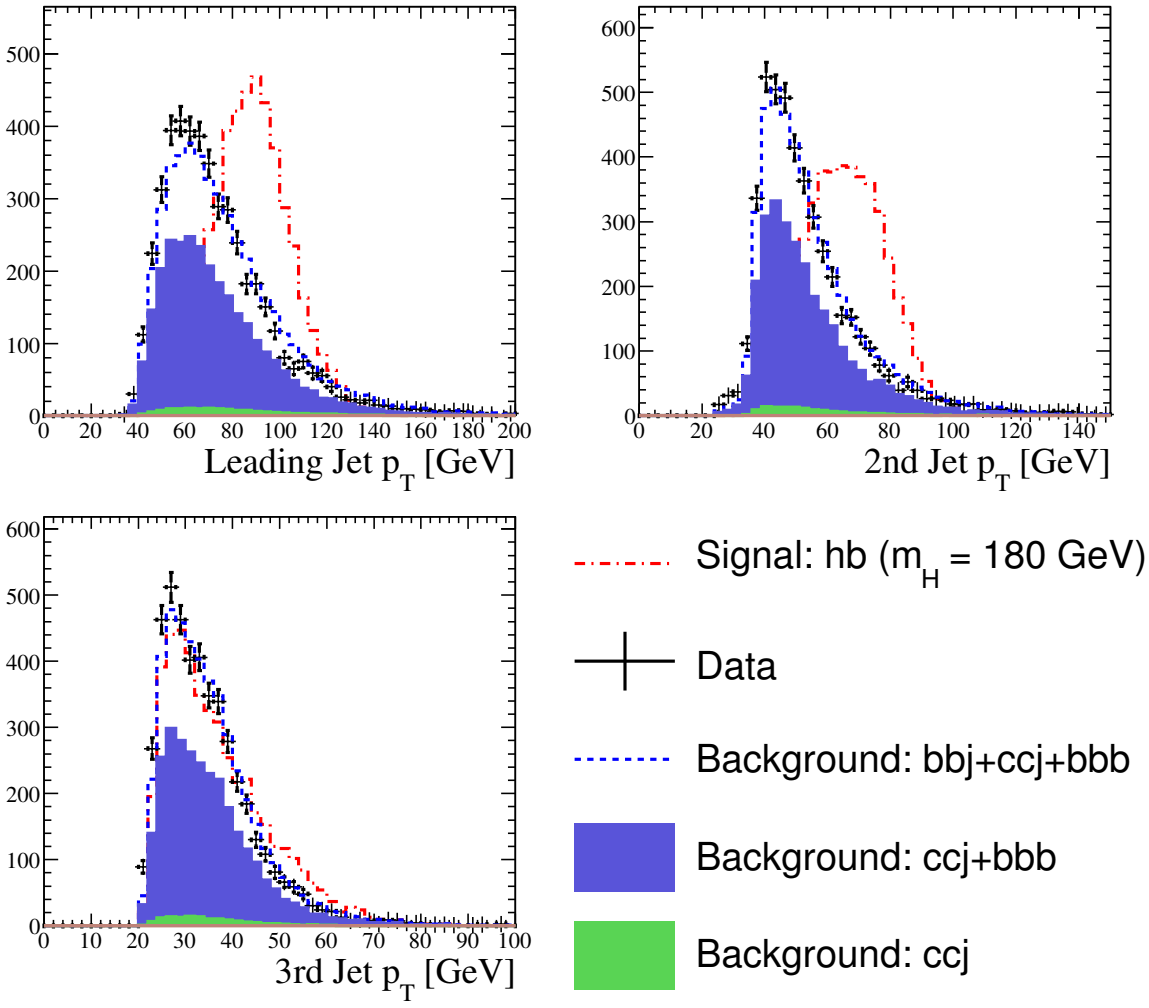


Figure 95: Data Monte Carlo comparison for 3 jets, 3 $b$-tag sample with a 180 GeV Higgs Sample used as signal. Shown is jet $p_T$ for the three jets with the highest $p_T$ in the event.

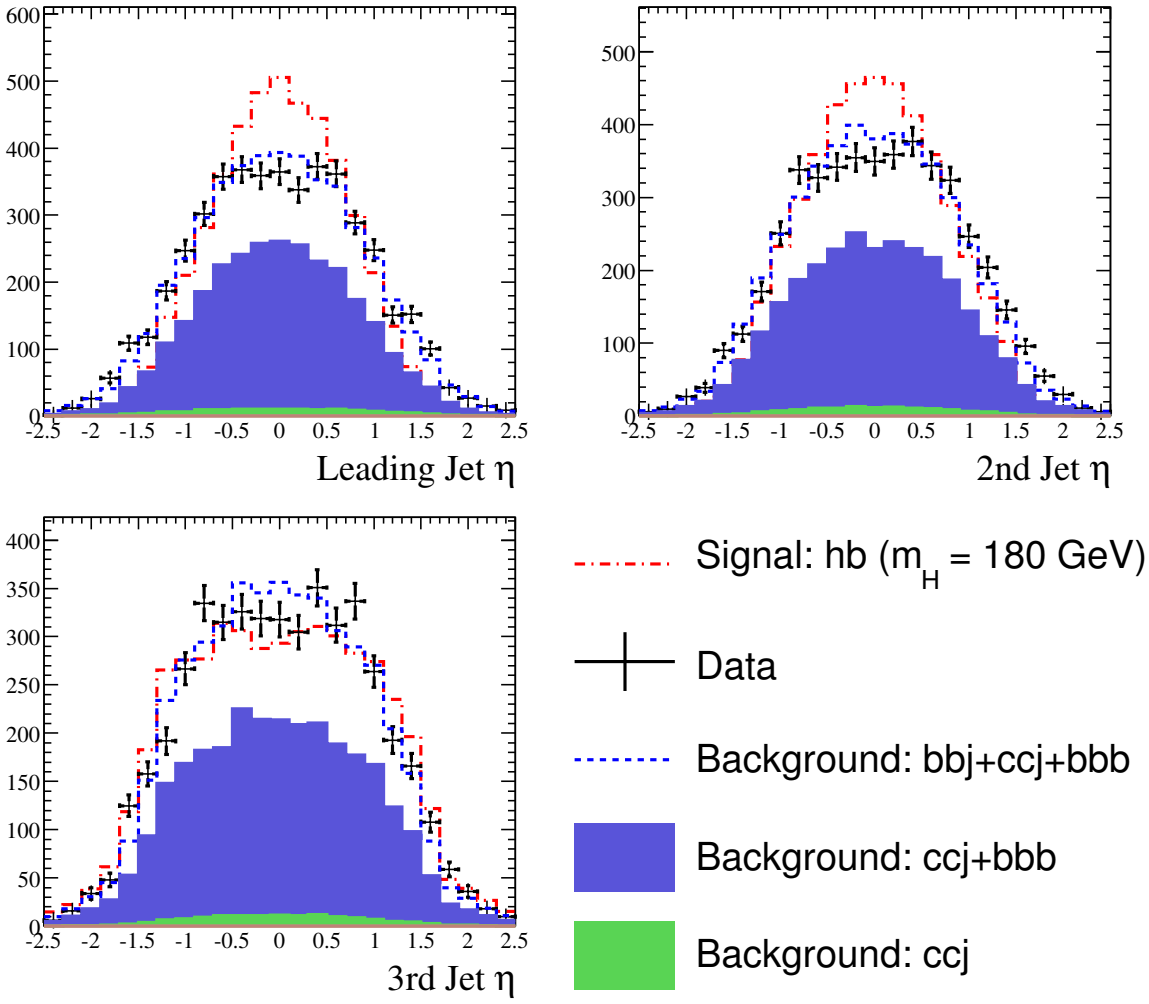


Figure 96: Data Monte Carlo comparison for 3 jets, 3 $b$-tag sample with a 180 GeV Higgs Sample used as signal. Shown is jet $\eta$ for the three jets with the highest $p_T$ in the event.

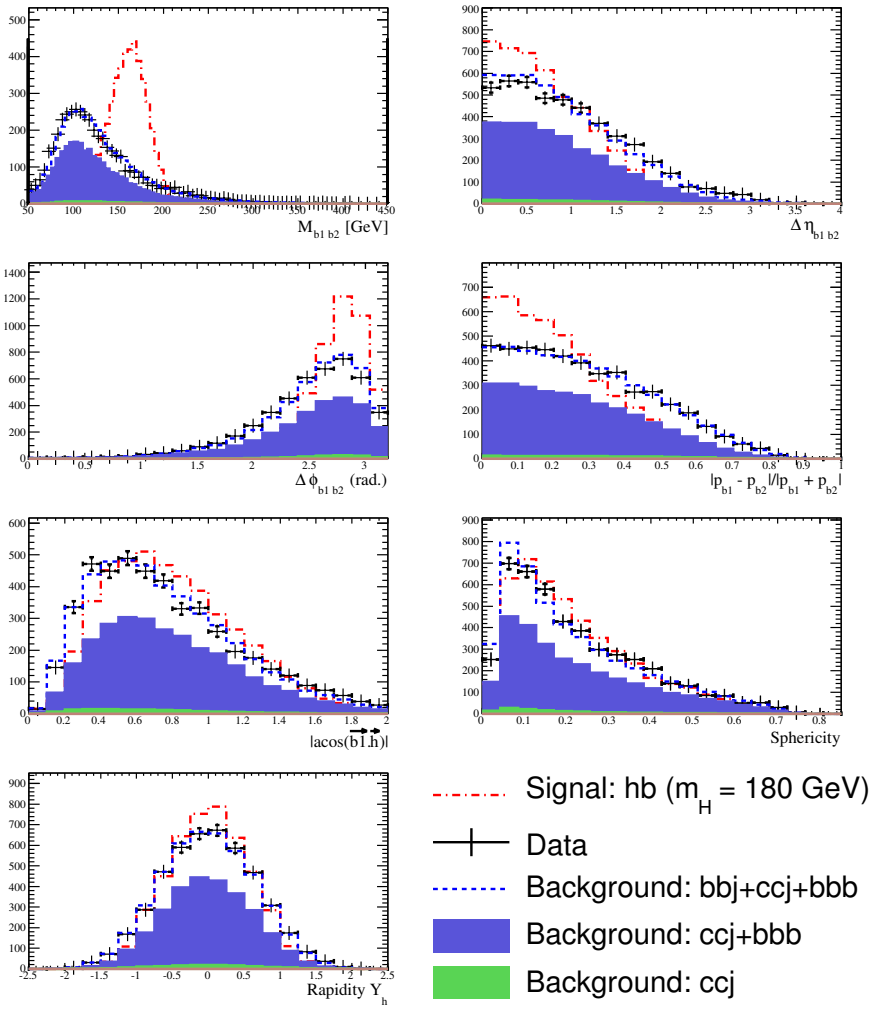


Figure 97: Data Monte Carlo comparison for 3 jets, 3 $b$-tag sample with a 180 GeV Higgs Sample used as signal. Likelihood.

### C.2.5 Four jet, three tag sample

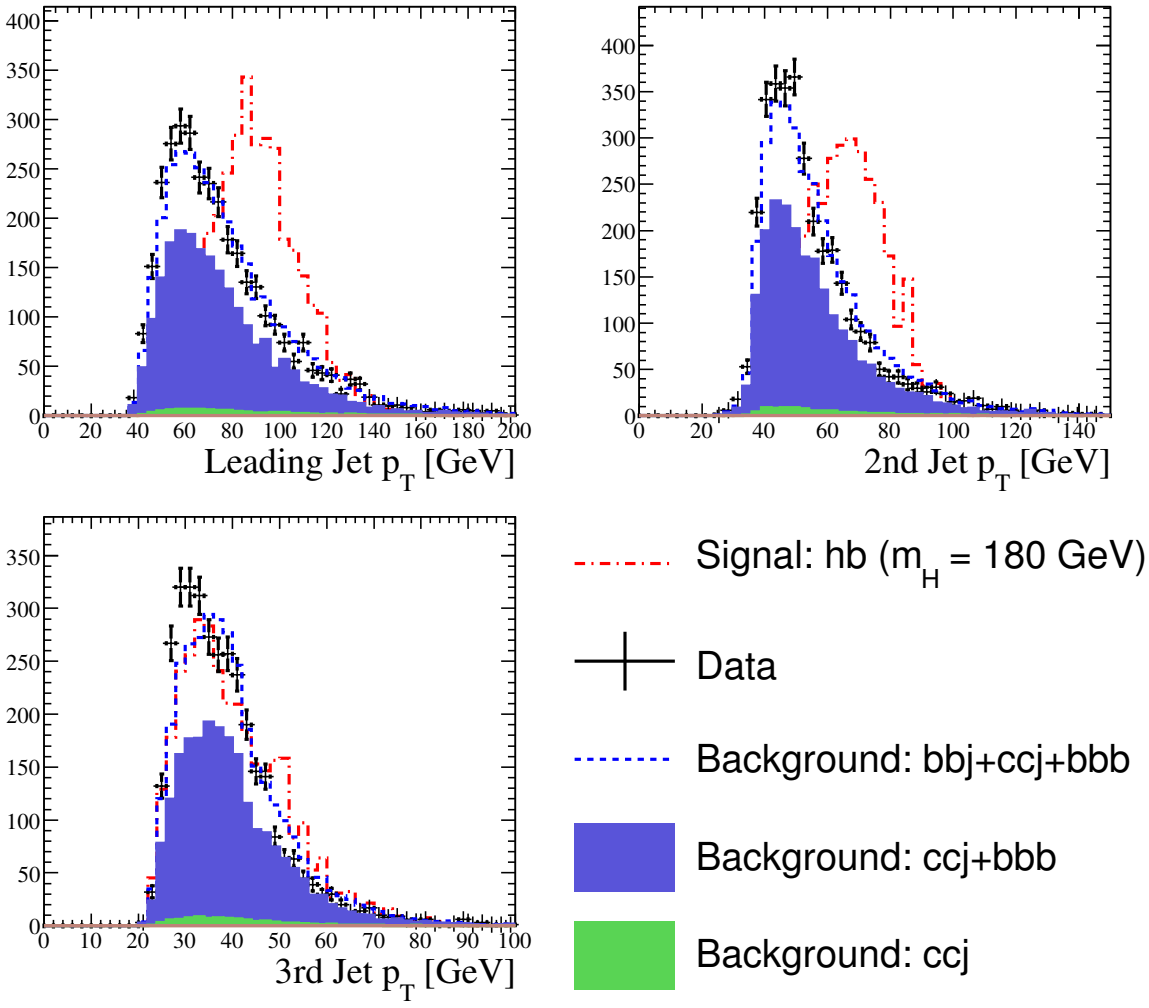


Figure 98: Data Monte Carlo comparison for 4 jets, 3 $b$-tag sample with a 180 GeV Higgs Sample used as signal. Shown is jet $p_T$ for the three jets with the highest $p_T$ in the event.

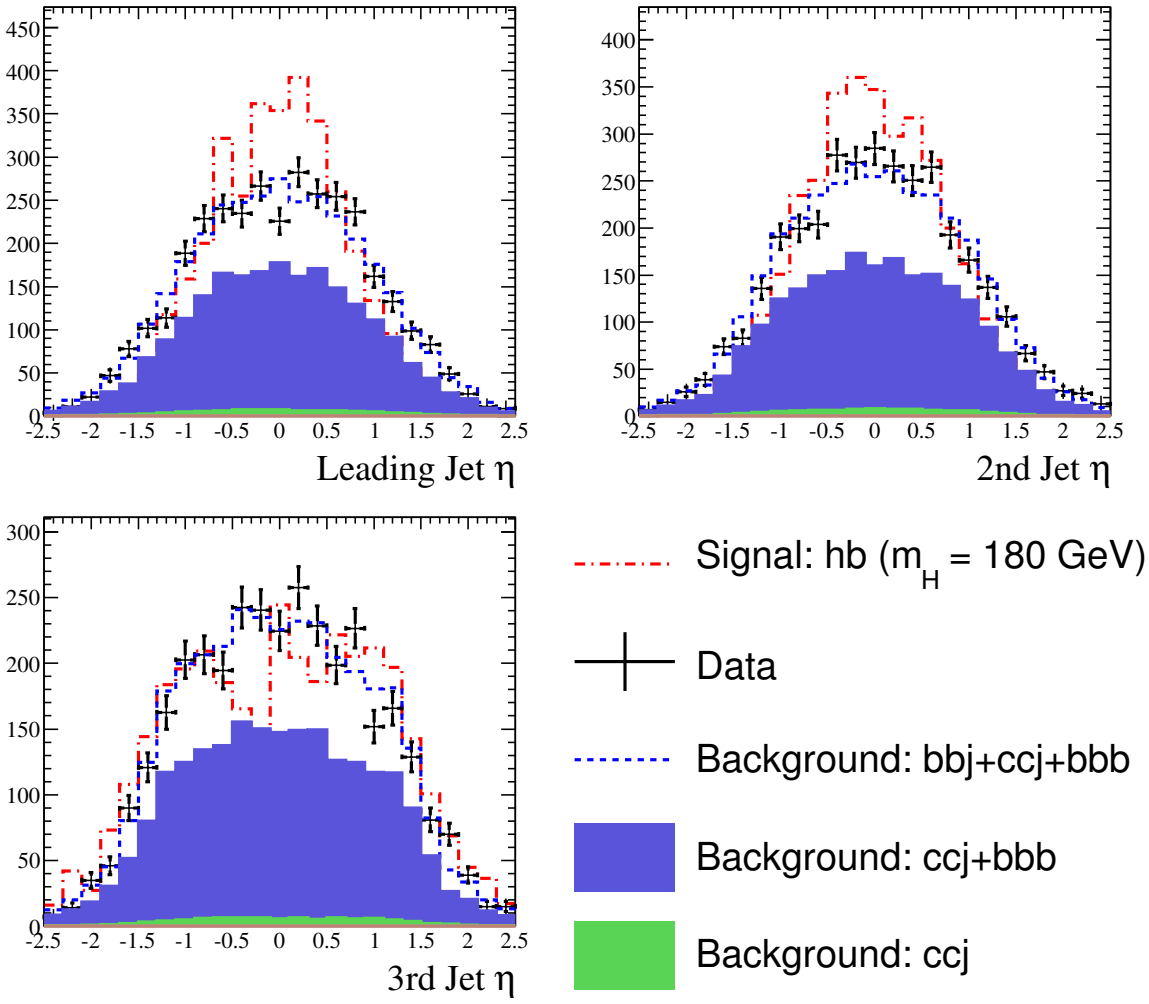


Figure 99: Data Monte Carlo comparison for 4 jets, 3 $b$-tag sample with a 180 GeV Higgs Sample used as signal. Shown is jet $\eta$ for the three jets with the highest $p_T$ in the event.

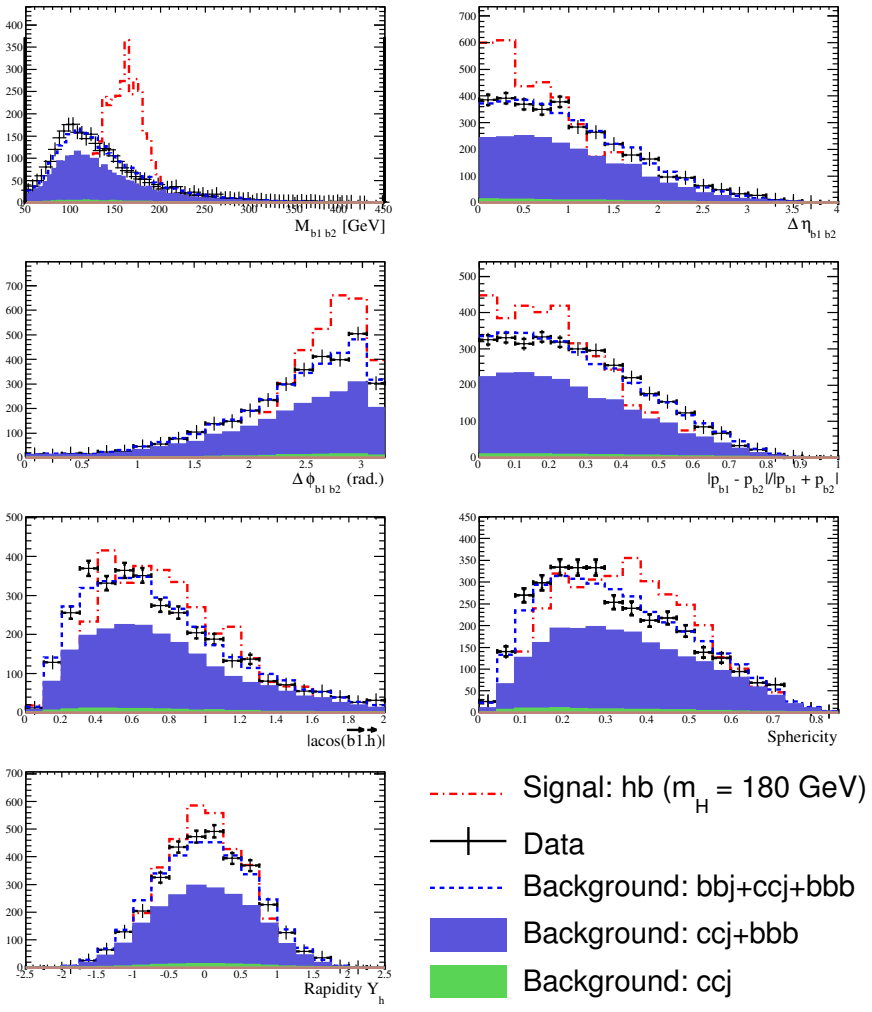


Figure 100: Data Monte Carlo comparison for 4 jets, 3 $b$-tag sample with a 180 GeV Higgs Sample used as signal. Shown are the variables used to determine the signal likelihood (see table 13).

### C.2.6 Five jet, three tag sample

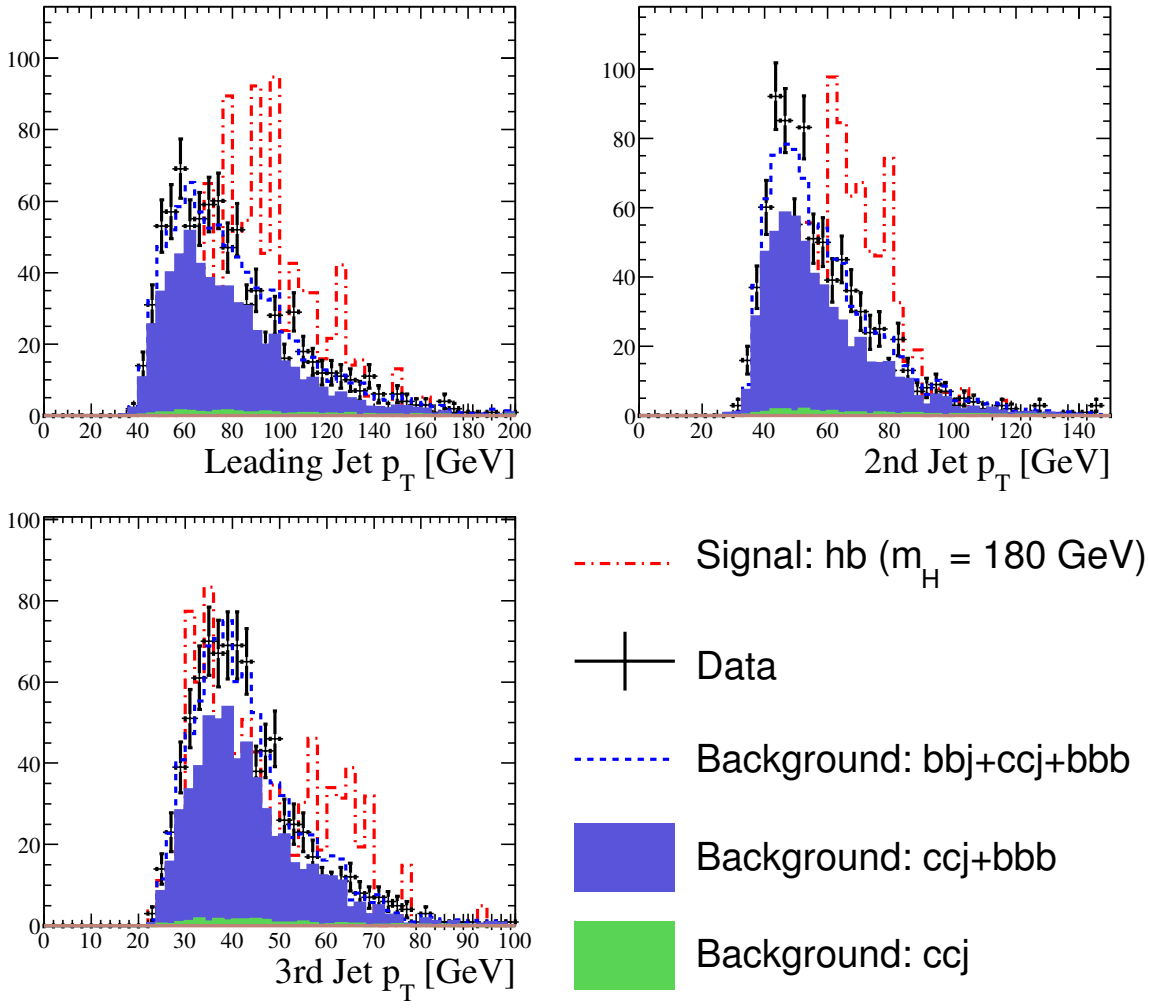


Figure 101: Data Monte Carlo comparison for 5 jets, 3 $b$-tag sample with a 180 GeV Higgs Sample used as signal. Shown is jet $p_T$ for the three jets with the highest $p_T$ in the event.

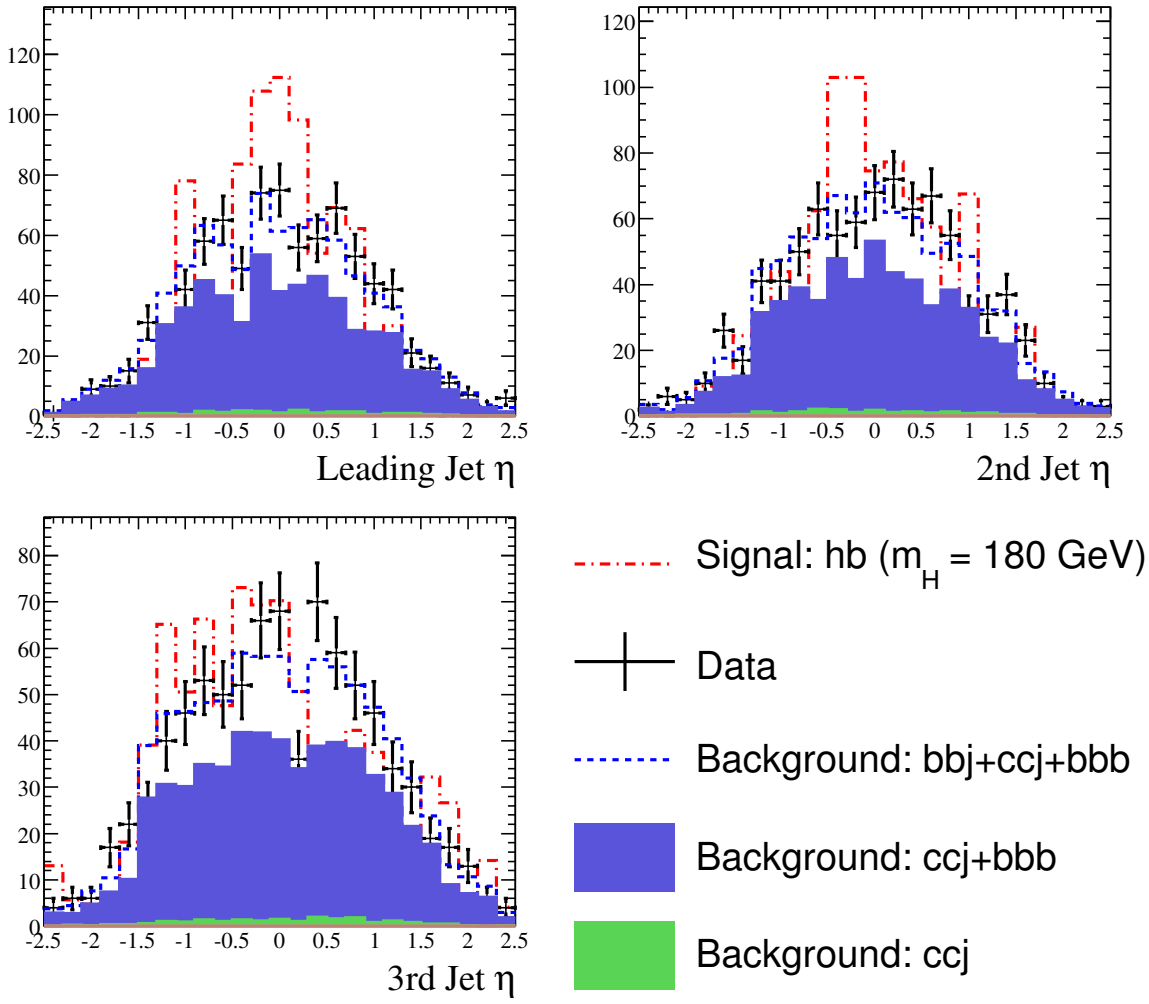


Figure 102: Data Monte Carlo comparison for 5 jets, 3 $b$-tag sample with a 180 GeV Higgs Sample used as signal. Shown is jet $\eta$ for the three jets with the highest $p_T$ in the event.

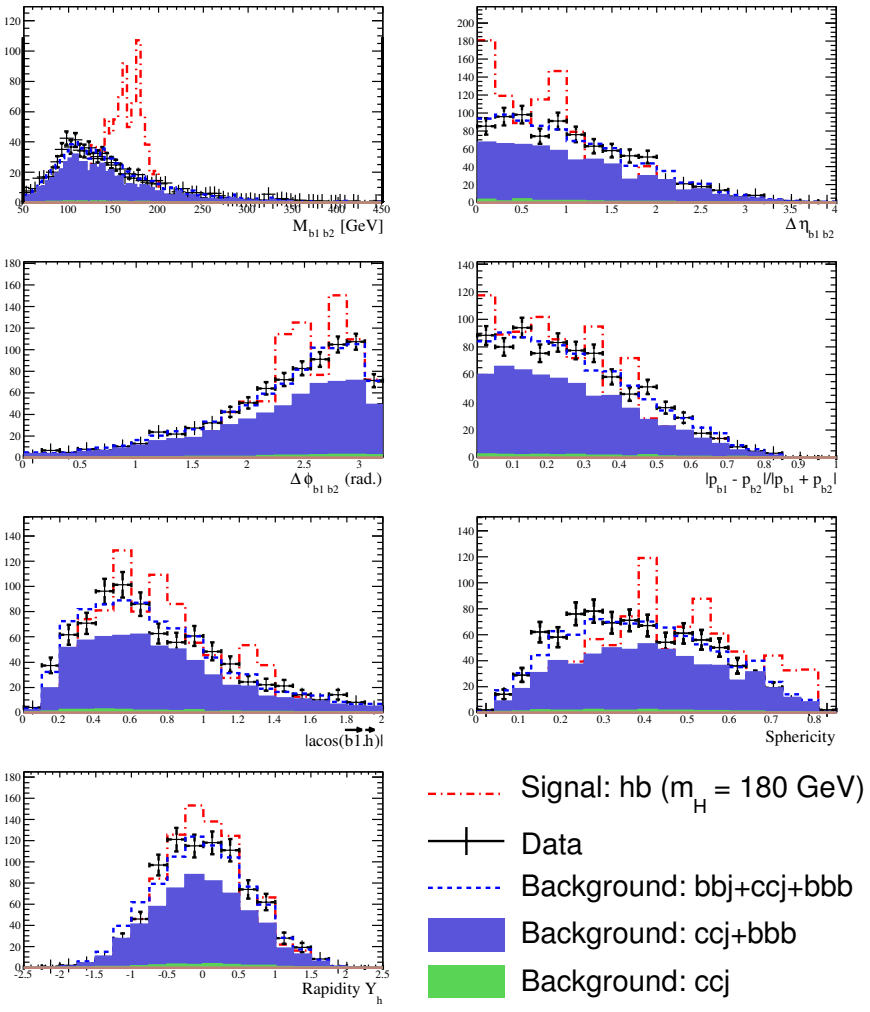


Figure 103: Data Monte Carlo comparison for 5 jets, 3 $b$-tag sample with a 180 GeV Higgs Sample used as signal. Shown are the variables used to determine the signal likelihood (see table 13).

# D Likelihoods

The probability density functions (pdf) used in the likelihood functions are first smoothed and then interpolated with the help of spline (order 3). Examples of these pdfs are given in Figs. 104 - 106 for the low mass likelihood and in Figs. 107 - 109 for the high mass likelihood.

## D.1 Low Mass Likelihood

### D.1.1 3 jet events

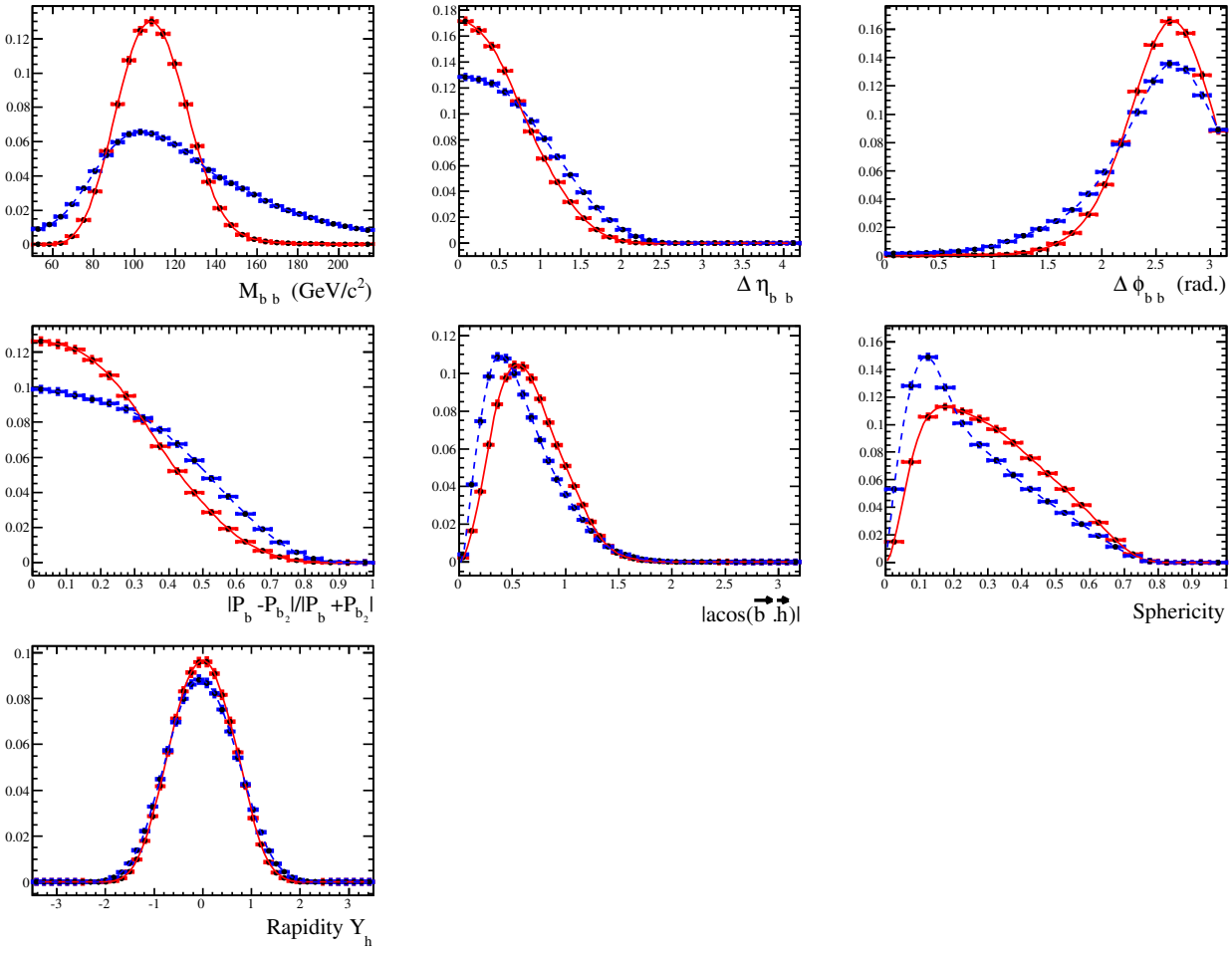


Figure 104: Fits to the kinematic variables in the 3-jet sample. The red (blue) curve is the signal for a Higgs boson mass of 120 GeV/$c^2$ (background) pdfs after 3 tags. Though the invariant mass of each pairing is not actually used in the likelihood computation, it is displayed here.

### D.1.2 4 jet events

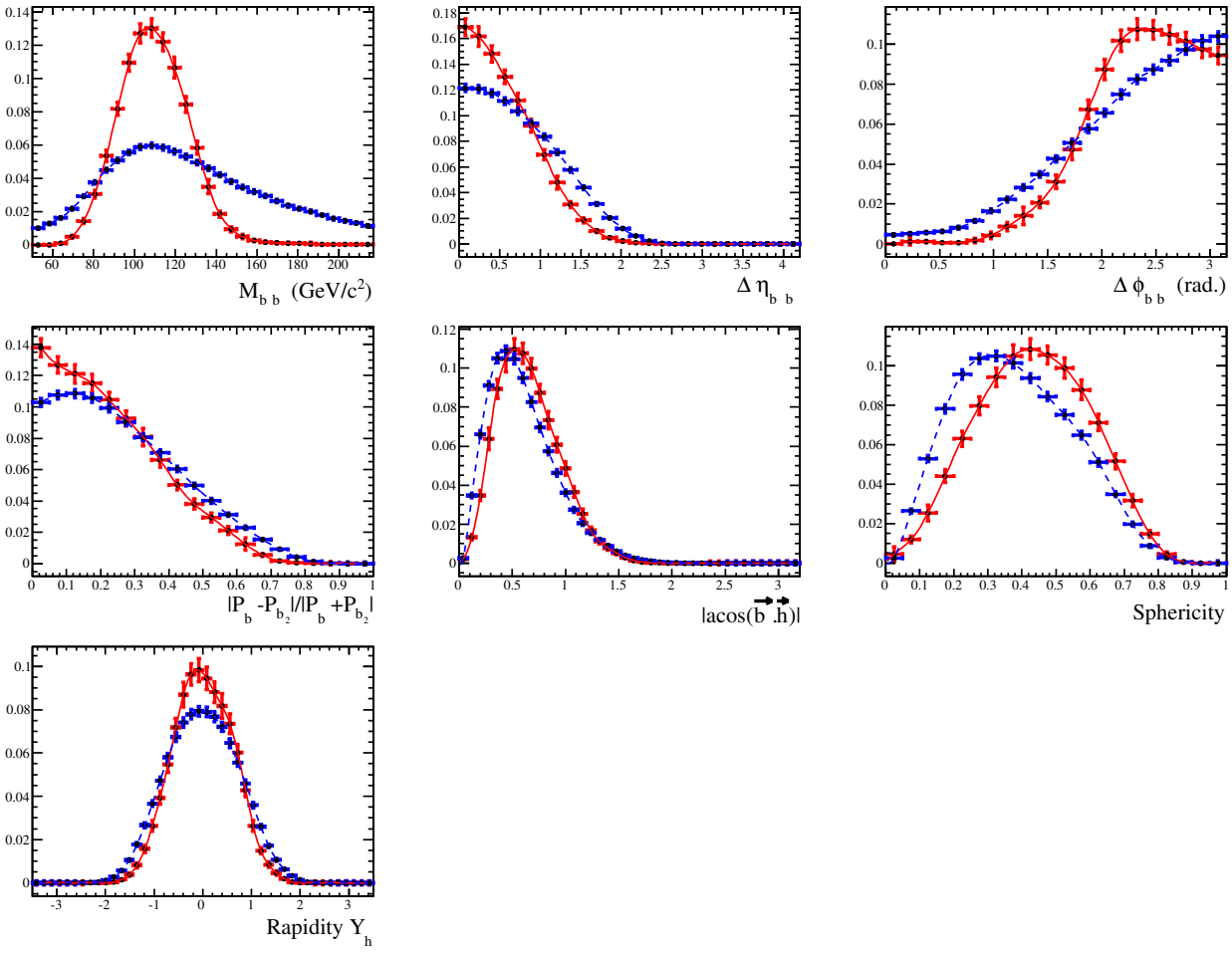


Figure 105: Fits to the kinematic variables in the 4-jet sample. The red (blue) curve is the signal for a Higgs boson mass of 120 GeV/$c^2$ (background) pdfs after 3 tags. Though the invariant mass of each pairing is not actually used in the likelihood computation, it is displayed here.

### D.1.3 5 jet events

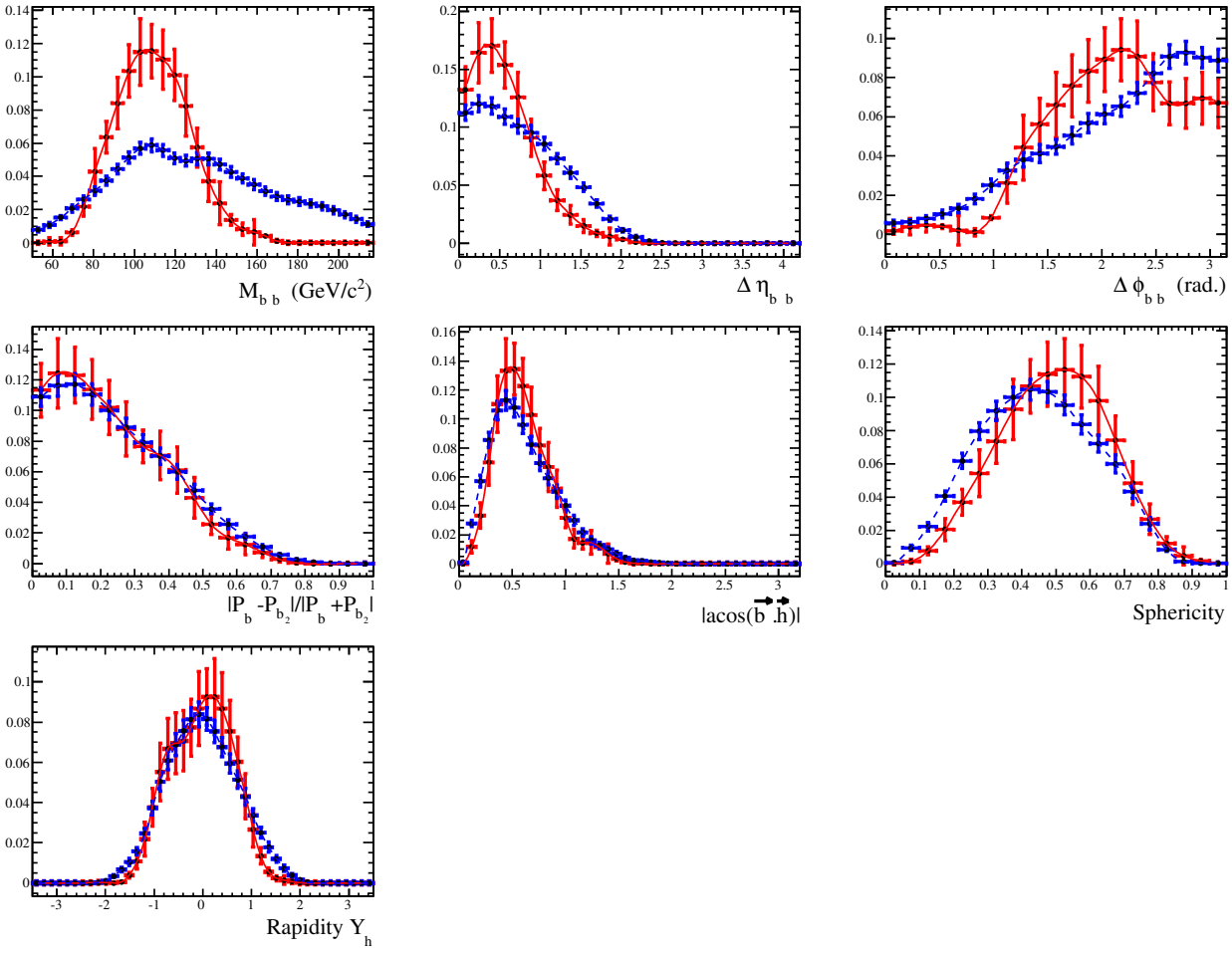


Figure 106: Fits to the kinematic variables in the 5-jet sample. The red (blue) curve is the signal for a Higgs boson mass of 120 GeV/$c^2$ (background) pdfs after 3 tags. Though the invariant mass of each pairing is not actually used in the likelihood computation, it is displayed here.

## D.2 High Mass Likelihood

### D.2.1 3 jet events

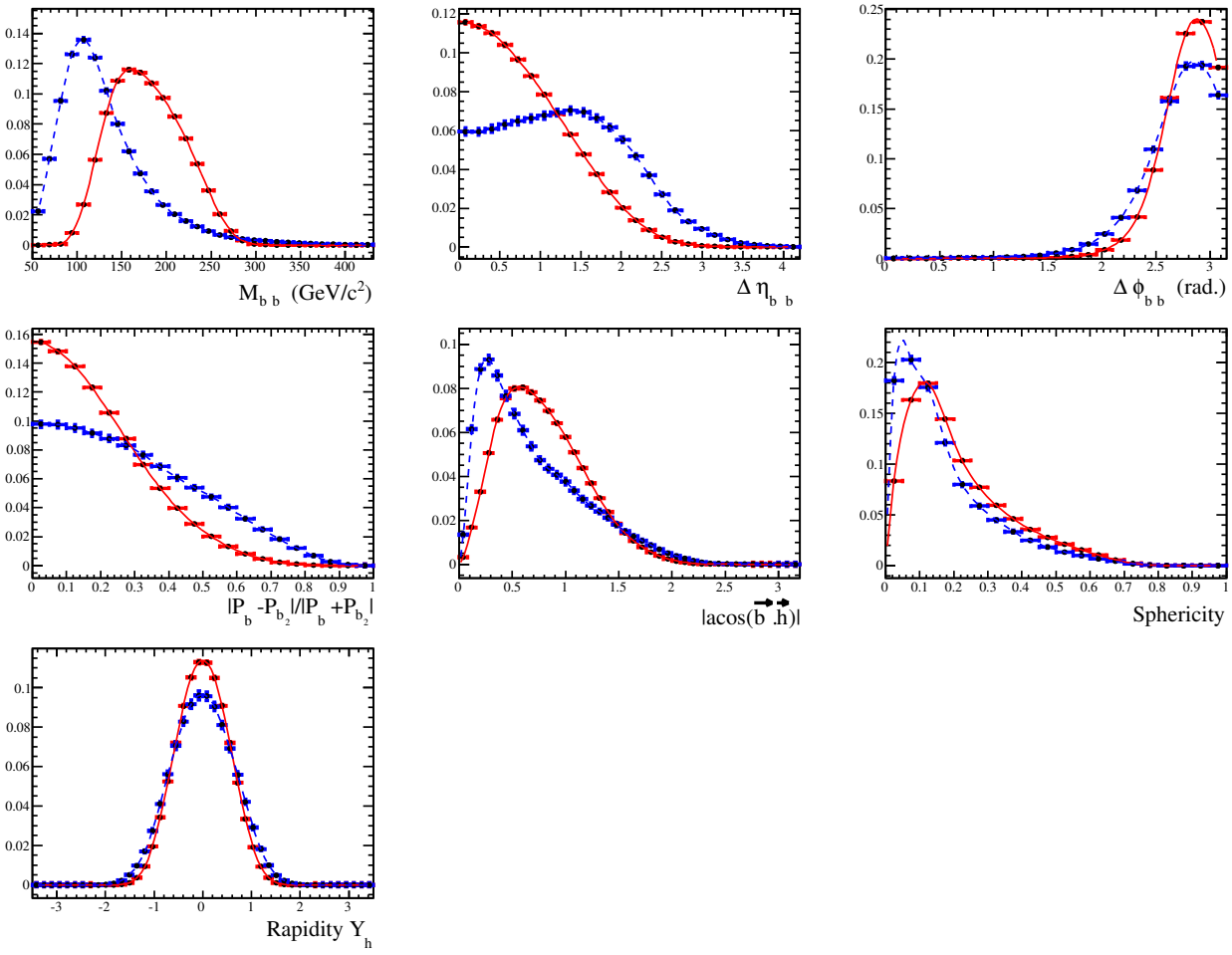


Figure 107: Fits to the kinematic variables in the 3-jet sample. The red (blue) curve is the signal for a Higgs boson mass of 180 GeV/$c^2$ (background) pdfs after 3 tags. Though the invariant mass of each pairing is not actually used in the likelihood computation, it is displayed here.

### D.2.2 4 jet events

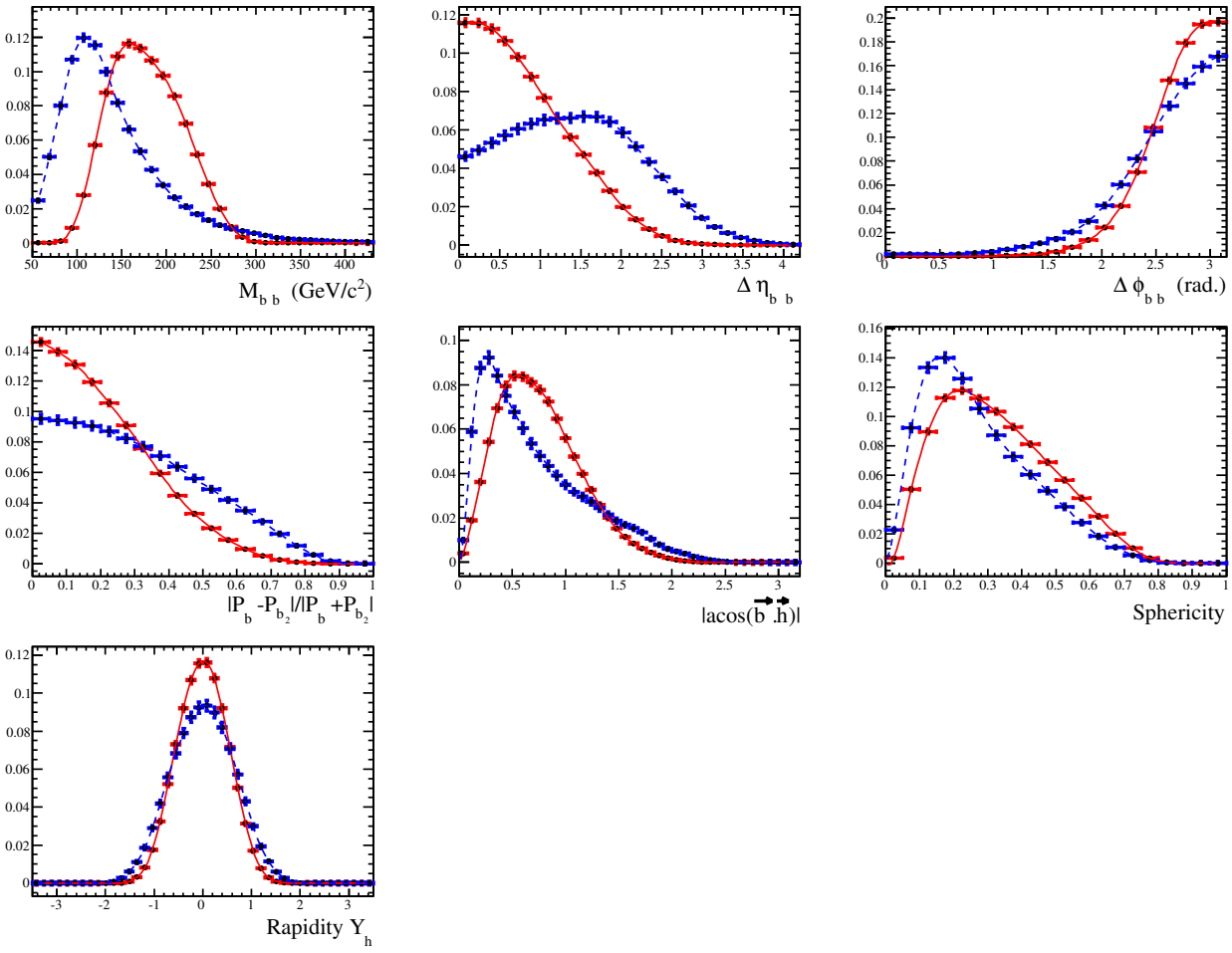


Figure 108: Fits to the kinematic variables in the 4-jet sample. The red (blue) curve is the signal for a Higgs boson mass of 180 GeV/$c^2$ (background) pdfs after 3 tags. Though the invariant mass of each pairing is not actually used in the likelihood computation, it is displayed here.

### D.2.3 5 jet events

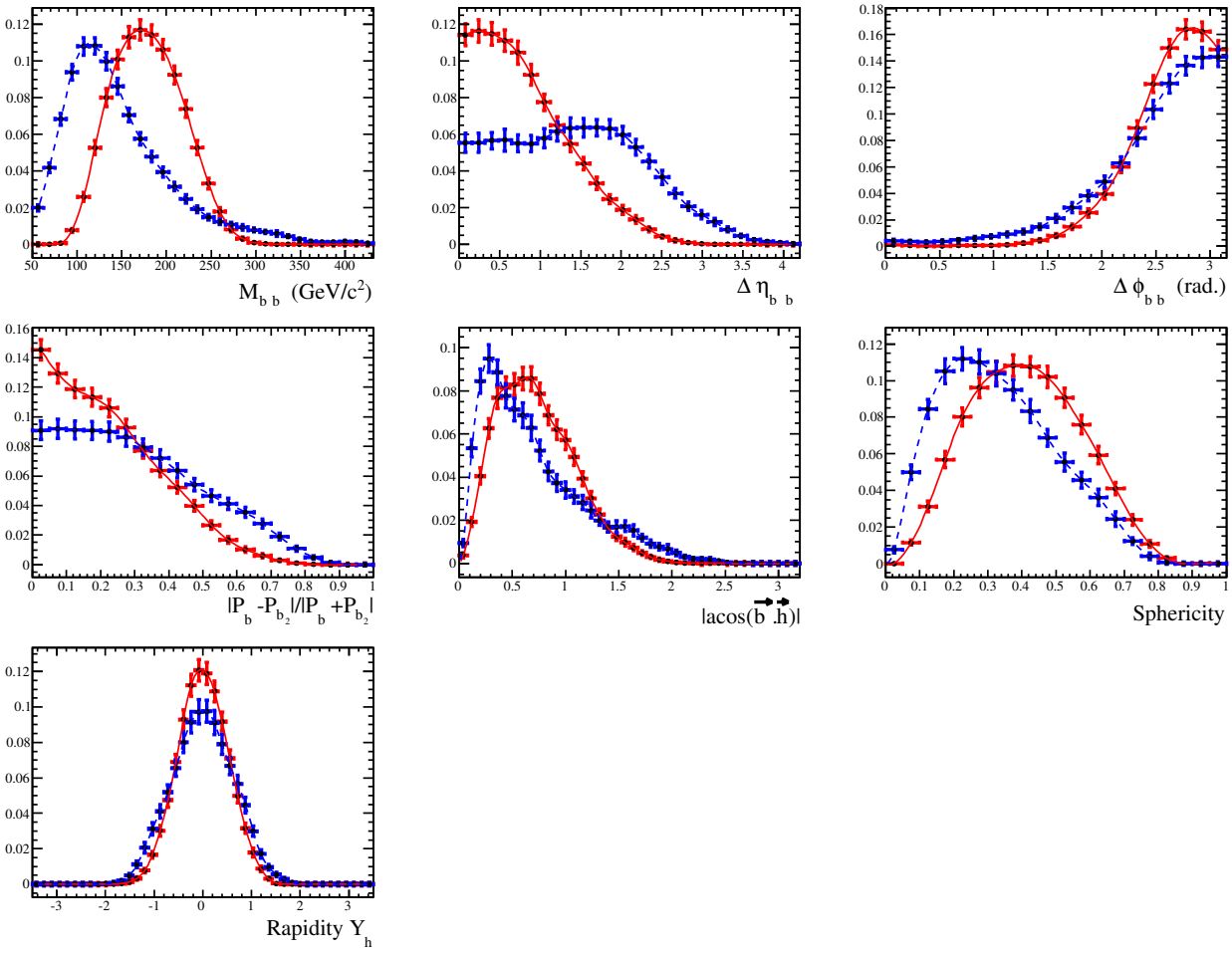


Figure 109: Fits to the kinematic variables in the 5-jet sample. The red (blue) curve is the signal for a Higgs boson mass of 180 GeV/$c^2$ (background) pdfs after 3 tags. Though the invariant mass of each pairing is not actually used in the likelihood computation, it is displayed here.

# E Taggability

For a jet to be taggable the calorimeter jet must be matched to a track jet, which in turn is built from 'good' tracks, i.e. tracks with $p_T > 0.5$ GeV (plus at least one track with $p_T > 1.0$ GeV, at least one SMT hit and impact parameters of less than 0.4 cm in $z$ and 0.2 cm (in $xy$). Generally the taggability in Monte Carlo tends to be higher than in data, hence we apply the weighting factors show in figs. 110 - 115. The taggability is parametrised in the product of $|\eta_{jet}|$ and $z_{pv}$. If the product is negative the jet will be pointing back to the centre of the detector and will usually have good tracking information. For jets pointing outwards, the taggability is also divided into two regions of $|z_{pv}| < 20$ cm and $20 < |z_{pv}| < 35$ cm. (We discard events with $|z_{pv}| > 35$ cm.)

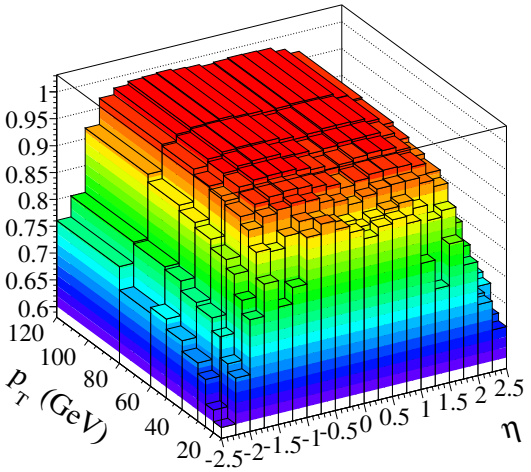


Figure 110: Taggability corrections for $b$-jets where $|\eta_{jet}| \times z_{pv}$ is negative.

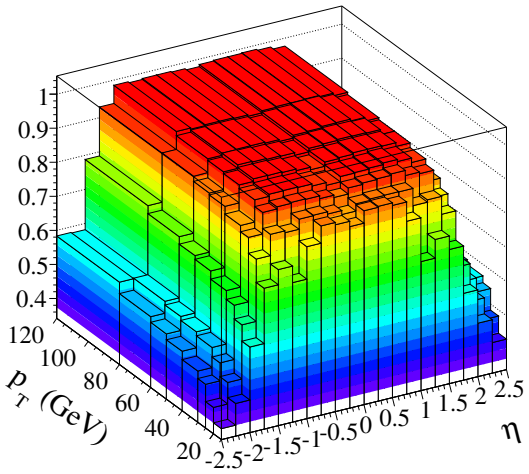


Figure 111: Taggability corrections for $b$-jets where $|\eta_{jet}| \times z_{pv}$ is positive and $|z_{pv}| <$ 20 cm

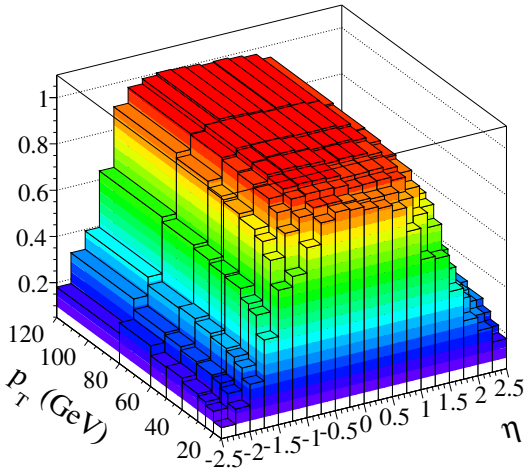


Figure 112: Taggability corrections for $b$-jets where $|\eta_{jet}| \times z_{pv}$ is positive and 20 cm $< |z_{pv}| <$ 35 cm.

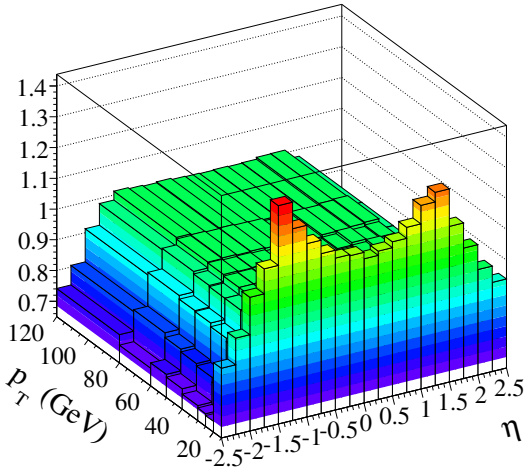


Figure 113: Taggability corrections for light jets where $|\eta_{jet}| \times z_{pv}$ is negative.

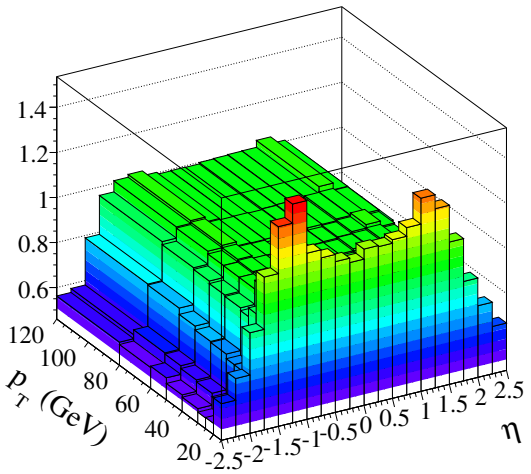


Figure 114: Taggability corrections for light jets where $|\eta_{jet}| \times z_{pv}$ is positive and $|z_{pv}| < 20$ cm

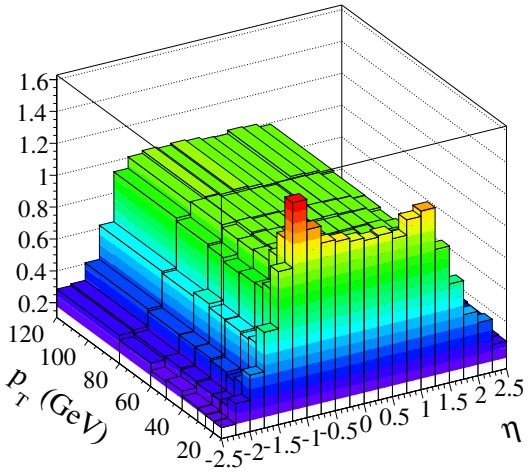


Figure 115: Taggability corrections for light jets where $|\eta_{jet}| \times z_{pv}$ is positive and 20 cm ¡ $|z_{pv}| < 35$ cm.

# F Luminosity Reweighting

The analysis requires data and Monte Carlo to have the same instantaneous luminosity profiles. For this purpose we determine the data and MC luminosity profiles in our final samples (for an example see fig. 116) and derive an event weight (see fig. 117). Fig. 118 shows the result of the closure test and Fig. 119 shows the ratio of the data and MC instantaneous luminosity profiles after reweighting.

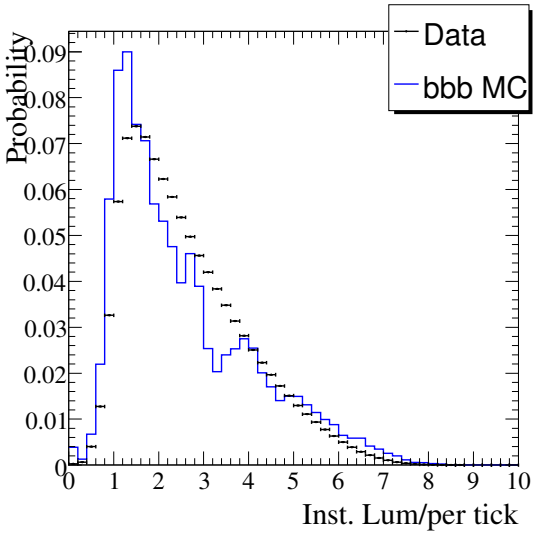


Figure 116: Instantaneous luminosity profiles for data and *bbb* Monte Carlo.

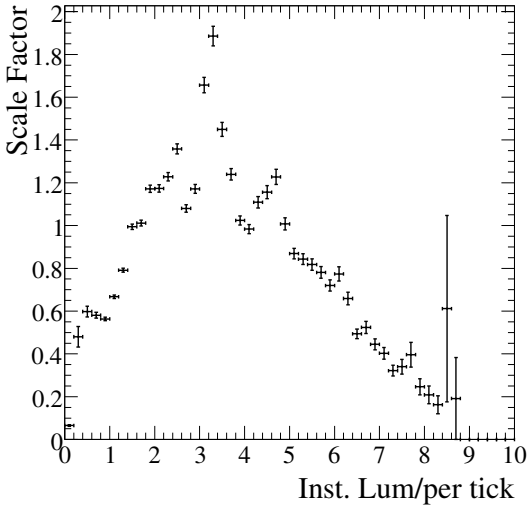


Figure 117: Event weight.

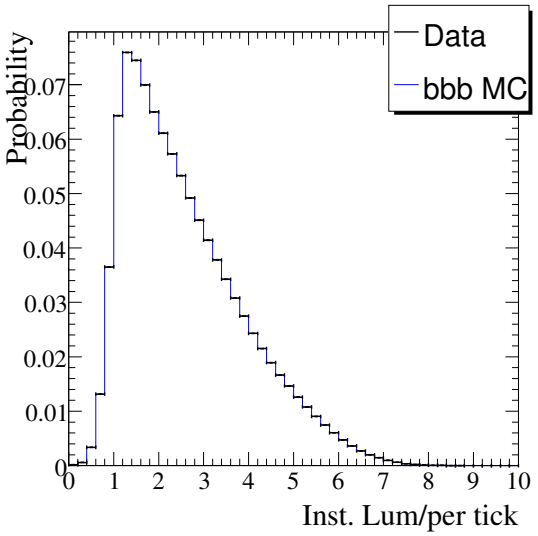


Figure 118: Closure plot for luminosity reweighting.

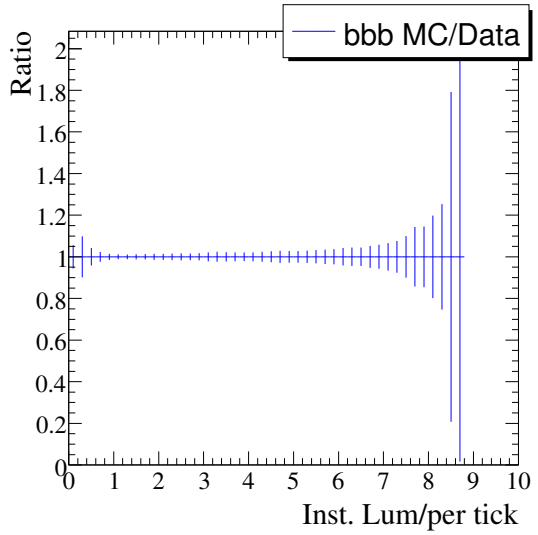


Figure 119: Ratio of the bbb MC and Data instantaneous luminosity profiles after reweighting.

# G Deficit Crosschecks

Several crosschecks have been carried out into the deficit around 130 GeV. The results of some of these investigations are shown here, specifically the likelihood and jet variables in the:

- High likelihood region, represented by a likelihood cut $> 0.5$, see Section G.1.
- Mass window around the deficit, $120 < m_{bb} < 140$, see Section G.2.1.
- High likelihood region and mass window around the deficit, $120 < m_{bb} < 140$, see Section G.2.2.

In addition to these crosschecks the effect of each variable in the likelihood was tested by removing each variable in turn and retraining the likelihood. No significant change in the likelihood or deficit was seen.

## G.1 High Likelihood Region

The $p_T$, $\eta$ and likelihood distributions are shown in Figs. 120, 121 and 122 respectively for the high likelihood region. Fig. 123 shows the residuals between the data and predicted background likelihood variable distributions.

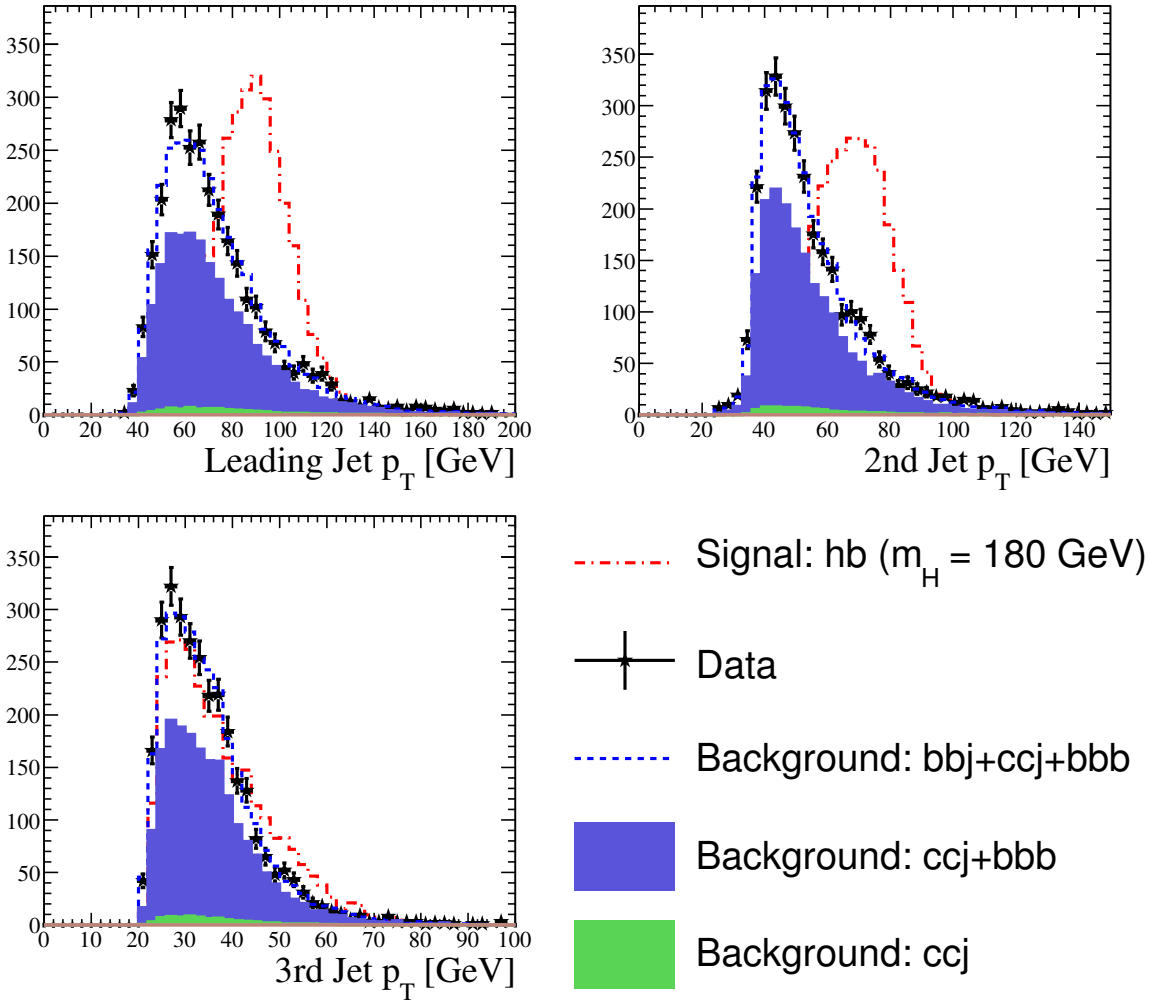


Figure 120: Data predicted background comparison for 3 jets, 3 $b$-tag sample with a 180 GeV Higgs Sample used as signal. Shown is jet $p_T$ for the three jets with the highest $p_T$ in the event after a likelihood cut of $> 0.5$ has been applied.

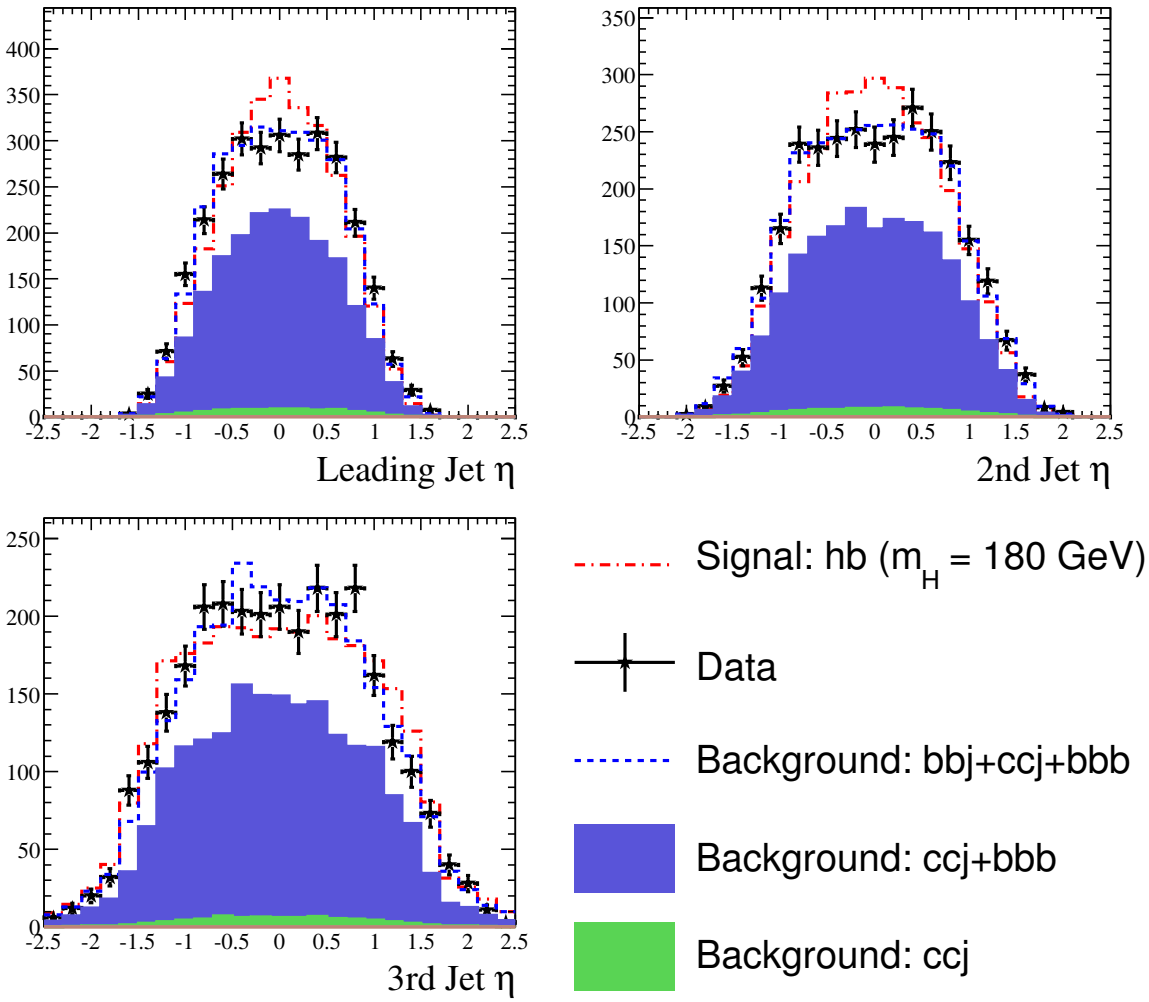


Figure 121: Data predicted background comparison for 3 jets, 3 $b$-tag sample with a 180 GeV Higgs Sample used as signal. Shown is jet $\eta$ for the three jets with the highest $p_T$ in the event after a likelihood cut of $> 0.5$ has been applied.

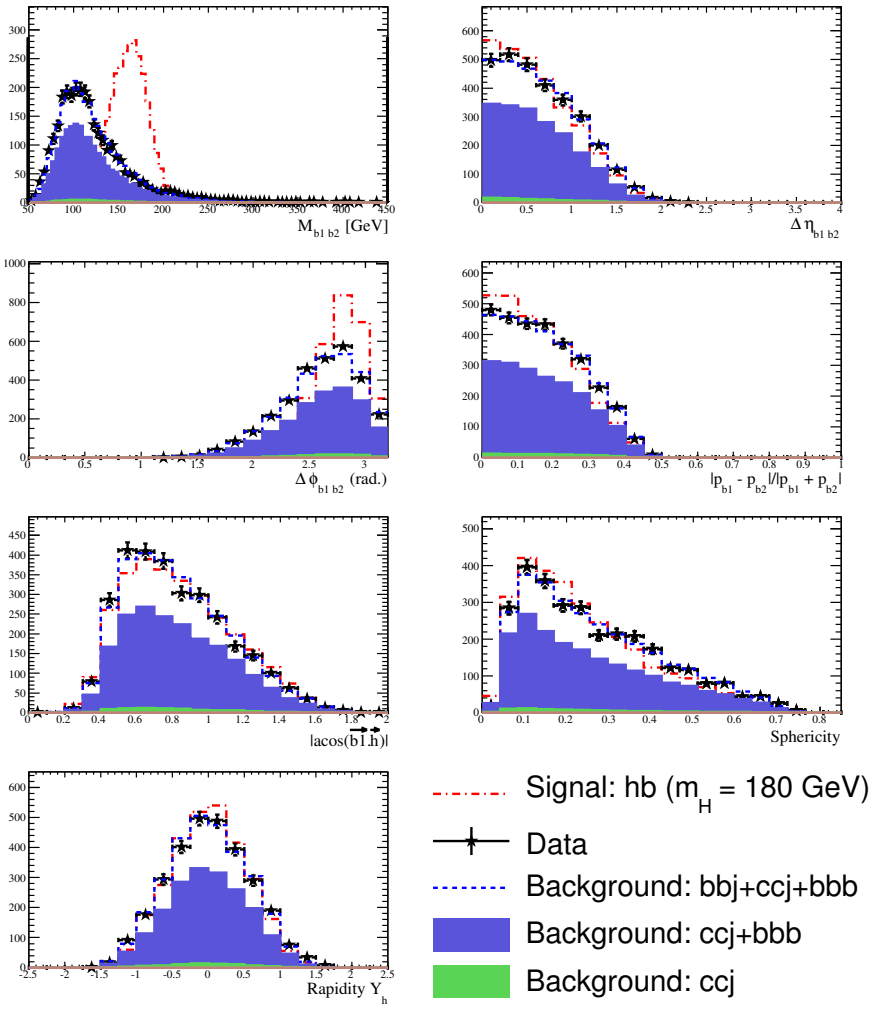


Figure 122: Data predicted background comparison for 3 jets, 3 $b$-tag sample with a 180 GeV Higgs Sample used as signal. Shown are the variables used to determine the signal likelihood (see table 13) after a likelihood cut of $> 0.5$ has been applied.

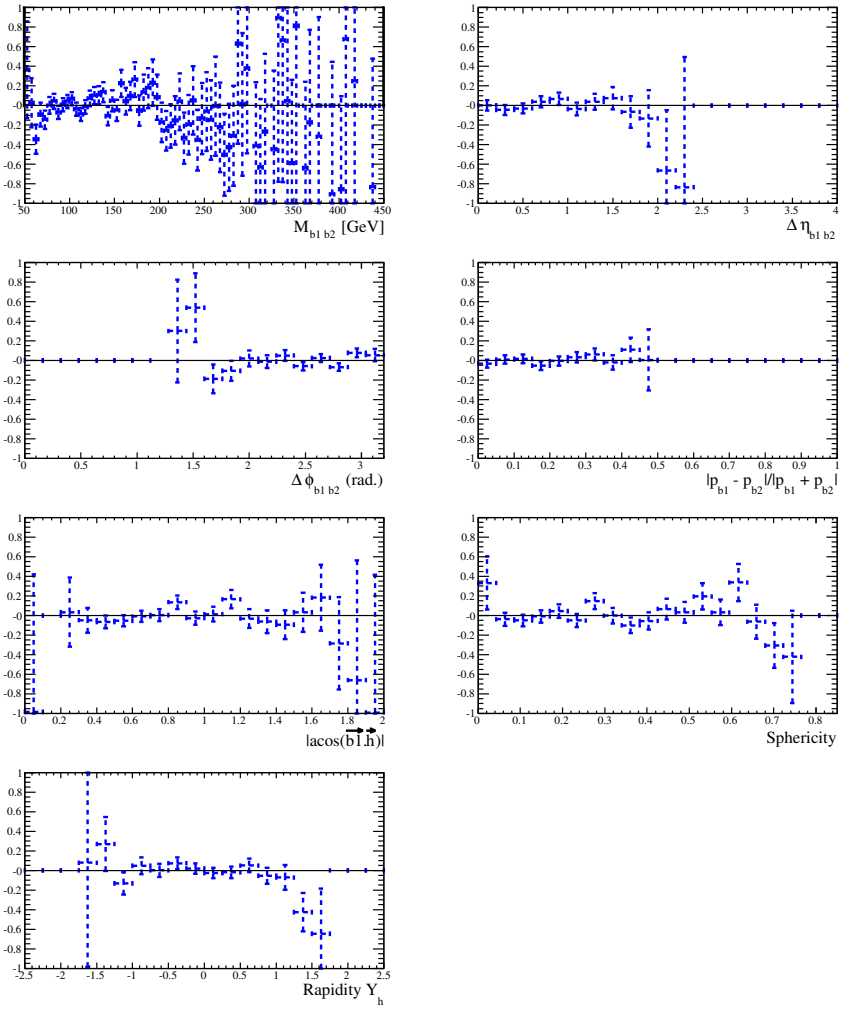


Figure 123: Residuals between predicted background and data for 3 jets, 3 $b$-tag sample with a 180 GeV Higgs Sample used as signal. Shown are the variables used to determine the signal likelihood (see table 13) after a likelihood cut of $> 0.5$ has been applied.

## G.2 Deficit Mass Region

### G.2.1 All Likelihood Region

The $p_T$, $\eta$ and likelihood distributions are shown in Figs. 124, 125 and 126 respectively for the full likelihood region in a mass window $120 < m_{bb} < 140$. Fig. 127 shows the residuals between the data and predicted background likelihood variable distributions.

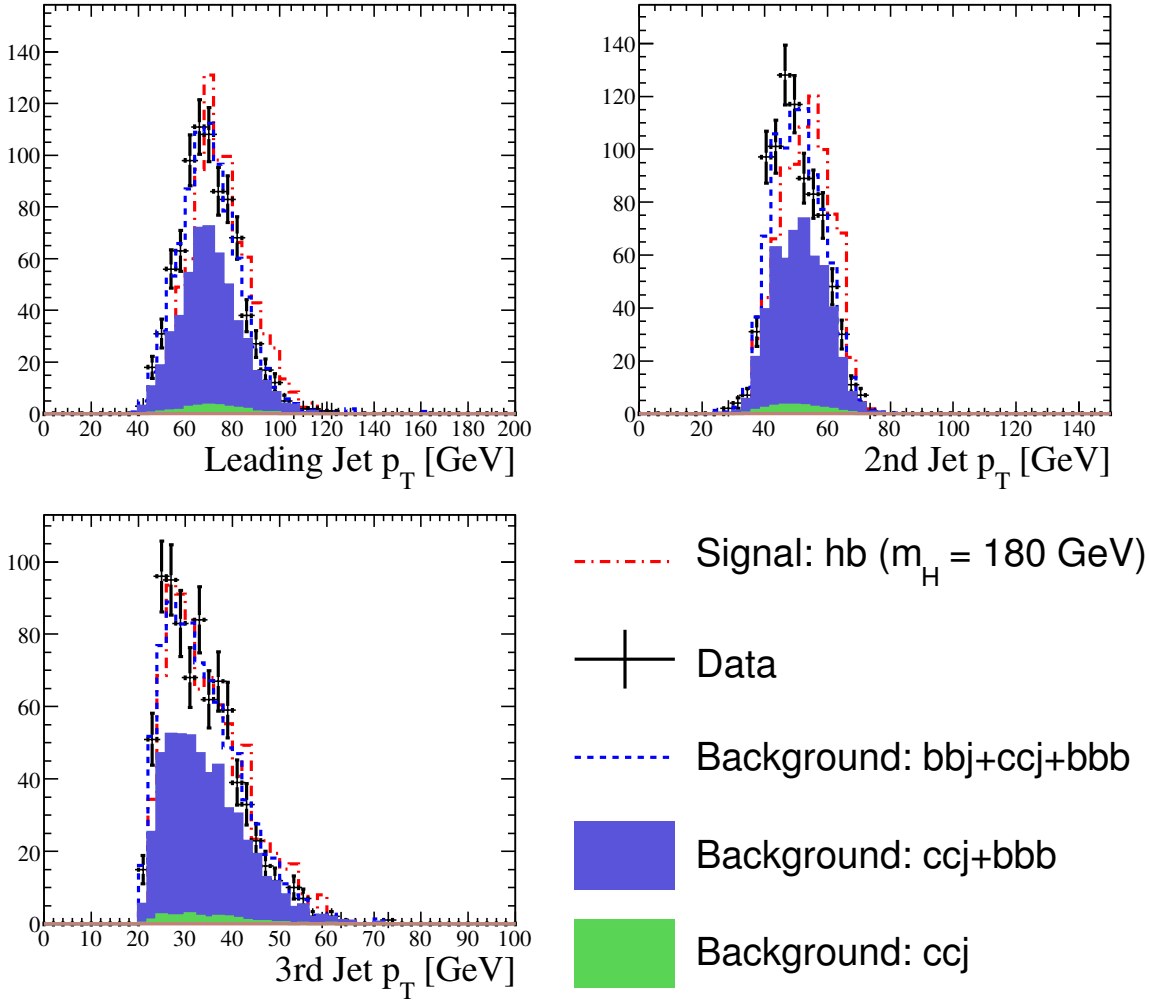


Figure 124: Data predicted background comparison for 3 jets, 3 $b$-tag sample with a 180 GeV Higgs Sample used as signal. Shown is jet $p_T$ for the three jets with the highest $p_T$ in the event after a mass window $120 < m_{bb} < 140$ has been applied.

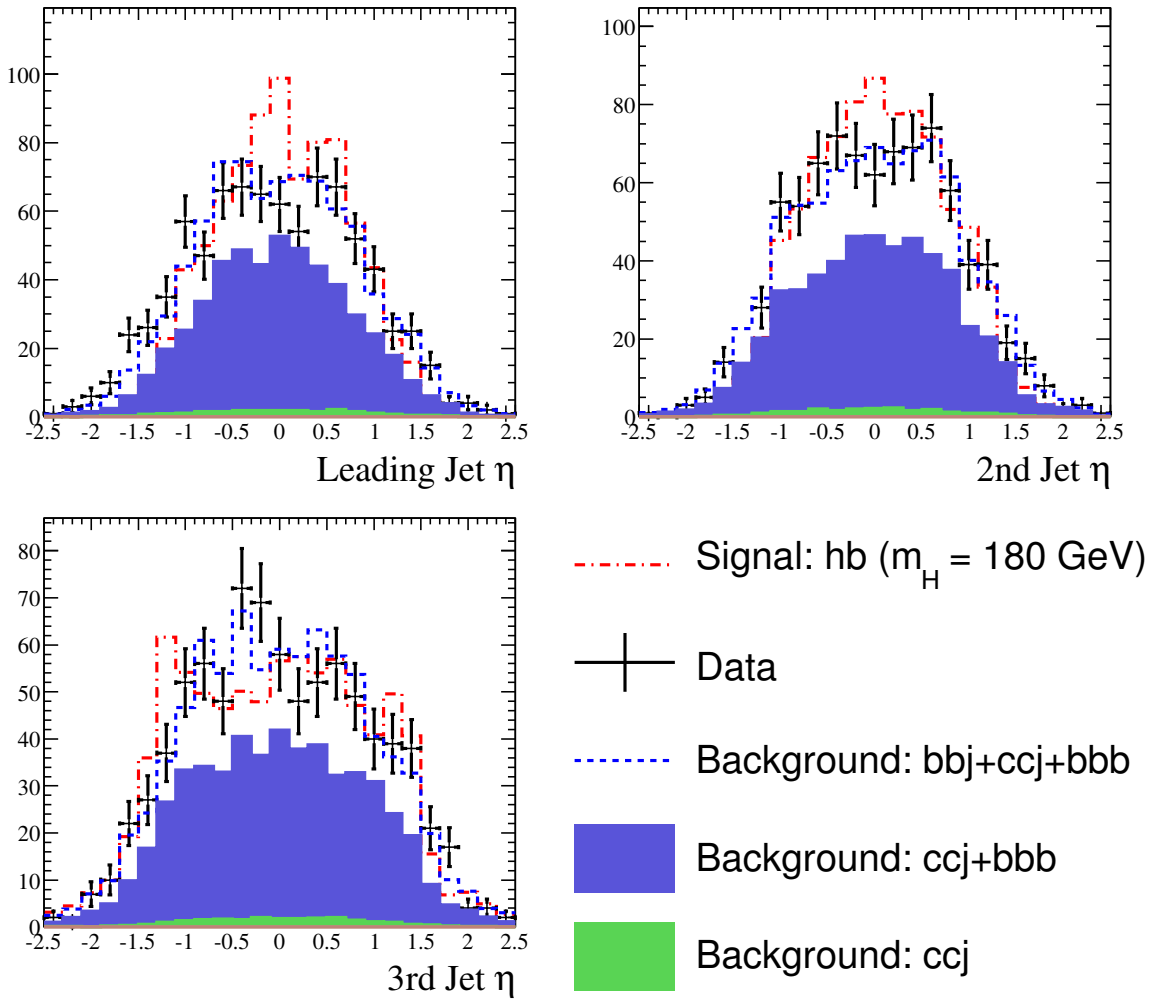


Figure 125: Data predicted background comparison for 3 jets, 3 $b$-tag sample with a 180 GeV Higgs Sample used as signal. Shown is jet $\eta$ for the three jets with the highest $p_T$ in the event after a mass window $120 < m_{bb} < 140$ has been applied.

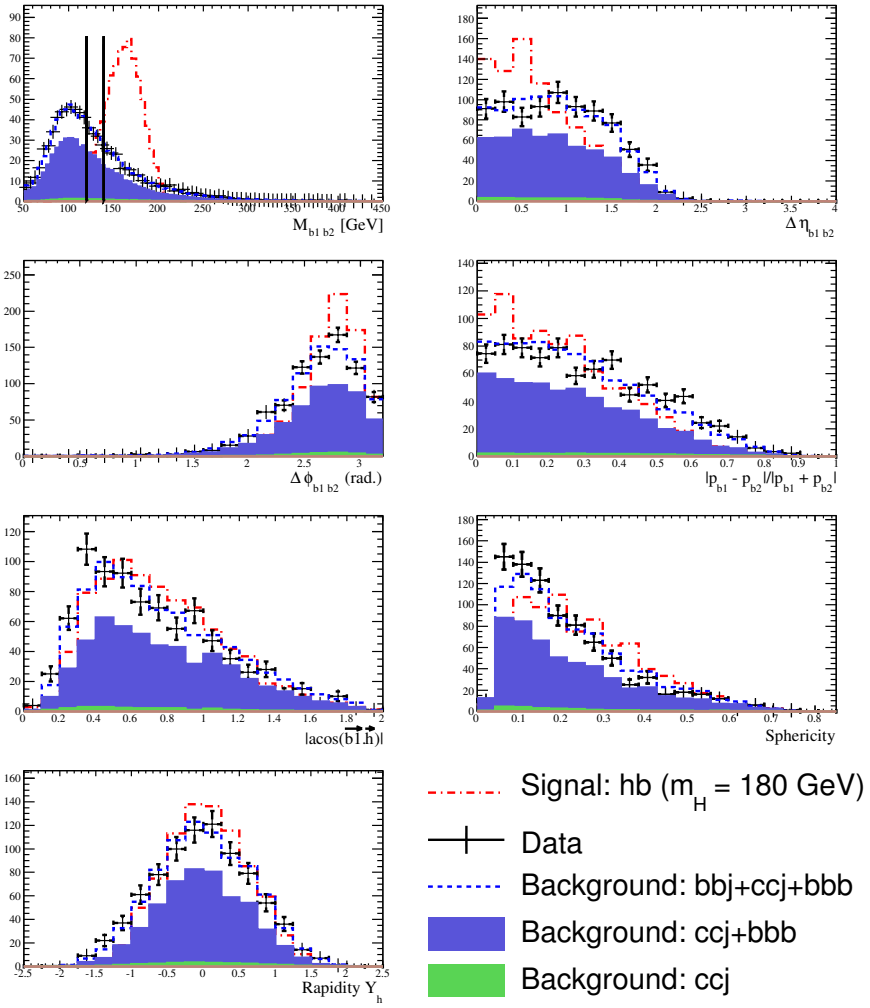


Figure 126: Data predicted background comparison for 3 jets, 3 $b$-tag sample with a 180 GeV Higgs Sample used as signal. Shown are the variables used to determine the signal likelihood (see table 13) after a mass window $120 < m_{bb} < 140$ has been applied.

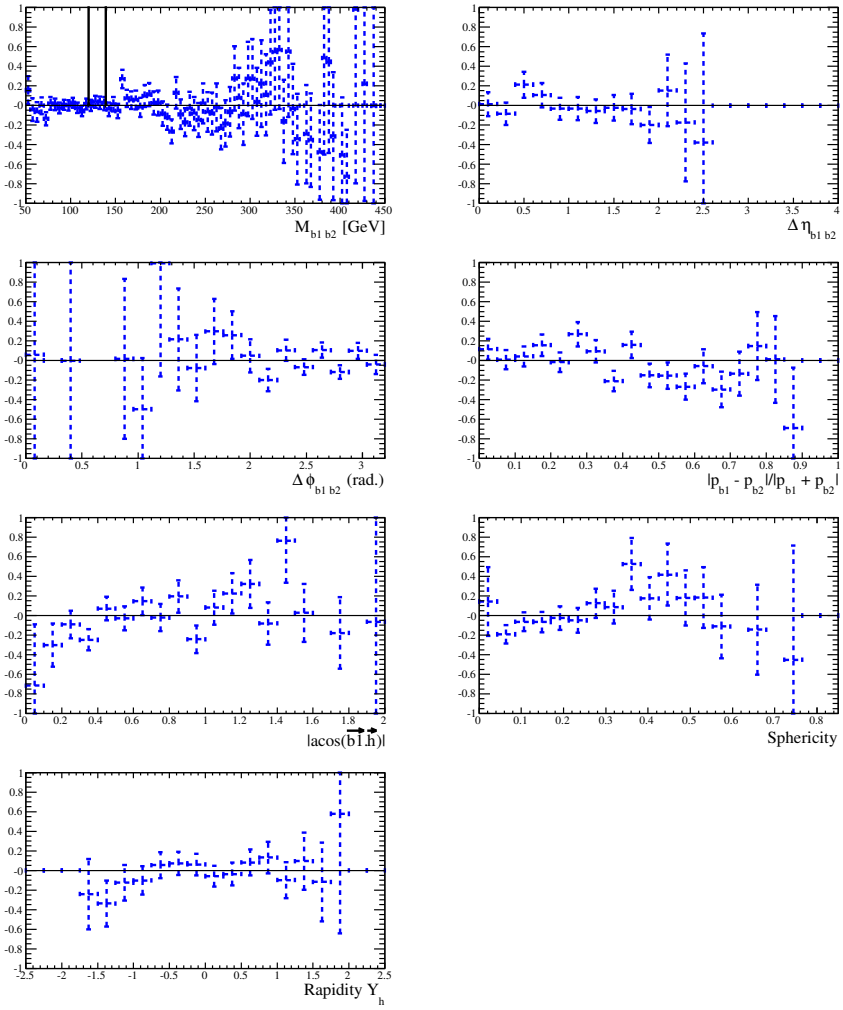


Figure 127: Residuals between predicted background and data for 3 jets, 3 $b$-tag sample with a 180 GeV Higgs Sample used as signal. Shown are the variables used to determine the signal likelihood (see table 13) after a mass window $120 < m_{bb} < 140$ has been applied.

### G.2.2 High Likelihood Region

The $p_T$, $\eta$ and likelihood distributions are shown in Figs. 128, 129 and 130 respectively for the high likelihood region in a mass window $120 < m_{bb} < 140$. Fig. 131 shows the residuals between the data and predicted background likelihood variable distributions.

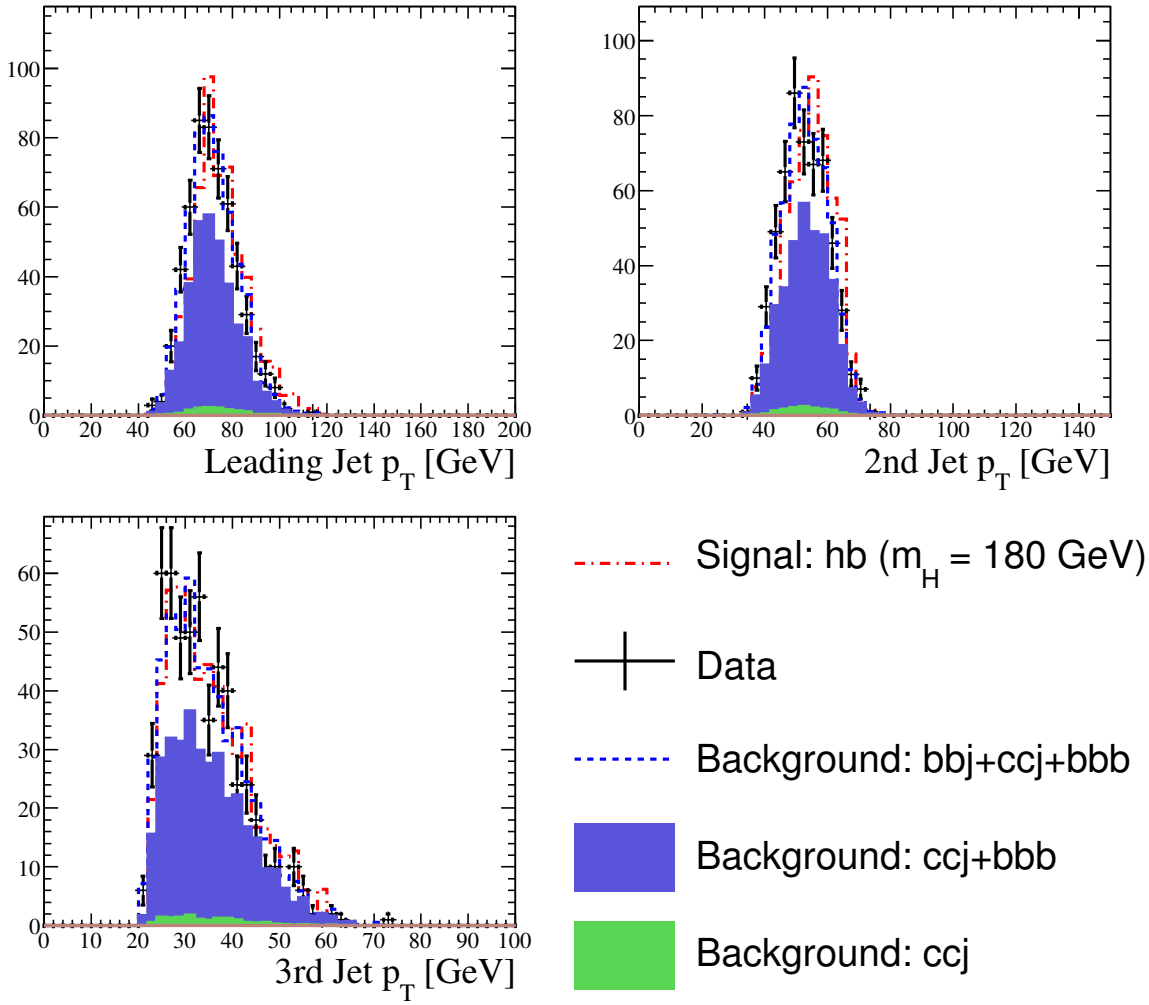


Figure 128: Data predicted background comparison for 3 jets, 3 $b$-tag sample with a 180 GeV Higgs Sample used as signal. Shown is jet $p_T$ for the three jets with the highest $p_T$ in the event after a likelihood cut $> 0.5$ and a mass window $120 < m_{bb} < 140$ has been applied.

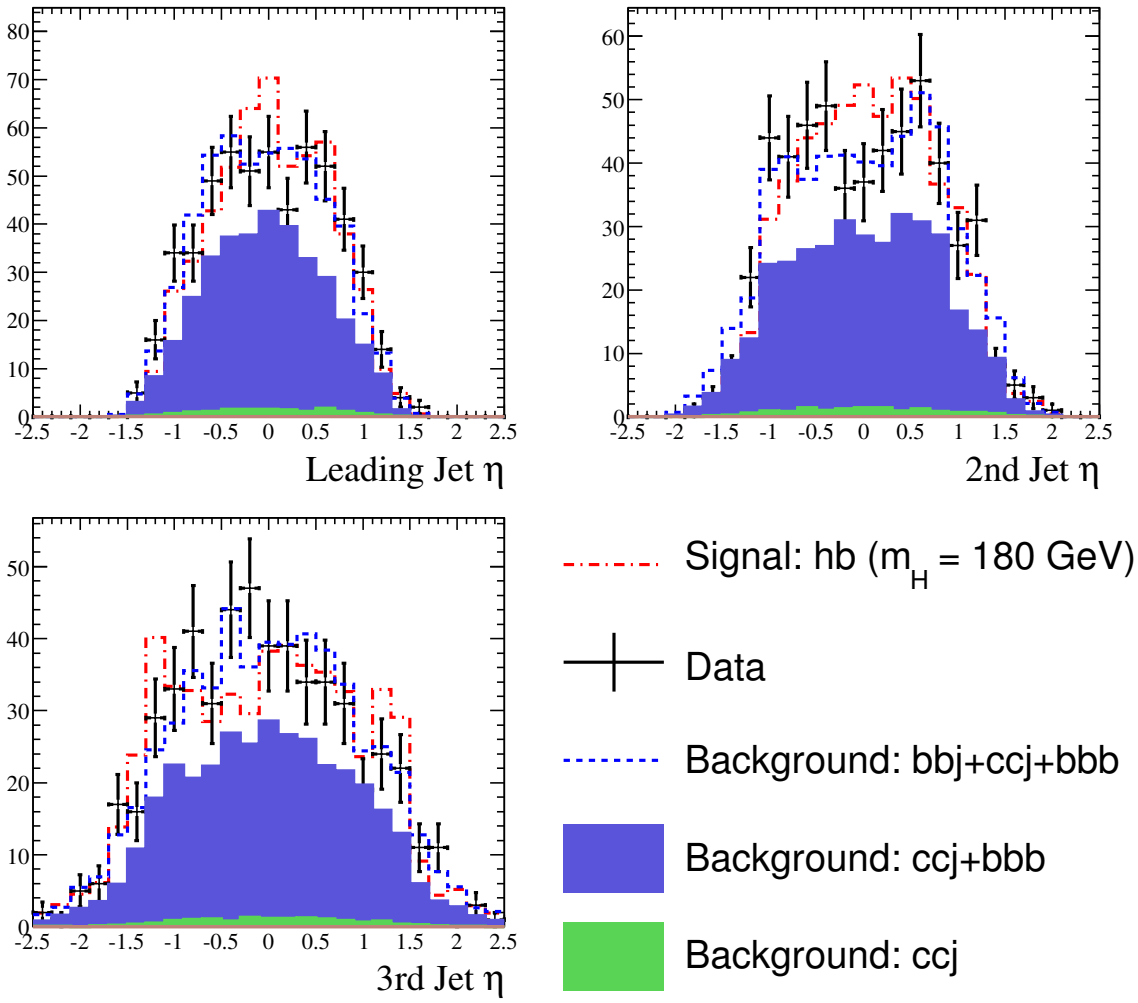


Figure 129: Data predicted background comparison for 3 jets, 3 $b$-tag sample with a 180 GeV Higgs Sample used as signal. Shown is jet $\eta$ for the three jets with the highest $p_T$ in the event after a likelihood cut $> 0.5$ and mass window $120 < m_{bb} < 140$ has been applied.

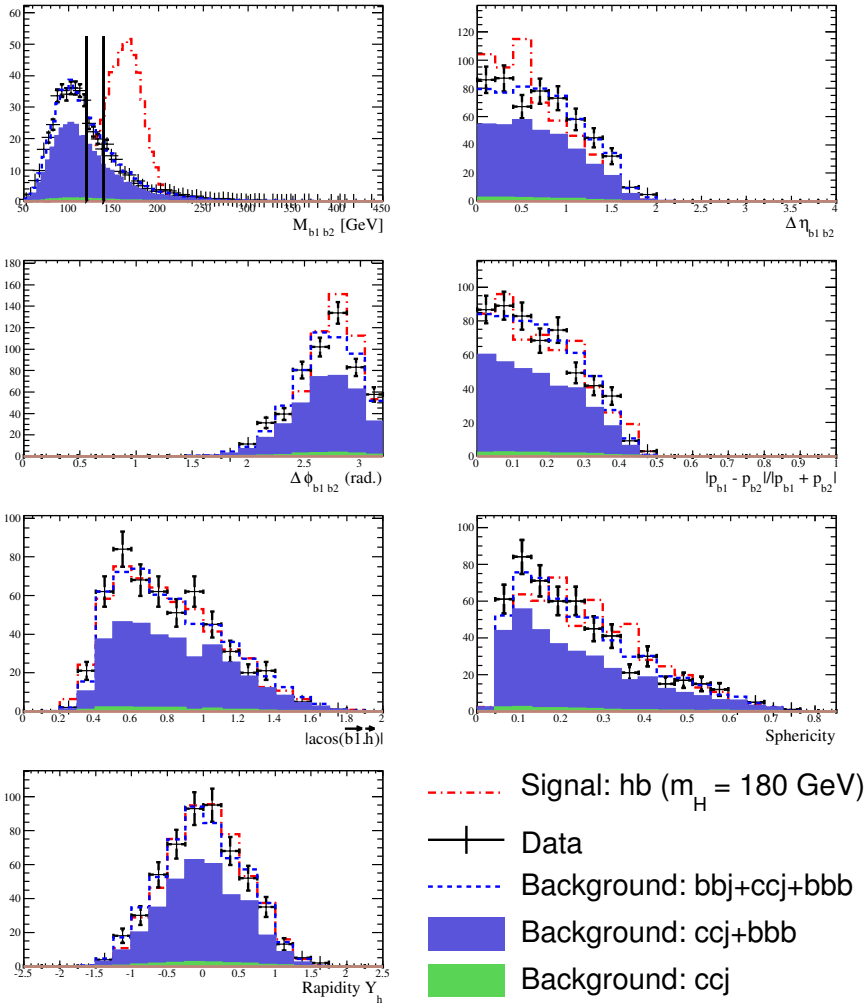


Figure 130: Data predicted background comparison for 3 jets, 3 $b$-tag sample with a 180 GeV Higgs Sample used as signal. Shown are the variables used to determine the signal likelihood (see table 13) after a likelihood cut $> 0.5$ and mass window $120 < m_{bb} < 140$ has been applied.

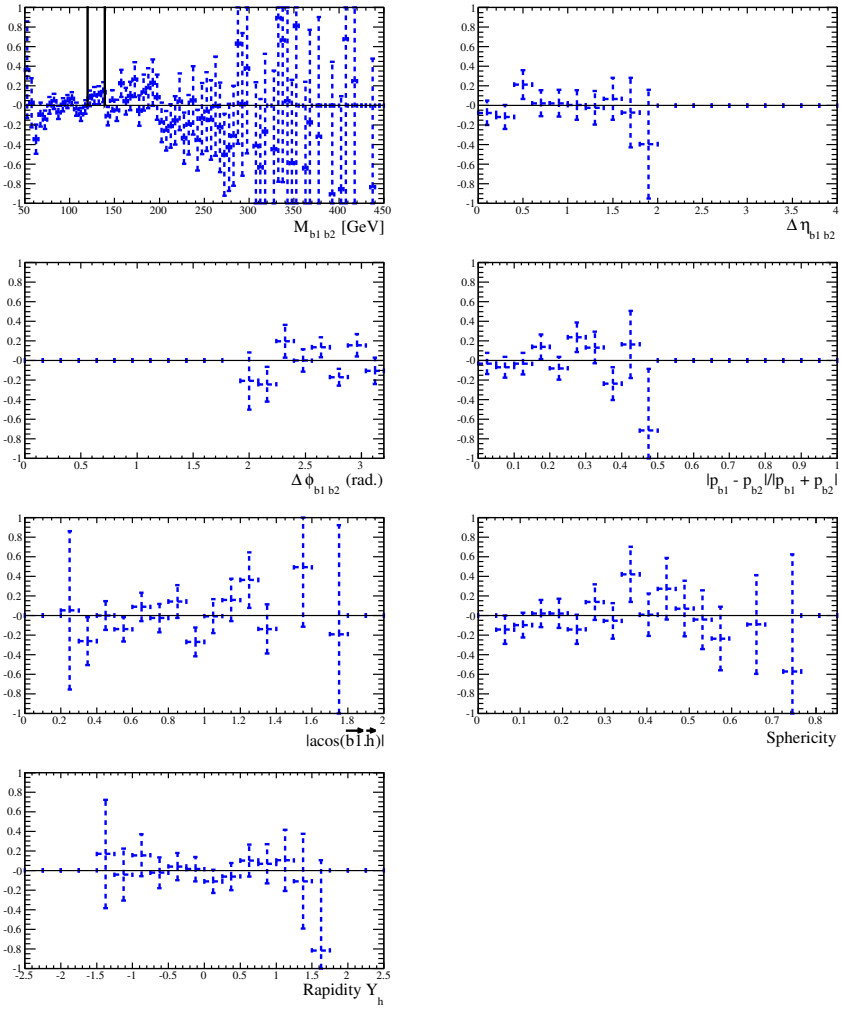


Figure 131: Residuals between predicted background and data for 3 jets, 3 $b$-tag sample with a 180 GeV Higgs Sample used as signal. Shown are the variables used to determine the signal likelihood (see table 13) after a likelihood cut $> 0.5$ and mass window $120 < m_{bb} < 140$ has been applied.

# References


[1] F. Couderc, B. Tuchming, G. Davies, P. Jonsson, S. Robinson, T. Scanlon, *DØ search for neutral Higgs bosons at high tan $\beta$ in multi-jet events using p17 data*, DØ Note 5341.

[2] ICHEP $b$-id instructions on the DØ Wiki. Reference to follow.

[3] W. Fisher, *Collie: A Confidence Level Limit Evaluator*.

[4] `http://www-d0.fnal.gov/Run2Physics/cs/skimming/p20_pass2_skims.html`

[5] Common Analysis Format `http://www-d0.fnal.gov/Run2Physics/cs/caf/`

[6] T. Sjöstrand, L. Lönnblad, S. Mrenna and P. Skands, *Pythia 6.3 Physics and manual*, hep-ph/0308153. We use Pythia 6.323.

[7] M. L. Mangano, M. Moretti, F. Piccinini, R. Pittau and A. D. Polosa, *ALPGEN, a generator for hard multiparton processes in hadronic collisions*, JHEP **0307**, 001 (2003) [arXiv:hep-ph/0206293].

[8] J.M. Campbell, R.K. Ellis, F. Maltoni and S. Willenbrock, *Higgs boson production in association with a single bottom quark*, hep-ph/0204093.

[9] J.M. Campbell *et al.*, *Higgs boson production in association with bottom quarks*, hep-ph/0405302.

[10] J.M. Campbell, R.K. Ellis, `http://mcfm.fnal.gov`.

[11] T. Gadfort, A. Haas, D. Johnston, D. Lincoln, T. Scanlon, S. Schlobohm, *Performance of the Dzero NN b-tagging Tool on p20 Data*, DØ Note 5554.

[12] Cecilia Gerber, Elizaveta Chabalina, Gustavo Otero y Garzon, DØ Note 4995.

[13] N. Makovec and J.-F. Grivaz, *Shifting, Smearing and Removing Simulated Jets*, DØ Note 4914.

[14] F. Couderc, M. Michaut, B. Tuchming, P. Jonsson, S. Robinson, T. Scanlon, *DØ search for neutral Higgs bosons at high tan $\beta$ in multi-jet events using p17 data*, DØ Note 5202.

[15] M. Carena, S. Heinemeyer, C. E. M. Wagner and G. Weiglein, *Suggestions for benchmark scenarios for MSSM Higgs boson searches at hadron colliders*, Eur. Phys. J. C **26**, 601 (2003) [arXiv:hep-ph/0202167].

[16] M. Carena, S. Heinemeyer, C. E. M. Wagner and G. Weiglein, *MSSM Higgs boson searches at the Tevatron and the LHC: Impact of different benchmark scenarios*, Eur. Phys. J. C **45**, 797 (2006) [arXiv:hep-ph/0511023].